THEORETICAL AND COMPUTATIONAL INVESTIGATIONS OF NONLINEAR WAVES IN MAGNETOHYDRODYNAMICS

by

Rho Shin Myong

A dissertation submitted in partial fulfillment
of the requirements for the degree of
Doctor of Philosophy
(Aerospace Engineering)
in The University of Michigan
1996

Doctoral Committee:

Professor Philip L. Roe, Chairperson
Professor Tamas I. Gombosi
Associate Professor Kenneth G. Powell
Professor Bram van Leer

To the memory of my father and my grandmother.

ACKNOWLEDGEMENTS

I would like to express my sincere gratitude to Professor Philip L. Roe for steering me toward this research and for giving fruitful suggestions during all phases of this study. Without his never-ending advice, I might still wander the nonlinear MHD wave world hidden in mist. Especially, a discussion with him last spring will remain the most creative one I have ever had.

I thank Professor Bram van Leer whose compressible flow class provided me a basic mathematical skill to explore the nonlinear hyperbolic world, Professor Kenneth G. Powell for the insight he provided to numerical problems such as MHD eigensystem, and Professor Thamas I. Gombosi for serving on my dissertation committee and whose space plasma physics course provided much of enhancement for my understanding of MHD.

I would like to acknowledge the Korean Ministry of Education for its financial support at the initial stage of my graduate studies, and the financial support from the Department of Aerospace Engineering at the University of Michigan.

Most of all, I would like to thank my beloved wife, Grace, for her full support of my endeavor at Ann Arbor and my five month-old daughter, Rahyun, for all the joy she brings to my life.

TABLE OF CONTENTS

LIST OF FIGURES

Figure

LIST OF TABLES

Table

LIST OF APPENDICES

Appendix

CHAPTER I

INTRODUCTION

1.1 Motivation

Magnetohydrodynamics (MHD), which studies the hydrodynamic description of a plasma, has been regarded as a powerful tool for describing the large-scale structure and processes of a magnetized fluid. For instance, MHD is used to investigate the macroscopic motion of plasmas such as space plasmas (cf. the earth-solar wind interaction [89, 18, 96], the interaction between the bow shock and interplanetary MHD waves [69]), hot fusion plasma (cf. Tokamak) [110, 12, 7, 38], and the temporal variations of time-dependent plasmas. Some processes arising in engineering problems, for example, plasma accelerator in space propulsion [103] and MHD power generator [19] can be also explained by magnetohydrodynamic approximations.

However, because of the great difficulty attached to laboratory experiments, and also to the interpretation of natural phenomena, it remains uncertain how complete and accurate the mathematical description of MHD is. Furthermore, due to the mathematical difficulty in full MHD, some reduced MHD [135], for example, the linearized MHD and incompressible MHD are considered without rigorous explanation of their relevance to the full compressible MHD.

The core problem of MHD is the nonlinear evolution and stability of resistive

MHD processes. The reason is that disruptive processes[1] (disruption of the Tokamak confinement magnetic fields and substorm of the magnetosphere) which is of fundamental importance in understanding of plasmas may develop as a nonlinear evolution of resistive MHD processes. These disruptive processes seem to be related with the reconnection of magnetic field lines and the instability, which are major consequences of finite resistivity.

The investigation of the nonlinear evolution and stability of resistive MHD processes requires solving the time-dependent resistive nonlinear MHD equations, which turn out to be very difficult even by numerical methods. However, because most of problems occurring in space and fusion plasmas involve the high magnetic conductivity [2], the Riemann problem is the simplest model which retains the effect of time-dependency and convection, if the resistivity is included at least in the vanishing limit.

The Riemann problem describes the evolution of nonlinear waves, and thus its solution reveals general features of the MHD description. It can be applied directly to the magnetic field reconnection problem that can be approximated by colliding plasma jets [132, 113, 121, 115, 74, 124]. More importantly, it serves as a starting point for numerical boundary conditions [117] and as the building block of high resolution Godunov-type numerical methods [43, 118, 99, 48].

The Riemann solution defines the large time asymptotics of a general resistive solution and also the instantaneous response to discontinuities. In gasdynamics, the

[1] "A common feature of disruptive processes in Tokamak is that they seem to be two-stage processor consisting of a coherent precursor which can be associated with some MHD instability and a usually faster turbulent phase, during which rapid transport occurs." "How can energy be stored efficiently without being released prematurely, and if it is finally released, what is the trigger mechanism?" [12, pages 240, 350].

[2] Note that $Re_m \approx u_o L T^{1.5}$. 1.6×10^{10} in magnetosphere, 1.6×10^{14} in solar wind, 1.6×10^2 in ionosphere, and $10^2 \sim 10^5$ in fusion plasmas [45].

large time asymptotics are not different from the instantaneous response. But the answer for MHD is not obvious. There are also possibilities of the interaction of nonlinear hyperbolic waves which may have a great influence on the study of the Riemann problem.

In this thesis, by considering the MHD Riemann problem, we investigate the evolution of nonlinear MHD waves theoretically and computationally. By studying the well-posedness of the MHD Riemann problem, we attempt to resolve two fundamental questions of MHD waves. **What is the consequence of the interaction of nonlinear waves? How can we apply the Godunov-type numerical methods to MHD whose well-posedness is questionable?** The studies focus on the shock stability and the well-posedness of the MHD Riemann problem: existence, uniqueness, and continuous dependence on reference states.

1.2 Historical Background

Previous studies of MHD nonlinear waves may be classified as three fields: physical approach, mathematical analysis, and numerical simulation.

1.2.1 Physical Approach

Since Alfvén showed the existence of electromagnetic-hydrodynamic waves known as Alfvén wave in 1942 [5], MHD waves have been studied extensively [50, 106, 81, 4, 108, 39, 71, 11, 70, 102, 29, 30, 62, 63, 49, 82, 128, 112, 33, 90, 79, 123]. De Hoffman and Teller [28] first obtained and discussed the MHD jump conditions, using the relativistic energy-momentum equation. Lüst [77] studied stationary MHD shock waves of arbitrary strength, while Bazer and Ericson [8, 31] derived an explicit form of the MHD Rankine-Hugoniot relations. Akhiezer *et al.* [3] developed the so-called evolutionary condition for MHD shocks, which has been considered a

major contribution to the study of MHD shocks. According to this theory, all intermediate shocks are considered non-physical. Germain [40] argued that a MHD shock for which the tangential magnetic field changes its sign is never stable. By considering the resistive MHD, Kulikovskii and Liubimov [66] showed that the fast and slow shock waves possess structure for arbitrary ratios of the dissipative coefficients. Then they argued that the intermediate shock waves may possess structure. Polovin [93] computed the Riemann invariants for MHD simple waves. Finally, by putting these works together, Gogosov [44] developed the theory of resolution of an arbitrary discontinuity in MHD, which corresponds to the exact solution of the MHD Riemann problem. But these works are far from showing the well-posedness of the Riemann problem, since it is known that if only evolutionary shocks are employed, not all Riemann problem have solution [58, pages 256]. All these studies are based on the analysis of MHD planar shocks and require the rotational discontinuity for the non-planar Riemann problem.

Due to this dilemma and the shift of the center of attention to the more complex kinetic theory, the study of MHD waves dwindled and remained only in some texts [6, 94] such as a famous book by Jeffrey and Taniuti [58], and instead some models of the non-planar problem of collisionless plasmas have begun to be studied. Rogister [101] investigated the parallel propagation of nonlinear low-frequency waves by using a model equation. Laminar wave-train structure of collisionless magnetic slow shocks considered by Coroniti [25], nonlinear evolution of parallel-propagating hydromagnetic waves by Cohen and Kulsrud [23], instability of long Alfvén waves parallel to the magnetic field by Mjølhus [83], structure and evolution of small-amplitude intermediate shocks by Kennel *et al.* [62], nonlinear evolution of Alfvén waves subject to growth and damping by Hada *et al.* [47] and Malkov *et al.* [78], and evolution

of small-amplitude intermediate shocks by Wu and Kennel [129] all lie in Rogister's approach in the sense that the governing equations are the form

$$\mathbf{B}_t + (|\mathbf{B}|^2\mathbf{B})_x = D\mathbf{B}_{xx}, \tag{1.1}$$

where $\mathbf{B}$ is magnetic field or fluctuation, and $D = \left((\eta,\chi)^T, (-\chi,\eta)^T\right)$. This is known as the CKB (Cohen-Kulsrud-Burgers) model [63] and also as derivative nonlinear Schrödinger equation (DNLS) when $\eta = 0$.

In the eighties interest shifted again to MHD due to increasing concern on denser plasmas and more complex methods of containment. From numerical solutions of resistive MHD equations [125-128, 131], Wu showed that at least some of the intermediate shocks are admissible and can be formed through nonlinear steepening from continuous waves in the planar problem, contrary to the evolutionary theory. By studying the nonlinear stability of MHD intermediate shock waves using an asymptotic 3×3 model system, Brio and Rosenau [17] also argued that the outcome of MHD numerical simulations may be sensitive to the type of the numerical scheme used. However, in spite of these numerical experiments, the behavior of nonlinear waves in MHD has remained far being completely understood, since the numerical results alone cannot yield a theory to explain all the complicated phenomena occurring in MHD which contain several hundred possibilities.

1.2.2 Mathematical Theory

Since Keyfitz and Kranzer [64] studied a system of non-strictly hyperbolic conservation laws arising in elasticity theory, the interactions of hyperbolic waves have been investigated extensively by many mathematicians. Freistühler [34] discussed the existence and uniqueness of solutions of the Riemann problem of the left-hand terms in derivative nonlinear Schrödinger equation. By studying the rotationally degenerate

hyperbolic model, Freistühler [32] argued that there is a considerable discrepancy between the approaches of dynamical stability (similar to evolutionary theory) and vanishing viscosity. But, the direct application of this work to MHD remained questionable since the rotational degeneracy is only part of MHD degeneracies[3].

Apparently without awareness of MHD application, Schaeffer, Shearer, Gomes and Isaacson *et al.* [104, 105, 107, 46, 53-56] classified the non-strictly hyperbolic system with isolated umbilic point and quadratic nonlinearity, and applied the solutions to oil recovery problem. According to their results, the 2×2 non-strictly hyperbolic system can be classified as four cases in which the Riemann solution patterns are qualitatively identical. In particular, by introducing a viscous profile entropy condition, Gomes showed that there are shocks which have viscous profiles but do not satisfy the Lax conditions. Isaacson *et al.* [57] also introduced a unifying framework for treating all of the fundamental waves occurring in non-strictly hyperbolic conservation laws.

1.2.3 Numerical Simulation

In the early eighties, some researchers in gasdynamics and astrophysics have begun to develop very efficient conservative finite difference schemes that could resolve discontinuities such as shocks very accurately [118, 99, 24, 48]. The idea behind these schemes can be traced to the pioneering work done by Godunov [43] in the late fifties which is developed on the basis of the Riemann problem.

The first application of this approach to MHD was done by Brio and Wu [15], who developed an approximate MHD Riemann solver. Bell *et al.* [10] extended high order Godunov-type methods to non-strict, having local linear degeneracies, hyperbolic system (oil recovery problem). By considering the rotationally degenerate

[3]See Section 2.5.

model, Freistühler[36] demonstrated that different schemes yield markedly different results for certain data and argued that precise control of the numerical viscosity introduced into a computational method is crucial for generating the correct numerical solution. Chen *et al.* [20] presented a numerical method based on a discrete Boltzmann equation. Zachary *et al.* [133, 134] applied BCT scheme (developed by Bell, Trangenstein and Colella [10]) to the MHD problem and also developed a high-order Godunov-type method based on operator-split approximation to the multidimensional equations. Dai and Woodward [26, 27] presented a MHD Riemann approximate solver which treats all waves emanating from the initial discontinuity as themselves discontinuous[4], and also developed a simple approximate Riemann solver based on characteristic formulations. Ogawa and Hayashi [89] presented a comparison among upwind, centered difference, and FCT (flux corrected transport) schemes with application to the problem of the interaction of a supersonic plasma flow with a two-dimensional dipole magnetic field. Tanaka [111] presented a three-dimensional high resolution MHD simulation scheme based on a linearized Riemann solver on an unstructured grid system. van Putten [119, 120] applied Roe's scheme to fully relativistic planar MHD shock problems. Aslan [7] carried out one-dimensional simulation of MHD waves using Roe's approximate Riemann solver. Powell *et al.* [96] developed a method enforcing the divergence-free condition and obtained some results for space physics simulation based on the Cartesian-based adaptive grid method. Interestingly, Wu, who first applied Roe's scheme to the MHD problem, argued that numerical schemes based on the Riemann problem might be inappropriate for solving the temporal dynamics of MHD shocks[5], and returned to two-step Lax-Wendroff

[4] It is limited to weak rarefaction.

[5] "To use a shock-capturing scheme, we already assume what the physical jump relations are. Thus, this kind of scheme is not appropriate to use here since we are concerned with the problem of deciding the admissibility of the Rankine-Hugoniot MHD jump relations." [125, page 669].

method for investigating the evolution of MHD shocks.

1.3 Scope of the Present Work

In this work we identify the critical issues of the evolution and stability of nonlinear waves in MHD that will be of great help to enhance the current understanding of resistive MHD processes. By showing the relationship between the 3×3 model system and the full MHD with mathematical rigor, we proved the well-posedness of the planar MHD Riemann problem.

In Chapter II, we examine the physical reasoning behind the MHD approximation and present various mathematical forms of large-scale plasma motions. In this chapter, we also present the general feature of the MHD singularity in more clear manner and derive model systems that preserve the MHD singularity and can be connected directly to recent mathematical works.

In Chapter III, based on Gomes' work, we present a global analysis of the dynamical system of the planar model. It is also shown that the simple geometric conditions are inappropriate as conditions for selecting admissible shocks of non-strictly hyperbolic conservation laws. In addition, the Riemann problem is investigated extensively and some recent mathematical theories for non-strictly hyperbolic conservation laws are applied to the model.

In Chapter IV, we derive the MHD Rankine-Hugoniot conditions and simple wave relations in a useful form, and construct the weak solutions to the planar MHD Riemann problem. With mathematical rigor, we prove that the planar MHD Riemann problem is well-posed and the solutions are always self-similar.

In Chapter V, we identify the fundamental difference between planar waves and non-planar waves. In coplanar case, we show that the solutions of the Riemann

problem depend not only on left and right states, but also on the magnetic field moments. In non-planar case, we demonstrate that the Riemann solutions exist but they are not necessarily unique.

In Chapter VI, we discuss how finite amplitude waves develop nonlinearly when they are subject to external disturbances. We obtain some patterns of the nonlinear evolution in canonical cases, and propose a general pattern of the nonlinear evolution in non-planar case, which is distinguished largely in time: very small, intermediate, and very large.

In Chapter VII, we discuss numerical issues arising in non-strictly hyperbolic conservation laws for MHD. We compute the Lagrangian MHD eigensystem which satisfies the mean-value property. We also raise the fundamental questions in developing Godunov-type numerical methods for MHD, and suggest a new approximate Riemann solver, which is simple and follows exactly the way to generate the large-time Riemann solution for the non-planar system from the well-posed planar problem.

In Appendix A, we show the exact relevance of the model and the MHD system with mathematical rigor.

In Appendix B, we describe the analytical tool for selecting shocks which admit a viscous profile.

In Appendix C, we study the MHD dynamical system and obtain the global phase portraits.

CHAPTER II

MATHEMATICAL DESCRIPTION OF THE LARGE-SCALE MOTIONS OF MAGNETIZED FLUIDS

When a conducting fluid moves in a magnetic field, an electric field is generated. As a result, the interaction of the electric current with the magnetic field changes the motion of the fluid and changes the magnetic field itself. This self-sustained process can be described by magnetohydrodynamic approximations which is a kind of continuum mechanics which studies the motion of electrically conducting media in the presence of a magnetic field [94].

The MHD approximation can be derived from the kinetic equations for ions and electrons [45], but we derive the MHD equations in a macroscopic way, valid for any electrically conducting fluid, the specific properties of which appear only in the equation of state. All quantities are expressed in the GS units.

2.1 Magnetohydrodynamic Approximation

MHD, which describes the large-scale motions of electrically conducting fluids, is the hydrodynamic description of a plasma. We neglect not only kinetic effects, but also the difference in motion of the various components of the plasmas. Its use can be justified if the characteristic frequency is appreciably smaller than the collision

frequency. This condition means small Knudsen numbers

$$Kn = \frac{l}{L} \ll 1, \tag{2.1}$$

where l is the mean free path and L is a characteristic length. Under this assumption, particles (ions, electrons, neutrals) are described by their own properties. In a fully ionized plasma, consisting only of electrons and a single kind of ions, it represents two-fluid MHD.

Strictly speaking, the hydrodynamic description of a plasma is valid only for high plasma densities and low plasma temperatures, when the Knudsen number is small. Therefore, a hydrodynamic approximation may be rejected in hot plasmas which have very long mean free path. This is true even for some astrophysical plasmas such as the solar wind, and so for hot laboratory plasmas such as in Tokamak. However, this argument turns out to be too restrictive [12, page 21] since (1) the plasma behavior is in general strongly anisotropic due to the magnetic field, and (2) a collisionless plasma is not dissipationless. The effective mean free path in the direction perpendicular to the field is usually very small giving rise to an anisotropic pressure tensor, and gradients parallel to the field where the mean free path is long tend to be much weaker than in the perpendicular direction. Furthermore, plasma particles feel a rather short effective mean free path due to the small-scale turbulence which causes stochastic particle orbits and phase mixing. Therefore, due to the effect of the short mean free path, a MHD approximation may be well justified for large-scale plasma motions.

A magnetohydrodynamic medium can be regarded as a single fluid, without distinguishing between the motion of the particles, provided that the characteristic frequency is much smaller than the ion cyclotron frequency. If the characteristic fre-

quency is appreciably smaller than the frequency for the exchange of energy between electrons and ions, the electron pressure and the ion pressure manage to become equal and the plasma is characterized by a single pressure. Since the electrons are much lighter than the ions, the mass density and the fluid velocity are then determined by ions, and the current density by the electrons. This is the simple fluid MHD approximation. The simple fluid model, considered as a single entity, is the simplest of a single fluid MHD.

In the non-relativistic case, the displacement current in Ampère's law can be neglected. Thus the current density $\mathbf{J}$ can be expressed in terms of magnetic induction,

$$\mathbf{J} = \nabla \times \mathbf{B}. \tag{2.2}$$

2.2 Conservation Laws in Ideal MHD

Conservation laws for the MHD quantities $\rho, p, \mathbf{u}, \mathbf{B}$ can be obtained by assuming that the fluid is ideal, that is, neglecting all dissipative and dispersive effects such as viscosity, magnetic resistivity, thermal conductivity and Hall effect. The mass conservation law in a differential form is

$$\frac{\partial \rho}{\partial t} + \nabla \cdot (\rho \mathbf{u}) = 0. \tag{2.3}$$

The conservation law of momentum is

$$\frac{\partial}{\partial t}(\rho \mathbf{u}) + \nabla \cdot (\rho \mathbf{u}\mathbf{u} + p\mathbf{I}) + \mathbf{B} \times \mathbf{J} = 0. \tag{2.4}$$

By Eq. 2.3 and a vector identity

$$\mathbf{B} \times (\nabla \times \mathbf{B}) = \nabla(\frac{\mathbf{B} \cdot \mathbf{B}}{2}) - (\mathbf{B} \cdot \nabla)\mathbf{B}, \tag{2.5}$$

it reduces to

$$\frac{\partial}{\partial t}(\rho \mathbf{u}) + \nabla \cdot \Big(\rho \mathbf{u}\mathbf{u} + \mathbf{I}(p + \frac{\mathbf{B} \cdot \mathbf{B}}{2}) - \mathbf{B}\mathbf{B}\Big) = -\mathbf{B}(\nabla \cdot \mathbf{B}). \tag{2.6}$$

The electromagnetic conservation law can be derived from the so-called freezing-in law that the fluid sticks to the magnetic field lines. The freezing-in law in any closed material contour which moves with the fluid is

$$\frac{D}{Dt}\int_{\Omega}\mathbf{B}\cdot\mathbf{n}\,dS \;=\; 0. \tag{2.7}$$

We can change the form of the freezing-in law by a kinematical relation [60, page 238]. The rate of change of outflow of $\mathbf{B}$ through any surface element $\mathbf{n}dS$ moving with the fluid is

$$\Big(\frac{\partial\mathbf{B}}{\partial t}+\mathbf{u}(\nabla\cdot\mathbf{B})-\nabla\times(\mathbf{u}\times\mathbf{B})\Big)\cdot\mathbf{n}dS \;=\; 0. \tag{2.8}$$

Using a vector identity

$$\nabla\times(\mathbf{u}\times\mathbf{B})=\mathbf{u}(\nabla\cdot\mathbf{B})+(\mathbf{B}\cdot\nabla)\mathbf{u}-\mathbf{B}(\nabla\cdot\mathbf{u})-(\mathbf{u}\cdot\nabla)\mathbf{B}, \tag{2.9}$$

it reduces to

$$\frac{\partial\mathbf{B}}{\partial t}+\nabla\cdot(\mathbf{uB}-\mathbf{Bu}) \;=\; -\mathbf{u}(\nabla\cdot\mathbf{B}). \tag{2.10}$$

Using the ideal gas assumption $p=\rho RT$ and the total energy

$$E=\frac{1}{2}\rho\mathbf{u}\cdot\mathbf{u}+\frac{p}{\gamma-1}+\frac{\mathbf{B}\cdot\mathbf{B}}{2}, \tag{2.11}$$

where γ is the ratio of the specific heats and is $5/3$ for a monatomic gas, the energy equation in the non-conservative form

$$\frac{\partial p}{\partial t}+(\mathbf{u}\cdot\nabla)p+\gamma p\nabla\cdot\mathbf{u} \;=\; 0 \tag{2.12}$$

can be cast in the conservative form,

$$\frac{\partial E}{\partial t}+\nabla\cdot\Big((E+p+\frac{\mathbf{B}\cdot\mathbf{B}}{2})\mathbf{u}-\mathbf{B}(\mathbf{B}\cdot\mathbf{u})\Big) \;=\; -(\mathbf{B}\cdot\mathbf{u})(\nabla\cdot\mathbf{B}). \tag{2.13}$$

Finally, the complete set of equations for ideal MHD has the form

$$\begin{pmatrix} \rho \\ \rho\mathbf{u} \\ \mathbf{B} \\ E \end{pmatrix}_t + \nabla \cdot \begin{pmatrix} \rho\mathbf{u} \\ \rho\mathbf{u}\mathbf{u} + \mathbf{I}(p + \frac{\mathbf{B}\cdot\mathbf{B}}{2}) - \mathbf{B}\mathbf{B} \\ \mathbf{u}\mathbf{B} - \mathbf{B}\mathbf{u} \\ (E + p + \frac{\mathbf{B}\cdot\mathbf{B}}{2})\mathbf{u} - \mathbf{B}(\mathbf{B}\cdot\mathbf{u}) \end{pmatrix} = -\begin{pmatrix} 0 \\ \mathbf{B} \\ \mathbf{u} \\ \mathbf{B}\cdot\mathbf{u} \end{pmatrix} (\nabla \cdot \mathbf{B}). \quad (2.14)$$

By the divergence-free condition, it recovers

$$\begin{pmatrix} \rho \\ \rho\mathbf{u} \\ \mathbf{B} \\ E \end{pmatrix}_t + \nabla \cdot \begin{pmatrix} \rho\mathbf{u} \\ \rho\mathbf{u}\mathbf{u} + \mathbf{I}(p + \frac{\mathbf{B}\cdot\mathbf{B}}{2}) - \mathbf{B}\mathbf{B} \\ \mathbf{u}\mathbf{B} - \mathbf{B}\mathbf{u} \\ (E + p + \frac{\mathbf{B}\cdot\mathbf{B}}{2})\mathbf{u} - \mathbf{B}(\mathbf{B}\cdot\mathbf{u}) \end{pmatrix} = 0. \quad (2.15)$$

In ideal MHD, $\mathbf{J}, \mathbf{E}$, and the charge density ρ_e are determined from the solution $\mathbf{u}(\mathbf{r}, t)$ and $\mathbf{B}(\mathbf{r}, t)$ by Eqs. 2.2, $\mathbf{E} = -\mathbf{u} \times \mathbf{B}$, and $\rho_e = \nabla \cdot \mathbf{E} = -\nabla \cdot (\mathbf{u} \times \mathbf{B})$.

2.3 Dissipative and Dispersive Effects

In the ideal MHD the fluid is stuck to the magnetic field line, whereas with dissipation (from collisions) the fluid slips away from the field line. Therefore, for strongly nonlinear dynamic processes we must include dissipative and dispersive effects, which are represented by various kinds of diffusion and dispersion processes. Such effects can be easily seen by determining how collisions affect the freezing-in law. Particle collisions or turbulence lead to the plasma not completely screening the electric field, and the electric field in the reference frame of the plasma becomes nonzero.

$$\mathbf{E} = -\mathbf{u} \times \mathbf{B} + \mathbf{E}'. \quad (2.16)$$

Then Faraday's law becomes

$$\frac{\partial \mathbf{B}}{\partial t} - \nabla \times (\mathbf{u} \times \mathbf{B}) = -\nabla \times \mathbf{E}'. \quad (2.17)$$

Here the divergence-free condition is applied. Using Ohm's law

$$\mathbf{J} = \frac{1}{\eta}\mathbf{E}', \tag{2.18}$$

where η is the magnetic resistivity, Eq. 2.2, and the vector identity $\nabla \times \nabla\mathbf{B} = \nabla\nabla \cdot \mathbf{B} - \nabla^2\mathbf{B}$, we find

$$\frac{\partial \mathbf{B}}{\partial t} - \nabla \times (\mathbf{u} \times \mathbf{B}) \;\; = \;\; \eta\nabla^2\mathbf{B}. \tag{2.19}$$

In general, in addition to dissipative coefficients, there are dispersive coefficients. Dissipative coefficients have positive sign and are related to energy dissipations. But dispersive coefficients can have any sign and are not related to energy dissipation. Among dispersive coefficients, the Hall coefficient is the most important. The Hall effect, which describes the current flowing at right angles to the electric and magnetic fields, can be explained by using a nonlinear transport theory. Ohm's law can be written in the form

$$\mathbf{E} + \mathbf{u} \times \mathbf{B} - \frac{1}{ne}\mathbf{J} \times \mathbf{B} \;\; = \;\; \eta\mathbf{J}, \tag{2.20}$$

where n, e are the electron density and charge. By combining Eqs. 2.2 and Faraday's law, we find

$$\frac{\partial \mathbf{B}}{\partial t} - \nabla \times (\mathbf{u} \times \mathbf{B}) \;\; = \;\; \eta\nabla^2\mathbf{B} - \frac{1}{ne}\nabla \times \Big((\nabla \times \mathbf{B}) \times \mathbf{B}\Big). \tag{2.21}$$

The left-hand side describes the freezing-in law while the first term in the right-hand side corresponds to the magnetic diffusion. A remaining term represents the Hall effect, which remains finite in a collisionless plasma. In the one-dimensional problem, the term becomes

$$(-\chi\frac{\partial^2 B_z}{\partial x^2}, \chi\frac{\partial^2 B_y}{\partial x^2}) \quad \text{for} \quad (B_y, B_z), \tag{2.22}$$

where χ defined as $\chi = B_x/(ne)$ is the Hall coefficient[1].

For dissipations, a conventional measure of their magnitude can be defined as

$$Re_m \equiv \frac{u_o L}{\eta}, \quad Re \equiv \frac{u_o L}{\mu}, \quad Pe \equiv \frac{u_o L}{\lambda}, \quad S \equiv \frac{c_a L}{\eta}, \tag{2.23}$$

where Re_m, Re represent the magnetic and kinetic Reynolds number, and Pe is Péclet number. u_o, L are the characteristic velocity and length, and λ is the thermal diffusivity defined as $\lambda = \kappa/(\rho c_p)$, where κ is the thermal conductivity, and c_a is the Alfvén velocity. The Lundquist number S is used mostly in measuring resistive effects of a static configuration.

In conclusion, for strongly nonlinear dynamic unsteady processes dissipation effects are important because large-scale motions rapidly build up small-scale structures, corresponding to singularities in the framework of the ideal MHD. Therefore the MHD Riemann problem is not free from such category, and thus dissipation effects have to be included for the MHD Riemann problem, at least, in the limit of vanishing dissipation coefficients.

2.4 Non-ideal MHD

The longitudinal viscosity μ, the shear viscosity ν, the magnetic resistivity η, and the thermal conductivity κ are the main dissipative coefficients, while the Hall coefficient χ is an important dispersive coefficient. If there are no external forces, the non-ideal MHD equations take the form in the one-dimensional problem

$$\begin{pmatrix} \rho \\ \rho\mathbf{u} \\ \mathbf{B}_\perp \\ E \end{pmatrix}_t + \begin{pmatrix} \rho u \\ \rho\mathbf{u}\mathbf{u} + \mathbf{I}(p + \frac{\mathbf{B}_\perp \cdot \mathbf{B}_\perp}{2}) - B_x\mathbf{B}_\perp \\ \mathbf{B}_\perp u - B_x\mathbf{v} \\ (E + p + \frac{\mathbf{B}_\perp \cdot \mathbf{B}_\perp}{2})u - B_x(\mathbf{B}_\perp \cdot \mathbf{v}) \end{pmatrix}_x = \begin{pmatrix} 0 \\ D_1\mathbf{u} \\ D_2\mathbf{B}_\perp \\ (\Sigma + \kappa T) \end{pmatrix}_{xx} \tag{2.24}$$

[1] It is assumed that the wave propagates in x direction.

where $\mathbf{B}_\perp, \mathbf{v}$ represent the transverse components of magnetic and velocity fields, and Σ denotes $(\mu u^2 + \nu \mathbf{v}\cdot\mathbf{v} + \eta \mathbf{B}_\perp \cdot \mathbf{B}_\perp)/2$. D_1, D_2 are defined as

$$D_1 = \begin{pmatrix} \mu & 0 & 0 \\ 0 & \nu & 0 \\ 0 & 0 & \nu \end{pmatrix}, \quad D_2 = \begin{pmatrix} \eta & -\chi \\ \chi & \eta \end{pmatrix}. \tag{2.25}$$

By means of the divergence-free condition for the magnetic field, B_x is constant in the one-dimensional problem.

The MHD equations can be put into the Lagrangian form. If we denote the specific volume by τ and define a material coordinates ξ as

$$\xi = \int_{x(t)}^{x} \rho(s,t) ds, \tag{2.26}$$

where $x(t)$ is a particle path satisfying $x'(t) = u(x(t),t)$, the MHD equations becomes

$$\begin{pmatrix} \tau \\ \mathbf{u} \\ \tau \mathbf{B}_\perp \\ e_t \end{pmatrix}_{t'} + \begin{pmatrix} -u \\ \mathbf{I}(p + \frac{\mathbf{B}_\perp \cdot \mathbf{B}_\perp}{2}) - B_x \mathbf{B}_\perp \\ -B_x \mathbf{v} \\ (p + \frac{\mathbf{B}_\perp \cdot \mathbf{B}_\perp}{2}) u - B_x (\mathbf{B}_\perp \cdot \mathbf{v}) \end{pmatrix}_{\xi} = \begin{pmatrix} 0 \\ D_1 \mathbf{u}_x \\ D_2 \mathbf{B}_{\perp x} \\ (\Sigma + \kappa T)_x \end{pmatrix}_{\xi}. \tag{2.27}$$

$\frac{\partial}{\partial t'}$ indicates the time derivative in the Lagrangian description. ($\tau E = e_t$.)

2.5 MHD Waves and Hyperbolic Singularity

From Eq. 2.15, the governing equations for the primitive variables $\mathbf{V}$, if their properties depend on x, can be written as ($\mathbf{V} = (\rho, u, \mathbf{v}, \mathbf{B}_\perp, p)$)

$$\mathbf{V}_t + \mathbf{A}\mathbf{V}_x = 0, \tag{2.28}$$

where

$$\mathbf{A} = \begin{pmatrix} u & \rho & 0 & 0 & 0 & 0 & 0 \\ 0 & u & 0 & 0 & \frac{B_y}{\rho} & \frac{B_z}{\rho} & \frac{1}{\rho} \\ 0 & 0 & u & 0 & -\frac{B_x}{\rho} & 0 & 0 \\ 0 & 0 & 0 & u & 0 & -\frac{B_x}{\rho} & 0 \\ 0 & B_y & -B_x & 0 & u & 0 & 0 \\ 0 & B_z & 0 & -B_x & 0 & u & 0 \\ 0 & \rho a^2 & 0 & 0 & 0 & 0 & u \end{pmatrix}, \tag{2.29}$$

and a, the acoustic wave speed, is given by $a^2 = \gamma p/\rho$ for an ideal gas. The system 2.28 yields seven types of wave motion whose speeds relative to the fluid velocity $(\lambda_i - u)$ are

$$0, \quad \pm c_s, \quad \pm c_a, \quad \pm c_f, \tag{2.30}$$

where $c_a = B_x/\sqrt{\rho}$, and $c_{f,s}$ are the fast and slow magnetoacoustic wave speed given by

$$2c_{f,s}^2 = a^2 + \frac{\mathbf{B}\cdot\mathbf{B}}{\rho} \pm \sqrt{\left(a^2 + \frac{\mathbf{B}\cdot\mathbf{B}}{\rho}\right)^2 - 4a^2 {c_a}^2}. \tag{2.31}$$

The first wave, which moves with the fluid velocity, is the entropy wave. It is well known that entropy and Alfvén waves are associated with linearly degenerate characteristic fields ($\nabla\lambda_i \cdot \mathbf{r}_i = 0$ for all phase space, where λ_i and $\mathbf{r}_i$ represent the eigenvalues and the right eigenvectors associated with i-waves), while slow and fast magnetoacoustic waves are associated with nonlinear characteristic field ($\nabla\lambda_i \cdot \mathbf{r}_i$ not generally zero). However, $\nabla\lambda_i \cdot \mathbf{r}_i$ may change the sign and is zero for certain critical states. This implies that the associated characteristic speeds for the magnetoacoustic waves are not convex.

In addition to the non-convexity, there are chances that those wave speeds are

not distinct. When $\mathbf{B}_\perp \cdot \mathbf{B}_\perp = 0$, then

$$c_s = c_a, \quad c_f = a \quad \text{for} \quad a > c_a, \tag{2.32}$$

$$c_f = c_a, \quad c_s = a \quad \text{for} \quad a < c_a. \tag{2.33}$$

In this case, the Alfvén wave interacts or resonates with one of the magnetoacoustic waves [2]. In particular, when $\mathbf{B}_\perp \cdot \mathbf{B}_\perp = 0$ and $c_a = a$, then

$$c_s = c_a = c_f = a. \tag{2.34}$$

This point is called the *triple umbilic* point. This represents the interaction of an Alfvén wave and slow, fast magnetoacoustic waves. Note that this triple umbilic point becomes a *double umbilic* point in the planar problem with variables (ρ, u, v, B_y, p) and such point represents the interaction of slow, fast magnetoacoustic waves at $c_a = a$.

The MHD singularity looks like a straight string which corresponds to the $(a^2 - {c_a}^2)$ axis in a space $(a^2 - {c_a}^2, B_y, B_z)$. The resonances have a profound effect on the construction of weak solutions to the hyperbolic conservation laws. Hyperbolic conservation laws with wave resonances are called non-strictly hyperbolic and have been studied extensively in the eighties by some mathematicians Keyfitz, Shearer, and Isaacson *et al.*, as mathematical models describing elasticity and oil recovery. They proposed a 2×2 non-strictly hyperbolic system and derived mathematical theorems of constructing the weak solutions near the double umbilic point.

In MHD, Wu and Freistühler have been working on a model system (DNLS) to describe the interaction of an Alfvén wave and a magnetoacoustic wave. As shown before, however, this resonance is only part of MHD resonances and thus the

[2] Among the non-convexity and the resonance, the non-convexity may be considered essential in the sense that it appears even in the scalar conservation laws.

application of their works to MHD is somewhat limited. In fact, a major contribution of current study is to fill the gap between the analysis of the interaction of linear and nonlinear fields and the analysis of the interaction of two nonlinear fields, and eventually to unify them in the three dimensional $(a^2 - c_a^2, B_y, B_z)$ phase space.

In the next section, we will derive a model system which preserves the behavior of the MHD singularity and MHD wave structures.

2.6 Derivation of Model Systems

Model systems, which preserve the MHD singularity and are easier to deal with, can be derived from the full MHD equations. Brio and Rosenau [17] developed a 3×3 model system in order to investigate MHD shocks, using the perturbation method [16]. But, we can also obtain the same system only by a physical reasoning. A close look of MHD waves suggests that the MHD wave structure near the triple umbilic point can be revealed in a three-dimensional phase space consisting of p, B_y and B_z. In other words, the nonlinear interactions can be explained by one-directional waves (either purely left-running waves or purely right-running waves), because six waves are symmetric about the entropy wave moving with the fluid particle. To this end, the MHD system is symmetrically non-strictly hyperbolic. Therefore, a 3×3 model system preserving the singularity can be derived by considering only the momentum equation of u and the conservation laws of the magnetic fields. Mass conservation law and energy equation are largely associated with the entropy wave, and momentum equations of v, w are related by the conservation laws of B_y, B_z. The

resulting equations are, from the Lagrangian form 2.27,

$$\begin{pmatrix} u \\ \tau B_y \\ \tau B_z \end{pmatrix}_{t'} + \begin{pmatrix} p + \frac{{B_y}^2 + {B_z}^2}{2} \\ -B_x v \\ -B_x w \end{pmatrix}_{\xi} = \begin{pmatrix} \mu u_x \\ \eta B_{y_x} - \chi B_{z x} \\ \chi B_{y_x} + \eta B_{z x} \end{pmatrix}_{\xi}, \tag{2.35}$$

with $\tau_{t'} = u_\xi$. Let us assume

$$B_x = 1,\ \tau \approx 1,\ v \approx B_y,\ w \approx B_z. \tag{2.36}$$

Noting that u has the same order of magnitude as a and thus $p \sim u^2$, the system of three equations reduces to the 3×3 model system developed by Brio and Rosenau [17].

$$\mathbf{u}_t + \mathbf{f}_x = D\mathbf{u}_{xx}, \tag{2.37}$$

where

$$\mathbf{u} = \begin{pmatrix} u \\ B_y \\ B_z \end{pmatrix},\ \mathbf{f} = \begin{pmatrix} \frac{1}{2}(cu^2 + {B_y}^2 + {B_z}^2) \\ (u-1)B_y \\ (u-1)B_z \end{pmatrix},\ D = \begin{pmatrix} \mu & 0 & 0 \\ 0 & \eta & -\chi \\ 0 & \chi & \eta \end{pmatrix}. \tag{2.38}$$

Here, u represents a thermodynamic property. The parameter c controls the behavior of the whole system, and Brio and Rosenau set its value $\gamma + 1$ although they omitted the proof.

In order to transform the system into a mathematically more manageable form[3], we consider the Taylor series of $f(\mathbf{u})$ about a triple umbilic point $\mathbf{u}^* = (1/(1-c), 0, 0)$ [104]:

$$f(\mathbf{u}) = f(\mathbf{u}^*) + df(\mathbf{u}^*)(\mathbf{u} - \mathbf{u}^*) + q(\mathbf{u} - \mathbf{u}^*) + h.o.t., \tag{2.39}$$

where $q : \mathbf{R}^3 \to \mathbf{R}^3$ is a homogeneous quadratic mapping and $h.o.t.$ represents the remainder. The truncated series $f_T(\mathbf{u})$ is

$$f(\mathbf{u}^*) + df(\mathbf{u}^*)(\mathbf{u} - \mathbf{u}^*) + q(\mathbf{u} - \mathbf{u}^*). \tag{2.40}$$

[3]This is the key step to relate the study of the MHD singularity with the recent mathematical works on 2×2 quadratic hyperbolic conservation laws.

In this case the following two relations are satisfied:

$df(\mathbf{u}^*)$ is diagonalizable.

$df_T(\mathbf{u})$ has distinct eigenvalues for all $\mathbf{u} \in \mathbf{R}^3 - \mathbf{u}^*$.

Then, the system can be simplified by the following steps. First, the system 2.37 is unchanged under replacing $f(\mathbf{u}) - f(\mathbf{u}^*)$ by $f(\mathbf{u})$. Next, using the first relation we have $df(\mathbf{u}^*) = \lambda \mathbf{I}$ for $\lambda = c/(1-c)$. Therefore, the linear terms in Eq. 2.40 can be eliminated by the change of variable $x' = x - \lambda t$. Finally, it does not matter to replace $(\mathbf{u} - \mathbf{u}^*)$ by $\mathbf{u}$ and to apply a transformation $\mathbf{u} = 2\mathbf{u}'$.

Therefore, if v, w are used to represent B_y, B_z, the nonlinear features in the system 2.37 can be represented by purely quadratic equations.

$$\begin{pmatrix} u \\ v \\ w \end{pmatrix}_t + \begin{pmatrix} cu^2 + v^2 + w^2 \\ 2uv \\ 2uw \end{pmatrix}_x = \begin{pmatrix} \mu & 0 & 0 \\ 0 & \eta & -\chi \\ 0 & \chi & \eta \end{pmatrix} \begin{pmatrix} u \\ v \\ w \end{pmatrix}_{xx}. \tag{2.41}$$

Surprisingly, the planar restriction of this system is nothing but the 2×2 quadratic system of non-strictly hyperbolic conservation laws developed by Schaeffer and Shearer [104],

$$\begin{pmatrix} u \\ v \end{pmatrix}_t + \begin{pmatrix} cu^2 + v^2 \\ 2uv \end{pmatrix}_x = \begin{pmatrix} \mu & 0 \\ 0 & \eta \end{pmatrix} \begin{pmatrix} u \\ v \end{pmatrix}_{xx}. \tag{2.42}$$

We call this system planar 2×2 model. It will be used to study the planar MHD problem. Schaeffer and Shearer showed that the wave structure of the system 2.42 is distinguished by four different cases (I : $c < 0$, II : $0 < c < 1$, III : $1 < c < 2$, IV : $2 < c$). By comparing the 2×2 model system with the 5×5 MHD system, we can prove that (see Appendix A)

$$c = \gamma + 1, \quad u = \left(\frac{a}{c_a}\right)^2 - 1, \quad v = \frac{B_y}{B_x}, \quad w = \frac{B_z}{B_x} \tag{2.43}$$

The first condition implies that the topology of MHD wave structure is identical with that of wave structure of case IV in the Schaeffer's model.

We can derive another model system by considering the second and third equations of the system 2.41. Let's assume that u is balanced by the transverse fields through

$$u = \frac{1}{2}(v^2 + w^2). \tag{2.44}$$

But, notice that by this assumption u has always a positive value[4]. Then, the system reduces to

$$\begin{pmatrix} v \\ w \end{pmatrix}_t + \begin{pmatrix} (v^2+w^2)v \\ (v^2+w^2)w \end{pmatrix}_x = \begin{pmatrix} \eta & -\chi \\ \chi & \eta \end{pmatrix} \begin{pmatrix} v \\ w \end{pmatrix}_{xx}. \tag{2.45}$$

We call this system rotational 2×2 model. This is a rotationally degenerate system of conservation laws with the cubic flux function and is similar to the CKB system [63] which describes the interaction of an Alfvén wave and a magnetoacoustic wave. It also belongs to the Keyfitz-Kranzer model which has been studied as a model for elastic string [64] and for multi-phase flow [56].

[4]In 3×3 model, u can have any sign.

CHAPTER III

NON-STRICTLY HYPERBOLIC CONSERVATION LAW

Since Keyfitz and Kranzer studied a system of non-strictly hyperbolic conservation laws arising in elasticity theory [64], new mathematical phenomena of the interaction of nonlinear hyperbolic waves have been identified in various physical systems modeling phase transition, real materials, chemically reactive flow, oil reservoirs, and MHD [41, 42]. In particular, it is shown by recent studies (Shearer and Isaacson *et al.* [104, 105, 107, 53-55, 57]) that the presence of an umbilic point complicates solving the Riemann initial value problem. Such complexity is related to the fact that the associated nonlinear waves are non-convex, meaning that the well-developed wave theories based on the convexity break down. In other words, discontinuities that satisfy the Rankine-Hugoniot conditions can not always be associated with a particular characteristic family, out of whose simple waves the discontinuity can be supposed to have evolved. Therefore, the most critical issue for the construction of a weak solution to non-strictly hyperbolic conservation laws is which of these discontinuities are admissible. In case I of the planar 2×2 model system, that is, oil recovery problem, a global analysis of the associated dynamical systems is given by Gomes [46], showing that there are shocks (undercompressive) which have viscous

profiles but do not satisfy the Lax condition and which are needed to solve certain Riemann problems.

In this chapter, based on Gomes' work, we present the global analysis of the dynamic system of case IV which corresponds to the planar MHD dynamical system. In addition, the Riemann solution to the system is given in more clear manner and some recent mathematical theories for non-strictly hyperbolic conservation laws are summarized.

3.1 Nonlinear Resonance and the Failure of Genuine Nonlinearity

The planar 2×2 model system may be written as

$$\mathbf{u}_t + \mathbf{f}_x = \mu \mathbf{u}_{xx}, \tag{3.1}$$

where

$$\mathbf{u} = \begin{pmatrix} u \\ v \end{pmatrix}, \ \mathbf{f} = \begin{pmatrix} cu^2 + v^2 \\ 2uv \end{pmatrix}, \tag{3.2}$$

and it is assumed that $\mu = \eta$ and $2 < c$. The waves will be described as slow and fast; their speeds are given by

$$\lambda_{f,s} = (c+1)u \pm \sqrt{(c-1)^2 u^2 + 4v^2} \tag{3.3}$$

always satisfying $\lambda_s \leq \lambda_f$, and the right eigenvectors are

$$\mathbf{r}_{f,s} = \begin{vmatrix} \frac{1}{2}\lambda_{f,s} - u \\ v \end{vmatrix}. \tag{3.4}$$

When $u = v = 0$, all wave speeds vanish simultaneously and the eigenvectors are indeterminate even when normalized. Also, the rarefaction wave construction breaks down if the wave speeds λ_i have extreme values on integral curves of $\mathbf{r}$. This condition can be expressed in mathematical terms as $\nabla\lambda \cdot \mathbf{r} = 0$. In the planar 2×2 model with $2 < c$, it is satisfied on the $v = 0$ axis.

3.2 Rankine-Hugoniot Jump Conditions

Travelling shock wave solutions

$$\mathbf{u}(x,t) = \begin{cases} \mathbf{u}_L, & \text{if } x < st \\ \mathbf{u}_R, & \text{if } x > st \end{cases}$$

are characterized by the Hugoniot waves $[\mathbf{f}] = s[\mathbf{u}]$. For the 2×2 model system, they are

$$s\,[u] = 2c\bar{u}\,[u] + 2\bar{v}\,[v] \tag{3.5}$$

$$s\,[v] = 2\bar{v}\,[u] + 2\bar{u}\,[v] \tag{3.6}$$

where the overbars indicate arithmetic averages taken across the discontinuity and $[Q]$ denotes the jump of a quantity Q, that is, $(Q_R - Q_L)$. The Hugoniot locus is obtained by eliminating s; it is

$$\bar{v}\,[u]^2 + (1-c)\bar{u}\,[u][v] - \bar{v}\,[v]^2 = 0. \tag{3.7}$$

If the state on one side, say the left, is taken as given, then this equation is cubic in v_R, and quadratic in u_R. Because the equation is homogeneous, the shape of the curve depends only the ratio v_L/u_L. There is a horizontal asymptote at the value $v_{\max}/v_L = c/(c-2)$, and a loop that passes around the origin. The highest and lowest points on the Hugoniot are given by

$$v = \frac{v_L}{c-2} \pm \frac{c-1}{c-2}\sqrt{v_L^2 + (c-2)u_L^2}. \tag{3.8}$$

Fig. 3.1 displays the Hugoniot curves for five cases. In all our illustrations we have taken $c = 8/3$. These cases are chosen because there is an aspect of the curves that depends on where the state $\mathbf{u}_L$ lies with respect to the critical lines $v^2/u^2 = c$ on which one of the wavespeeds vanishes. This aspect is the way that the Hugoniot curve divides into sections corresponding to different types of discontinuity.

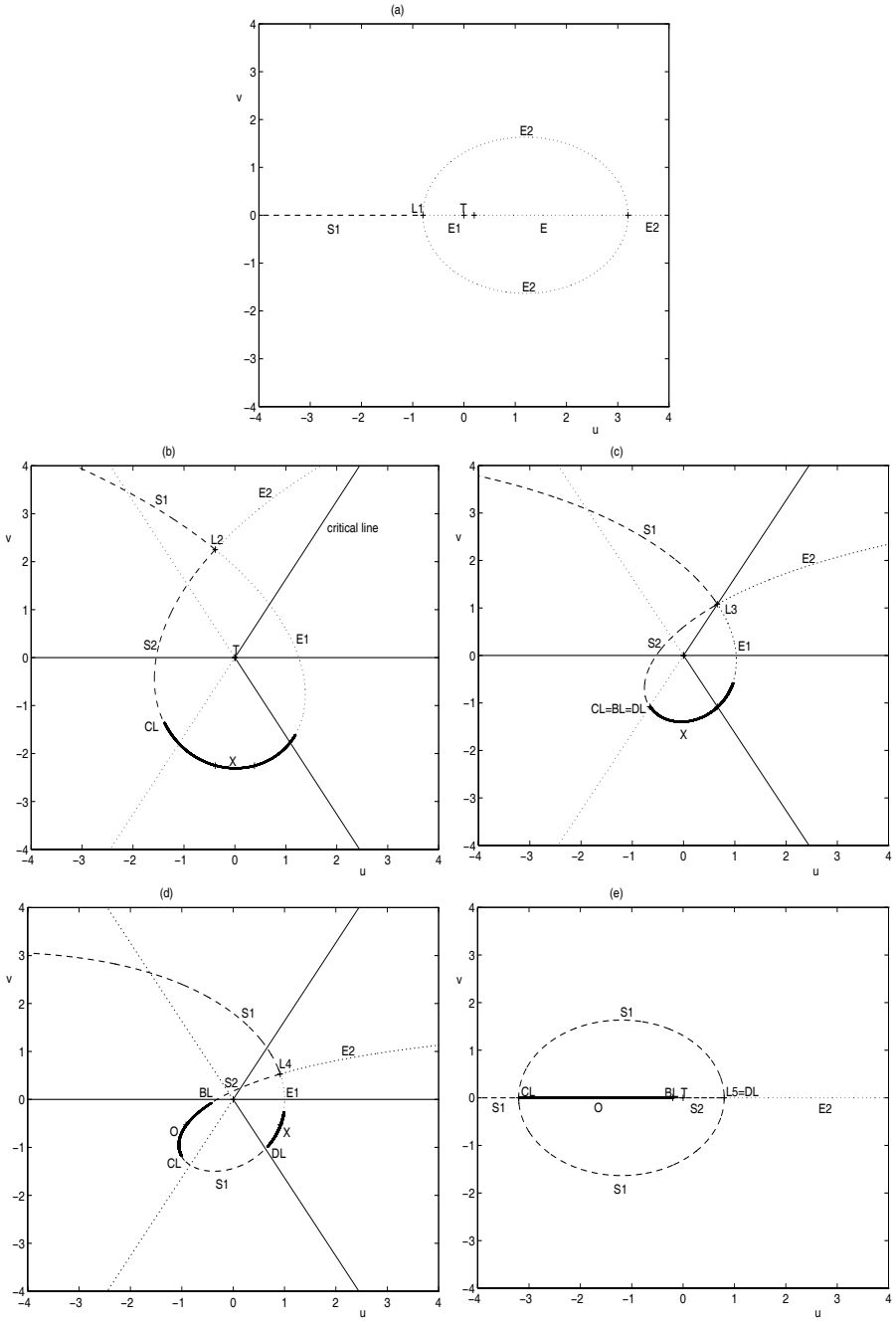

Figure 3.1: (a)-(e). Hugoniot loci and shock type: $S_1, S_2 - 1, 2$ regular, $E_1, E_2 - 1, 2$ expansive, E - expansive, O - overcompressive, X - undercompressive shocks. C_L, B_L, and D_L are critical points, which will be explained in Section 3.7.

3.3 Shock Types

In addition to the Rankine-Hugoniot jump conditions, supplementary conditions are needed to determine which jumps are physically admissible. Before considering such conditions, it is very useful to classify the discontinuities by how many characteristics enter them from each side. For a travelling shock, the signs of the following four parameters determine which of the slow, fast characteristics run into the shock:

$$P_1 = \lambda_f - s, \quad P_2 = s - \lambda_s, \quad P_3 = \lambda_{f\,L} - s, \quad P_4 = s - \lambda_{s\,L}. \tag{3.9}$$

There are sixteen possible sign distributions of discontinuities of these four parameters, but only nine can actually arise because the following relations must be satisfied.

$$c_s \leq c_f \quad \text{and} \quad c_{s\,L} \leq c_{f\,L}. \tag{3.10}$$

In Table 3.1 we classify nine types of shocks according to the signs of these parameters. 1,2 denote slow and fast waves. The relationship between the speed of a shock and characteristics in nine types of shocks is summarized in Fig. 3.2. The different types of shocks occurring in the planar 2×2 model system are illustrated in Fig. 3.1. The types are;

Regular shocks For just one of the families f, s it is true that the Lax condition

$$\lambda_R < s < \lambda_L, \tag{3.11}$$

holds, so that the shock arises from coalescing waves of that family. Shock jumps corresponding to slow waves are labelled S_1 in the diagrams, and jumps corresponding to fast waves are labelled S_2. These correspond to I→II or III→IV shocks in MHD. (See Section 5.2.)

Expansion shocks If the above inequality holds with signs reversed, the discontinuity is not evolutionary. These branches are labelled E, E_1, E_2.

Overcompressive shocks The above inequality is true for both families. This is a I→IV shock in MHD. It can be regarded as belonging to either family. It can be shown that the Hugoniot contains overcompressive shocks (labelled O) only if the left state lies in the region $|v_L/u_L| < \sqrt{c}$. Then a particular example (with $s = 0$) of an overcompressive shock is found by taking $u = -u_L, v = -v_L$.

Undercompressive shocks For these, we have

$$\lambda_{s,L} < s < \lambda_{f,L} \tag{3.12}$$

$$\lambda_{s,R} < s < \lambda_{f,R} \tag{3.13}$$

This is a II→III shock in MHD. It is also called *crossing shocks* since the fast and slow characteristics cross each other at the shock.

Hydrodynamic shocks There are cases corresponding to hydrodynamic shocks, that is, shocks along the axis $\overline{v} = [v] = 0$. Their speed is given by $s = 2c\bar{u}$, and represent evolutionary shocks if u decreases. They are overcompressive if

$$0 < u_L \quad \text{and} \quad \frac{c}{2-c}u_L < u < \frac{2-c}{c}u_L. \tag{3.14}$$

3.4 Integral Curves

From the right eigenvectors, the integral curves are defined by

$$\frac{dv}{du}\Big)_{f,s} = \frac{v}{\frac{1}{2}\lambda_{f,s} - u} \tag{3.15}$$

which are the paths taken in phase space, as the solution traverses a simple wave, have the general appearance shown in Fig. 3.3.

parameter\shock	$S1$	$E1$	$S2$	$E2$	O	E	X	Rt	Lt
P_1	+	+	−	+	−	+	+	+	−
P_2	+	−	+	+	+	−	+	−	+
P_3	+	+	+	−	+	−	+	+	−
P_4	−	+	+	+	−	+	+	−	+

Table 3.1: Types of shocks according to the sign of four parameters: $S_1, S_2 - 1, 2$ regular, $E_1, E_2 - 1, 2$ expansive, O, X - overcompressive, undercompressive, E - expansive, R_t, L_t - right, left transport shocks.

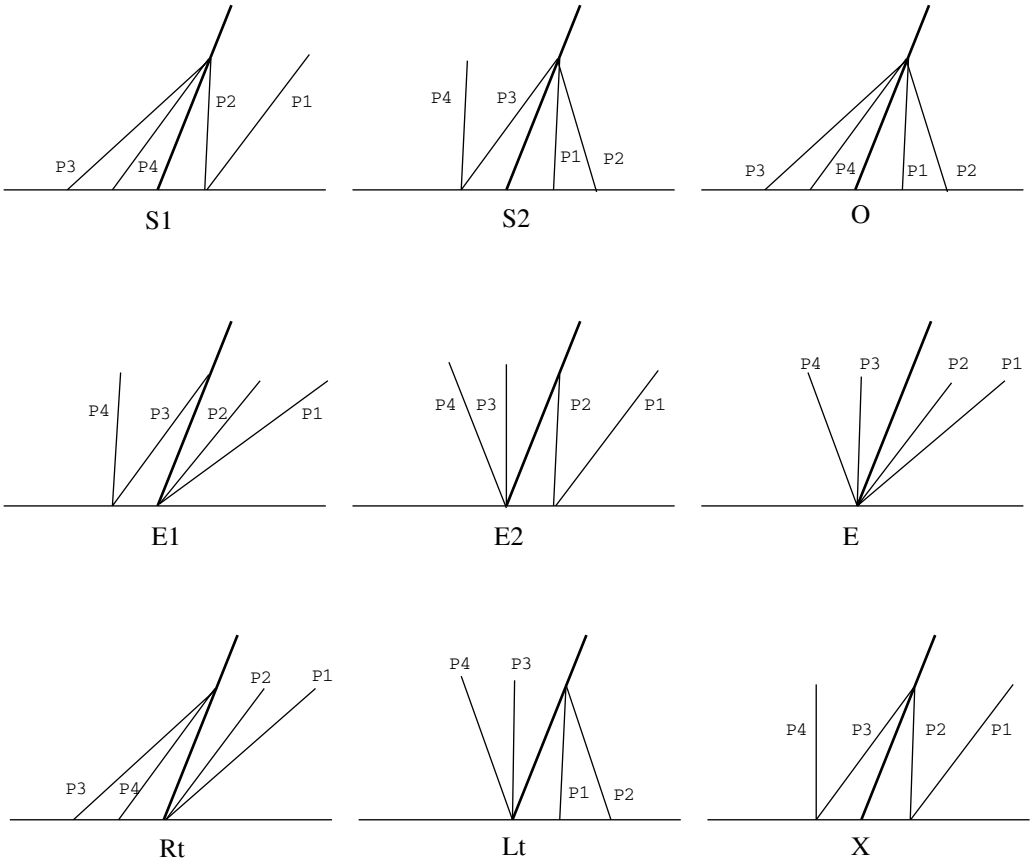

Figure 3.2: Shock classification according to the sign of four parameters in (x, t) space: $S_1, S_2 - 1, 2$ regular, $E_1, E_2 - 1, 2$ expansive, O, X - overcompressive, undercompressive, E - expansive, R_t, L_t - right, left transport shocks. The thick line represents a travelling shock, and the thin lines represent characteristics.

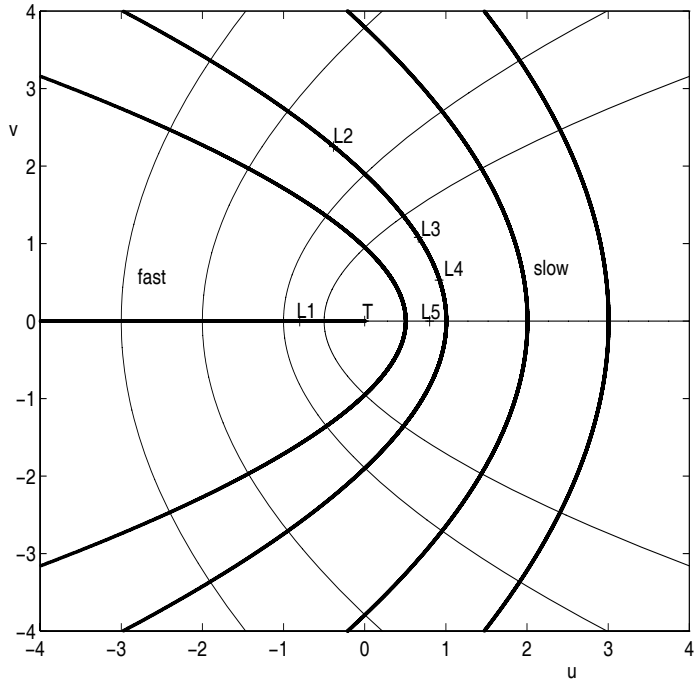

Figure 3.3: Integral curves. The thick lines indicate slow rarefaction waves, and the thin lines indicate fast rarefaction waves. T denotes the umbilic point and $L_{1,2,3,4,5}$ represent the five left states in the Hugoniot curves.

Invariants for integral curves can be calculated by introducing

$$u = r\cos\theta = \frac{2}{c-1}\, r'\cos\theta' \text{ and } v = r\sin\theta = r'\sin\theta'. \tag{3.16}$$

Then we have

$$\frac{r'^2(\cos\theta' \pm 1)^{\frac{c-1}{c-2}}}{\Big((3-c)\cos\theta' \pm (c-1)\Big)^{\frac{3-c}{c-2}}} = \text{const.} \tag{3.17}$$

with

$$\tan\theta = \frac{c-1}{2}\tan\theta' \text{ and } \frac{r^2}{r'^2} = \frac{4}{(c-1)^2}\cos^2\theta' + \sin^2\theta'. \tag{3.18}$$

Here $+, -$ denote fast wave and slow wave, respectively. For case IV, these integral curves are similar to the parabola. If the curves are followed from left to right in physical space in the direction of increasing u, the characteristics form diverging fans, and represent rarefaction waves.

Finally, we can show the non-convexity of waves of the model, which is illustrated in Fig. 3.4.

3.5 Conditions for Selecting Physically Admissible Shocks

In order to select physically admissible shocks, supplementary conditions are imposed on jumps. In gasdynamics, the entropy condition is regarded as such a condition. Although the condition works well in strict hyperbolic systems such as Euler equations, a simple extension of such condition to jumps that are not always associated with a particular characteristic family fails. In order to overcome this difficulty, several shock admissibility conditions have been proposed, but the exact relation between these conditions is a current research issue [34, 35, 65]. For the model system in which genuine nonlinearity fails and eigenvalues are not distinct everywhere, some admissibility criteria may be used to obtain well-posedness: geometric entropy condition (or Lax condition), entropy-flux criterion, viscosity admissibility criterion

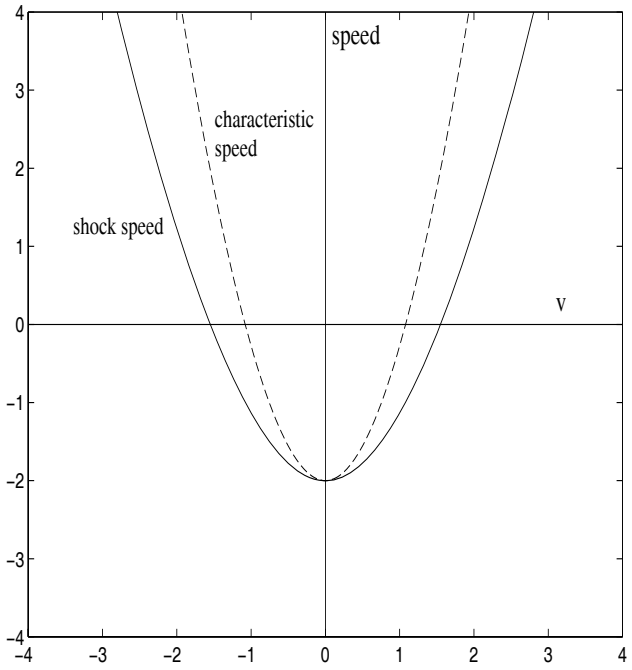

Figure 3.4: The shock speed and the characteristic speed as a function of v along a fast rarefaction wave with $u_L = -1,\ v_L = 0$.

[46], linearized stability [13], nonlinear stability, and asymptotic stability [76]. The first condition is based solely on the simple geometric interpretation, while the next two and three conditions are formulated as physical principles and self-contained analysis.

3.5.1 Geometric Condition

For $n \times n$ system, the Lax condition [68] is

$$\lambda_i(\mathbf{u}_R) \quad < \quad s \quad < \quad \lambda_i(\mathbf{u}_L) \tag{3.19}$$

for a shock of the i-family. For the 2×2 system, physically relevant shocks satisfy

$$\lambda_s(\mathbf{u}_R) \quad < \quad s \quad < \quad \lambda_s(\mathbf{u}_L) \quad \text{and} \quad s \quad < \lambda_f(\mathbf{u}_R) \tag{3.20}$$

$$\lambda_f(\mathbf{u}_R) \quad < \quad s \quad < \quad \lambda_f(\mathbf{u}_L) \quad \text{and} \quad s \quad > \lambda_s(\mathbf{u}_L). \tag{3.21}$$

For a scalar conservation law with convex flux function, it reduces to

$$\lambda(u_R) \quad < \quad s \quad < \quad \lambda(u_L). \tag{3.22}$$

3.5.2 Physical Conditions

The entropy-flux condition can be formulated as

$$\iint (e_t + h_x)\, dx\, dt \leq 0, \tag{3.23}$$

where e is a convex entropy function and h is the entropy flux.

The viscosity admissibility condition requires that admissible shocks satisfying the Rankine-Hugoniot conditions are those which can be approximated by the travelling wave solutions to the associated parabolic system. That is, a shock wave $x = st$ joining states $\mathbf{u}_L$ and $\mathbf{u}_R$ has a viscous profile if the system has a solution of the form

$$\mathbf{u} = \mathbf{u}(\xi \equiv (x - st)/\mu) \text{ satisfying } \mathbf{u}(\xi = -\infty) = \mathbf{u}_L \text{ and } \mathbf{u}(\xi = \infty) = \mathbf{u}_R. \tag{3.24}$$

Then we have the dynamical system that could be used to establish the existence of heteroclinic orbits.

3.5.3 Self-Contained Conditions

The linearized stability condition on a uniform shock is formulated as follows [58, 17]. Let us consider inviscid perturbation of a uniform shock

$$\mathbf{u}^o(x,t) = \begin{cases} \mathbf{u}^o_-, & \text{if } x < s_o t, \\ \\ \mathbf{u}^o_+, & \text{if } x > s_o t. \end{cases}$$

Across the shock the following jump relations must be satisfied.

$$\mathbf{f}(\mathbf{u}^o_+) - \mathbf{f}(\mathbf{u}^o_-) = s_o(\mathbf{u}^o_+ - \mathbf{u}^o_-). \tag{3.25}$$

Assuming that the shock is perturbed by small-amplitude waves impinging from both sides, we have the following perturbation data

$$\mathbf{u}_\pm(x,0) = \mathbf{u}^o_\pm(x) + \varepsilon \sum_{p=1}^{p_{in}} \mathbf{v}^p_\pm(x)\mathbf{r}^p_\pm, \quad \varepsilon \ll 1, \tag{3.26}$$

if we decompose the perturbed components in an eigenvector expansion. $\mathbf{r}^p_\pm$ denotes the right eigenvectors of $\mathbf{A}_\pm = \partial\mathbf{f}/\partial\mathbf{u}(\mathbf{u}^o_\pm)$, and $\mathbf{v}^p_\pm$ is the coefficient of $\mathbf{r}^p$ in an eigenvector expansion of the vector $\mathbf{u}(x,t)$. The initial perturbation leads to perturbation of the shock speed and the generation of outgoing waves from the shock.

Next, let us consider the linearized $n \times n$ system on each side of the shock,

$$\mathbf{u}_t + \mathbf{A}(\mathbf{u}_\pm)\mathbf{u}_x = 0. \tag{3.27}$$

The solution can be written as

$$\mathbf{u}_\pm(x,t) = \mathbf{u}^o_\pm + \varepsilon \sum_{p=1}^{n} \mathbf{v}^p_\pm(x - \lambda^p_\pm t, 0)\, \mathbf{r}^p_\pm, \tag{3.28}$$

where $\lambda^p_\pm$ are the characteristic speeds of the linear system in the frame of reference moving with the shock speed s_o. If we assume the shock weak, the perturbation

jump relations

$$\mathbf{f}(\mathbf{u}_+) - \mathbf{f}(\mathbf{u}_-) \;=\; (s_o + \varepsilon\tilde{s})(\mathbf{u}_+ - \mathbf{u}_-) \tag{3.29}$$

yield a linear system

$$\tilde{s}[\mathbf{u}^o] + \sum_{p=1}^{p_{out}} \lambda_\pm^p \mathbf{v}_\pm^p(x - \lambda_\pm^p t, 0)\,\mathbf{r}_\pm^p \;=\; \sum_{p=1}^{p_{in}} \lambda_\pm^p \mathbf{v}_\pm^p(x - \lambda_\pm^p t, 0)\,\mathbf{r}_\pm^p \tag{3.30}$$

for the unknowns $p_{out} + 1$ when incoming distributions are given. Hence the system has a non-trivial solution only if (1) $p_{out} = n - 1$ (2) the vectors $\mathbf{r}_{out}^p$ and $[\mathbf{u}^o]$ are linearly independent. Since there are $2n$ waves present $p_{in} = n - 1$ and two waves get *lost* in the shock. If these are waves of the same family then this is the Lax condition.

Also, the nonlinear stability condition can be formulated from the linearized stability condition by relaxing the weakness of perturbation, becoming a nonlinear existence problem that the perturbed data lead to a unique classical solution to the quasilinear problem on each side of the shock.

Finally, the asymptotic stability condition is related to the question, whether the discontinuity evolves from smooth data approximating a uniform shock.

If eigenvalue is a real, simple, genuinely nonlinear characteristic value at $\mathbf{u}_L$, all these conditions are known to be equivalent to the Lax condition for sufficiently small amplitude shocks. Especially, for a system whose characteristic speeds are all real, distinct, and depend monotonically on the corresponding characteristic variables, the geometric condition and the linear stability condition work well. However, for the 2×2 model system where these non-degeneracy conditions fail, such simple conditions turn out to be inappropriate.

For some non-classical shock types, the system 3.30 becomes insolvable [17].

A. The system has more unknowns than given equations, and thus there are infinitely many solutions possible. For the general quadratic 2×2 system, X, R_t, L_t are such shocks. (Expansive shocks are also such shocks, but they are obviously inadmissible.) For the 2×2 model system, such insolvability is found only in undercompressive shocks.

B. The system is overdetermined and thus it does not have a solution. Overcompressive shocks are such shocks. All characteristics run into the shock.

C. The system is invalid when waves move with the shock speed, and thus it can not be characterized as the incoming or the outgoing. Such cases can be found in compound waves, which will be explained later.

D. The matrix of the system becomes singular, which means large amplitude of the outgoing waves. For example, in the 3×3 model system, the evolution of w is governed by $w_t + (2uw)_x = 0$ and its jump relation for the small perturbation $\tilde{w}$ becomes

$$2\tilde{w}_+(u_+ + \tilde{u}_+) - 2\tilde{w}_-(u_- + \tilde{u}_-) = (s_o + \tilde{s})(\tilde{w}_+ - \tilde{w}_-). \tag{3.31}$$

The linearization yields

$$\tilde{w}_- = \tilde{w}_+ \frac{(2u_+ - s_o)}{(2u_- - s_o)}, \tag{3.32}$$

and then the amplitude of the outgoing wave tends to infinity as v approaches zero.

In conclusion, the linearized stability condition and the geometric condition fail for the scalar equation with non-convex flux function and for the system in which the associated waves are not convex, because they are based on the characteristic

speeds only at the end states. It is expected that nonlinear stability condition will give the correct result only if the perturbations are large enough.

3.6 Dynamical System

The failure of admissibility criteria based on the linear theory for non-strictly hyperbolic systems implies that a geometric consideration alone can not make the Riemann problem well-posed and thus there exist some missing physical effects. The most obvious one is the viscosity, so that the viscosity admissibility condition is considered to overcome the limitation of geometric approaches. It is based on the analysis of a dynamical system which is the essential tool for selecting shocks which admit a viscous profile. The dynamical system is determined by travelling wave solutions to the associated viscosity equation. Some important theorems of the dynamical system are summarized in Appendix B. The dynamical system of the planar problem 3.1 can be written as

$$u_\xi = f(\mathbf{u}) - f(\mathbf{u}_L) - s(u - u_L) \equiv \Theta(\mathbf{u}), \tag{3.33}$$

$$v_\xi = g(\mathbf{u}) - g(\mathbf{u}_L) - s(v - v_L) \equiv \Phi(\mathbf{u}), \tag{3.34}$$

where

$$\mathbf{f} = (f, g) = (cu^2 + v^2, 2uv), \tag{3.35}$$

and $2 < c$. In order to analyze this dynamical system, let us examine first singularities which will be determined by solving $\Theta = 0$ and $\Phi = 0$ for given s and $\mathbf{u}_L$. The reason for this is that we are interested only in profiles connecting singularities.

In general, singularities on the finite domain are the intersection of two curves (ellipse and hyperbola) defined by $\Theta = \Phi = 0$. In our case, we can observe two, three, and four singularities. Three singularities occur in a degenerate case. However, there

is a special case in which $\mathbf{u}_L$ is the umbilic point, so that eigenvalues become equal. In this case, singularities can be attained by considering the Hugoniot locus 3.7 at the umbilic point ($u_L = v_L = 0$), which is

$$v = 0. \tag{3.36}$$

Hence there are two singularities at infinity independent of s. These singularities can be revealed by the Poincaré transform.

Following the method given in the theorem 2.2 of Ref. [46] or summarized in Appendix B, the Jacobian matrix of the vector field (Θ, Φ) evaluated at singularities, which can be obtained by applying the Poincaré transformation $u = 1/z$ and $v = y/z$ to the vector field, is

$$\begin{pmatrix} \Gamma'(\alpha) & 0 \\ 0 & \Gamma(\alpha) \end{pmatrix}, \tag{3.37}$$

where

$$\Gamma'(y) = -f(1,y) - yf'(1,y) + g'(1,y), \tag{3.38}$$

$$\Gamma(y) = -f(1,y), \tag{3.39}$$

and $\alpha = 0$ for $2 < c$. Here $\alpha = 0$ corresponds to the $v = 0$ condition. For $c < 2$, α has three values $\alpha = \pm\sqrt{2-c}, 0$, which can be calculated from

$$\alpha f(1,\alpha) - g(1,\alpha) = 0. \tag{3.40}$$

Note that α is the slope of the Hugoniot through the umbilic point and is equal to y since singularities at infinity $(y, z = 0)$, if existent, satisfy Eq. 3.40. To determine the type of singularities at infinity, we consider the sign of $\Gamma(\alpha)\Gamma'(\alpha)$. At $y = 0$, we have

$$\Gamma'(y)(= 2 - c - 3y^2) = 2 - c, \tag{3.41}$$

$$\Gamma(y)(= -y^2 - c) = -c. \tag{3.42}$$

This indicates that singularities at infinity are two nodes for $2 < c$ (including an antipodal point of the Poincaré sphere).

Once we find singularities, we can determine their type using the index theory, without resolving orbits in detail. An important result of the index theory is the Poincaré index theorem, which shows that the sum of indices of singularities on a two-dimensional surface is 2. (See Appendix B.) In four singularities in the finite domain, the index theorem yields $2N - 2S + 2 = 2,\ N + S = 4$. Then, we obtain two nodes and two saddles as singularities in the finite domain. Similarly, we can find a node and a saddle for two singularities. In case of three singularities, we have one saddle, one node and non-hyperbolic saddle-node in which the index is zero. The global phase portraits are given in Fig. 3.5 (a-c). It is shown that all regular shocks and overcompressive shocks have viscous profiles since there are saddle-node and node-node connections, but undercompressive shocks do not have viscous profiles since there is no saddle-saddle connection.

3.7 Compound Waves

In Section 3.5, it was noted that rarefaction waves can move with the shock and in that case the linearized theory fails. Here, we introduce *compound waves*, also known as *composite waves*, as substitutes for undercompressive shocks which are inadmissible by the viscous admissibility condition. Historically, these waves are identified in a model for multi-phase flow in a porous medium [9]. In MHD, they are first identified by Wu [125] from the numerical solutions to the full MHD[1].

[1]Interestingly, MHD slow compound waves were discovered in an experimental observation performed by Patrick and James. "The experimental observations show that the density ratio across the shock wave does drop rather sharply, which is, we think, some confirmation of the characteristic theory and the fact that the expansion has actually caught up with the shock front." [22, pages

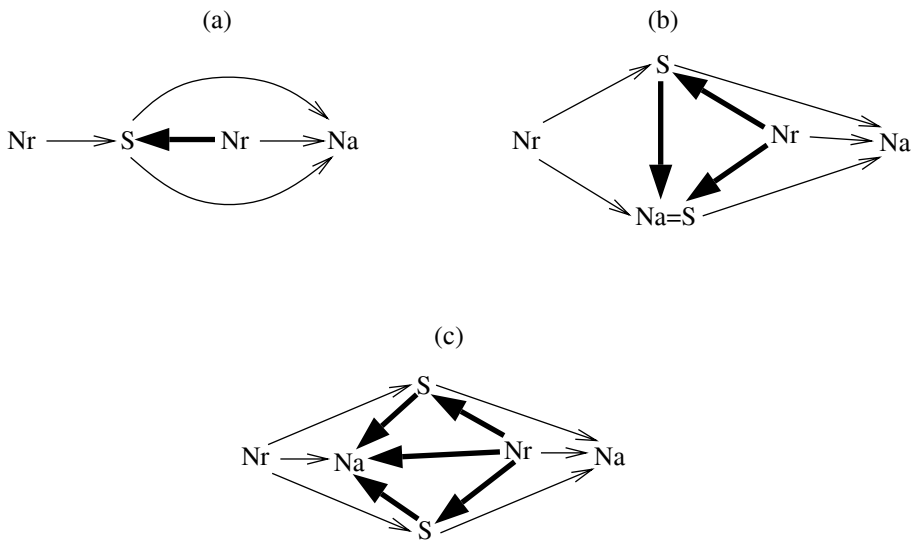

Figure 3.5: (a)-(c). Examples of the global phase portrait of the planar model problem. Nr, Na, S denote repelling node, attracting node and saddle, respectively.

Here, the simplest of this kind of models will be considered in order to show how compound waves are constructed.

$$u_t + (u^3)_x = 0. \tag{3.43}$$

The characteristic speed for this model $\lambda = 3u^2$ which is parabola-like about $u = 0$. For the Riemann problem with the initial data $u_R = -u_L, 0 < u_L$, the solution can be obtained by constructing the convex hull [72], that is, the smallest convex set, which is illustrated in Fig. 3.6. At u^*, $s^* = \Big(f(u^*) - f(u_L)\Big)/(u^* - u_L)$ is identical with $f'(u^*)$, which means the shock moves as the same speed as the adjacent characteristics.

For the planar 2×2 model, they consist of waves of one family (slow and fast) and are of three types, shown in Fig. 3.7. There exist critical points in the Hugoniot curves that are very helpful for identifying compound waves. The critical point C_L is defined as the point where the Hugoniot locus is tangent to a fast integral curve,

205-206].

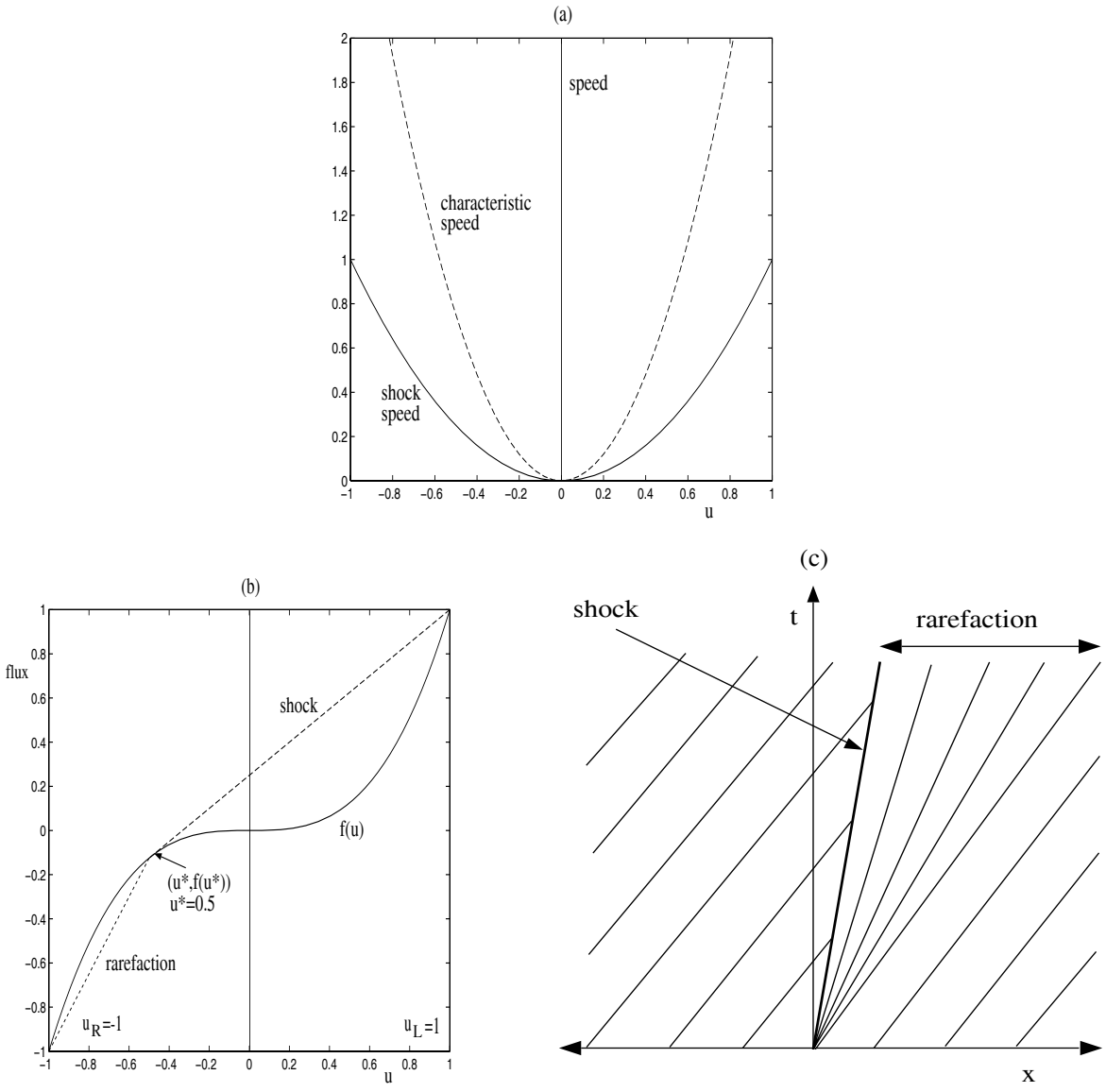

Figure 3.6: (a)-(c). (a) The shock speed and the characteristic speed for $u_L = 0$. Compare with Fig. 3.4. (b) The convex hull construction. (c) Compound wave.

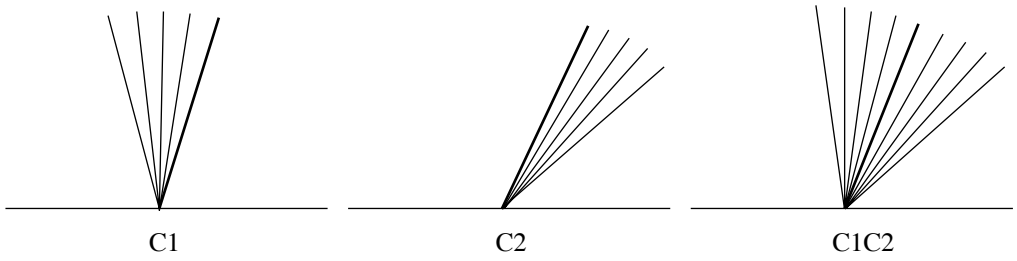

Figure 3.7: Compound waves in (x,t) space: $C_1, C_2 - 1,2$ compound, C_1C_2- transitional waves. The shock is shown by the thick line, while characteristics are shown by the thin lines.

which satisfies

$$\lambda_f(\mathbf{u}) - s(\mathbf{u}_L, \mathbf{u}) = 0. \tag{3.44}$$

Similarly, B_L, D_L can be defined as points satisfying

$$\lambda_s(\mathbf{u}_L) - s(\mathbf{u}_L, \mathbf{u}) = 0. \tag{3.45}$$

Therefore, a slow compound wave C_1 can be defined as a rarefaction wave followed by a slow shock, consisting of a slow rarefaction wave and a jump to the point D_L. Similarly, a fast compound wave C_2 can be defined as a rarefaction wave followed by a fast shock, consisting of a jump to the point C_L and a fast rarefaction wave. For special left states at which C_L and D_L coincide, as found in Fig. 3.1 (c), there is a possibility of a slow rarefaction followed by a shock to a fast rarefaction. This is an example of the *transitional wave* [56].

3.8 Solution of the Riemann Problem for the Planar Model

We study the Riemann problem for the planar 2×2 model:

$$\mathbf{u}_t + \mathbf{f}_x = 0, \tag{3.46}$$

$$\mathbf{u}(x, t=0) = \begin{cases} \mathbf{u}_L, & x \le 0, \\ \mathbf{u}_R, & x > 0. \end{cases}$$

The wave curve for a given state $\mathbf{u}_L$ is defined as the set of all states that can be connected to $\mathbf{u}_L$ by a single, physically relevant wave. In a sense, it is the union of the integral curves and the Hugoniot curves. However, we eliminate from the integral curves those branches that imply a steepening of the characteristics. Likewise, we eliminate from the Hugoniot curves those branches that would imply characteristic divergence.

Close to $\mathbf{u}_L$, this is straightforward. In Fig. 3.8 (a-e), we take $\mathbf{u}_L$ to be the points $L_{1,2,3,4,5}$, and we see departing from these points the slow (S_1) and fast (S_2) shock curves, along which u and λ both decrease, together with the slow (R_1) and fast (R_2)rarefaction curves, along which u and λ increase. We should also eliminate from the Hugoniot curves those shocks that are undercompressive, since these turn out to have unstable viscous profiles, and it needs to be noted that this branch includes the special point $u = u_L,\ v = -v_L$ corresponding to the Alfvén wave that rotates the transverse field through an angle π.

Finally, we need to add those states that can be reached through compound waves. These involve shocks that are on the border between regular and undercompressive shocks. This occurs when

$$s(\mathbf{u}_L, \mathbf{u}_R) = \lambda_1(\mathbf{u}_L), \ \text{ slow waves}, \qquad s(\mathbf{u}_L, \mathbf{u}_R) = \lambda_2(\mathbf{u}_R) \ \text{ fast waves}.$$

Such shocks can be contiguous with rarefaction waves of the same family. The curve C_1 is defined by taking an arbitrary point $\mathbf{u}_M$ on R_1, and then finding the unique point $\mathbf{u}_N$ on the Hugoniot of $\mathbf{u_M}$ such that $s(\mathbf{u}_M, \mathbf{u}_N) = \lambda_1(\mathbf{u}_M)$. The curve C_2 is defined by finding the unique point $\mathbf{u}_K$ on the Hugoniot of $\mathbf{u}_L$ such that $s(\mathbf{u}_L, \mathbf{u}_K) = \lambda_2(\mathbf{u}_K)$ and then continuing the R_2 curve from $\mathbf{u}_K$.

To solve the Riemann problem, take $\mathbf{u}_L$ to be fixed, and let $\mathbf{u}_R$ range over the

phase space. Whenever $\mathbf{u}_R$ happens to lie on some branch of the wave curve for $\mathbf{u}_L$ the Riemann solution is simply the single wave indicated. That branch is therefore a boundary across which the other wave changes sign. Thus, the regions either side of the S_1 wave curve correspond to wave patterns S_1R_1 or S_1S_2 and are so labelled. In Fig. 3.9, exact solution of the full coplanar Riemann problem, we denote these boundaries by continuous lines.

On a second type of boundary one of the waves does not vanish, but changes character. This occurs when a compound wave becomes either a regular shock or else a pure rarefaction. We denote these boundaries with dashed lines.

Finally, the O branch of the Hugoniot is a third kind of boundary, appearing in the middle of the S_1S_2 region. It corresponds to a limiting case in which the two shocks are parallel to each other, and merge to form a single overcompressive shock. It is shown, when it occurs, with a dotted line. Note that these waves required to solve the Riemann problem are precisely those admitted under the viscosity criterion.

Even though only two unknowns are involved, the reasoning involved in constructing the Riemann solution is intricate and not easy to formalize. Although we have independently verified the results in Refs. [104, 53], our 'method' consisted mostly of staring hard enough at the diagrams to become convinced that no case had been overlooked. We were, however, aided in doing this by the fact that for the model problem several theorems and analytical results are available.

3.9 Fundamental Wave Manifolds

In the previous section we showed how the solutions to the Riemann problem are constructed. With the help of the complicated diagrams, we can construct the global solutions to the Riemann problem. However, it is also possible to develop a

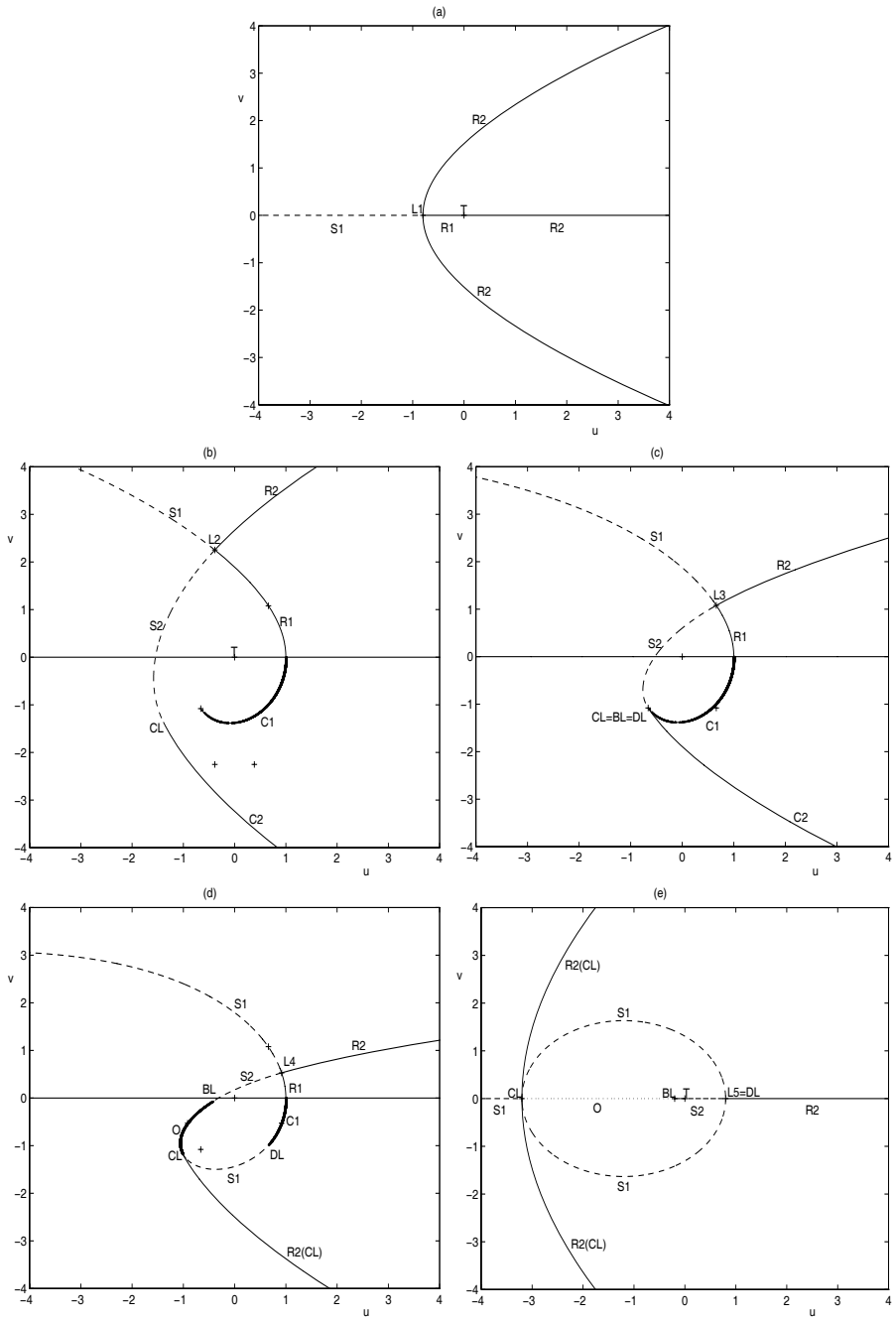

Figure 3.8: (a)-(e). Wave curves. $R_2(C_L)$ denotes a fast rarefaction wave curve originating from the point C_L.

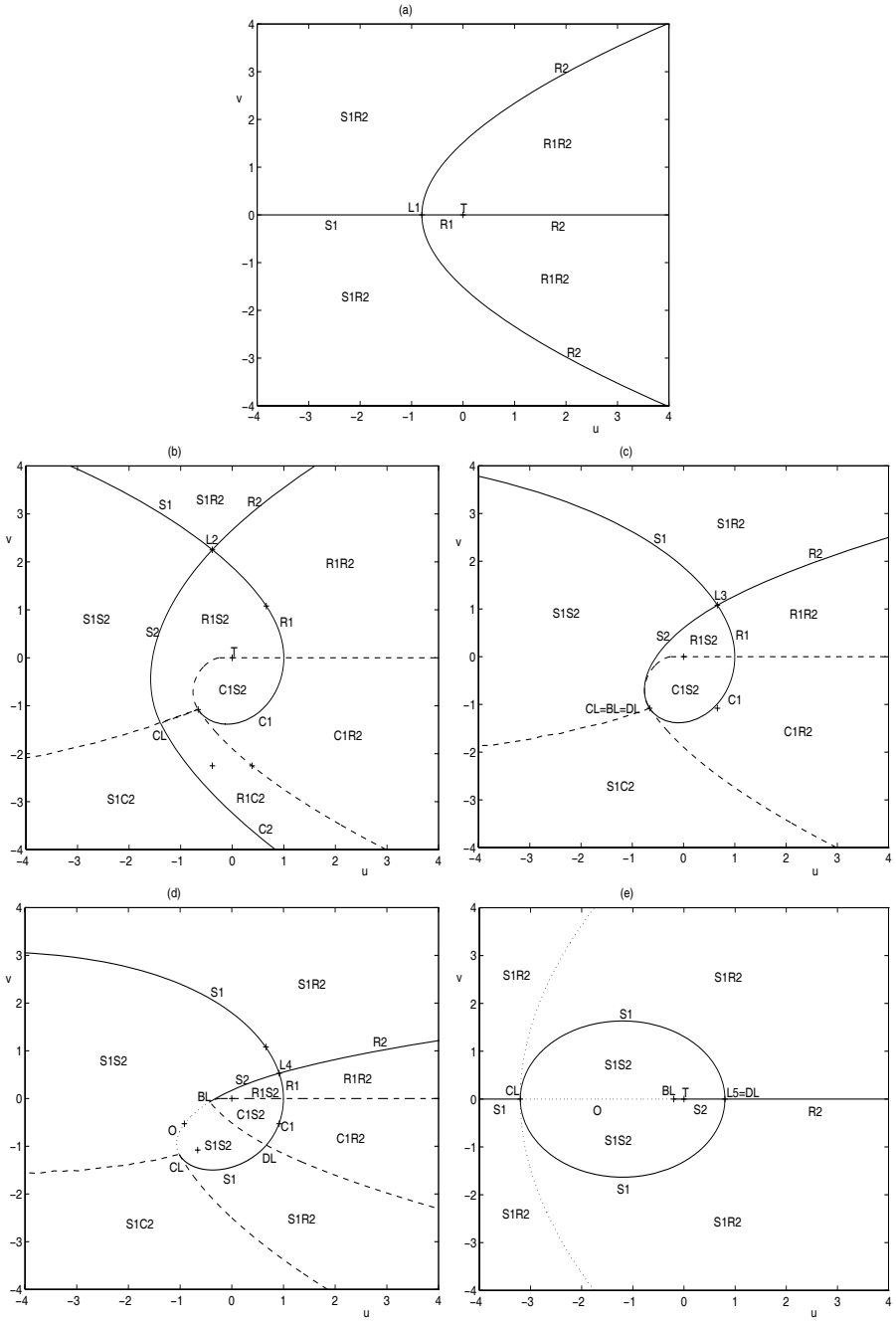

Figure 3.9: (a)-(e). Exact solution of Riemann problem: solid line - boundary line across which one wave is zero, dashed line - one wave changes character, dot line - two waves coincide.

simple geometric framework which incorporates all the elementary waves in a single space[2]. Such framework becomes more important in non-strictly hyperbolic systems (where the nonlinear coupling in linearized modes leads to non-classical shocks) than in strict hyperbolic systems (where solutions are obtained by traversing the wave curves, which are one-parameter families of solutions associated with a particular mode). Isaacson *et al.* [57] introduced such framework based on the *fundamental wave manifold*, which consists of a distinguished n-dimensional submanifold containing a single one-dimensional foliation that represents the rarefaction curves for all families, and a foliation that represents shock waves.

A reason for introducing the fundamental wave manifold is that it provides a natural setting for the study of two fundamental problems on the theory of conservation laws: the physical admissibility of shock waves and the bifurcation of wave curves. It can parameterize the dynamical systems associated to shock waves. It can also describe the wave curve bifurcation, in other words, how solutions of Riemann problems depend on the initial data, $\mathbf{u}_L$ and $\mathbf{u}_R$. But, in this study, we apply this concept to the planar 2×2 model only for the purpose of extracting a geometric information on Rankine-Hugoniot relations.

The key idea of their construction is a reformulation of the Rankine-Hugoniot conditions by introducing a blow-up procedure. They noticed that three variables $(\mathbf{u}_L, \mathbf{u}_R, s)$ satisfying the Rankine-Hugoniot conditions are of three types: (1) solutions with $\mathbf{u}_R \neq \mathbf{u}_L$, representing shock waves (2) limits, as $|\mathbf{u}_R - \mathbf{u}_L| \to 0$, of shock wave solutions, which represent rarefaction waves; for these solutions, s is an eigenvalue of the $\mathbf{f}'(\bar{\mathbf{u}})$ at $\bar{\mathbf{u}} = \mathbf{u}_R = \mathbf{u}_L$ (3) solutions with $\mathbf{u}_R = \mathbf{u}_L$ and other values of s, which represent constant states in solutions of Riemann problems. Then, they

[2] The idea is in common with an argument by Kaku [59, page 12]. "The laws of nature become simpler and elegant when expressed in higher dimension."

introduced R and $\mathbf{r}(\phi) = (\cos\phi, \sin\phi)$ such that $[\mathbf{u}] = R\mathbf{r}(\phi)$. By doing this, they develop a single manifold which represents both rarefaction waves and shocks. In this framework, the idea that shock waves with infinitesimal strength are infinitesimal rarefaction fans is successfully implemented. That is, the Rankine-Hugoniot conditions can be written as

$$-s[\mathbf{u}] + \mathbf{f}(\mathbf{u}_R) - \mathbf{f}(\mathbf{u}_L) \quad = \quad R \cdot \mathcal{H}(\bar{\mathbf{u}}, R, \phi, s) \tag{3.47}$$

for $R \neq 0$. For $R = 0$, noting that $\mathbf{f}(\mathbf{u}_R) - \mathbf{f}(\mathbf{u}_L) = R \cdot \mathbf{A}(\bar{\mathbf{u}}, R, \phi)\mathbf{r}(\phi)$ where

$$\mathbf{A}(\bar{\mathbf{u}}, R, \phi)\mathbf{r}(\phi) = \int_{-\frac{1}{2}}^{\frac{1}{2}} \mathbf{f}'(\bar{\mathbf{u}} + \alpha R\mathbf{r}(\phi))\, d\alpha \quad \text{and} \quad \mathbf{A}(\bar{\mathbf{u}}, 0, \phi)\mathbf{r}(\phi) = \mathbf{f}'(\bar{\mathbf{u}})\mathbf{r}(\phi), \tag{3.48}$$

we have

$$\mathcal{H}(\bar{\mathbf{u}}, 0, \phi, s) \quad = \quad [-s + \mathbf{f}'(\bar{\mathbf{u}})]\mathbf{r}(\phi). \tag{3.49}$$

(For the quadratic model, $\mathbf{A}(\bar{\mathbf{u}}, R, \phi) = \mathbf{f}'(\bar{\mathbf{u}})$.) When this derivation is applied to the 2×2 model system, the Hugoniot function becomes, for given $\mathbf{u}_L$,

$$\mathcal{H}(u, v) \quad = \quad R^2\Big(\frac{1}{2}R(\alpha(\phi)\cos\phi + \beta(\phi)\sin\phi) + \alpha(\phi)u_L + \beta(\phi)v_L\Big), \tag{3.50}$$

$$s \quad = \quad \frac{1}{2}R(\tilde{\alpha}(\phi)\cos\phi + \tilde{\beta}(\phi)\sin\phi) + \tilde{\alpha}(\phi)u_L + \tilde{\beta}(\phi)v_L, \tag{3.51}$$

where

$$\alpha(\phi) = (1-c)\sin 2\phi, \quad \beta(\phi) = 2\cos 2\phi, \tag{3.52}$$

$$\tilde{\alpha}(\phi) = (c-1)\cos 2\phi + c + 1, \quad \tilde{\beta}(\phi) = 2\sin 2\phi. \tag{3.53}$$

By putting $R = 0$, we have the following relations for characteristics

$$\mathcal{F}(u, v, \phi) \quad = \quad \alpha(\phi)u + \beta(\phi)v, \tag{3.54}$$

$$\lambda(u, v, \phi) \quad = \quad \tilde{\alpha}(\phi)u + \tilde{\beta}(\phi)v. \tag{3.55}$$

Then any solution (u, v) of $\mathcal{F}(u, v, \phi) = 0$ takes the form

$$u = -\beta(\phi) \cdot \kappa, \quad v = \alpha(\phi) \cdot \kappa \tag{3.56}$$

for some real κ. The equation defining integral curves is

$$-\sin\phi du + \cos\phi dv = 0, \tag{3.57}$$

$$(\alpha\cos\phi + \beta\sin\phi)d\kappa + (\alpha_\phi\cos\phi + \beta_\phi\sin\phi)\cdot\kappa d\phi = 0. \tag{3.58}$$

Thus integral curves may be obtained locally by solving

$$\dot{\phi} = -(\alpha\cos\phi + \beta\sin\phi), \tag{3.59}$$

$$\dot{\kappa} = (\alpha_\phi\cos\phi + \beta_\phi\sin\phi)\kappa. \tag{3.60}$$

They can be written as a first-order ordinary differential equation.

$$\frac{d\kappa}{\kappa} = -\frac{\alpha_\phi\cos\phi + \beta_\phi\sin\phi}{\alpha\cos\phi + \beta\sin\phi}d\phi. \tag{3.61}$$

The solution is

$$\kappa = \kappa_L\Big(\frac{\sin^2\phi_L}{\sin^2\phi}\Big)^{\frac{c-1}{2(c-2)}}\Big(\frac{(3-c)\cos^2\phi - 1}{(3-c)\cos^2\phi_L - 1}\Big)^{\frac{3-c}{2(c-2)}}. \tag{3.62}$$

On the other hand, $\mathcal{H}(u, v) = 0$ gives

$$R = -2\frac{\alpha u_L + \beta v_L}{\alpha\cos\phi + \beta\sin\phi}, \tag{3.63}$$

$$s = \cos\phi\Big(R(c\cos^2\phi + \sin^2\phi) + 2(c\cos\phi u_L + \sin\phi v_L)\Big) \tag{3.64}$$

$$+2\sin\phi\Big(R\cos\phi\sin\phi + (u_L\sin\phi + v_L\cos\phi)\Big). \tag{3.65}$$

Here, ϕ satisfying $\alpha\cos\phi + \beta\sin\phi = 0$ is called *asymptotic angle* where the genuine nonlinearity breaks down and ϕ satisfying $\alpha u_L + \beta v_L = 0$ is called *characteristic angle*.

CHAPTER IV

PLANAR MHD RIEMANN PROBLEM

In the previous chapter, by considering a planar model system, we showed that the simple geometric condition and linearized theory are inappropriate for conditions for selecting admissible shocks of non-strictly hyperbolic conservation laws, while the viscosity admissibility condition works well for such system. As a result, non-classical shocks are needed to ensure the uniqueness and existence of the weak solutions to the planar 2×2 model. In this chapter, by observing that MHD shocks are determined on a domain essentially consisting of the transverse magnetic field and the pressure (which makes it possible to apply the theory of the planar 2×2 model system to the problem of the 5×5 planar MHD system), we present MHD Rankine-Hugoniot conditions and simple wave relations in a useful form, and construct the weak solutions to the planar Riemann problem in MHD [87].

Most of the results are new and their ultimate contribution is the proof of well-posedness of the planar MHD Riemann problem. In other words, with mathematical rigor, we prove the validity of the MHD approximation in the limit of vanishing dissipations.

4.1 MHD Rankine-Hugoniot Conditions

From the ideal MHD equations in the Lagrangian description given in Section 2.4, the MHD shock relations are expressed as follows.

$$
\begin{aligned}
m[\tau] - [u] &= 0, && (4.1)\\
m[u] + [p] + \bar{B_\perp}[B_\perp] &= 0, && (4.2)\\
m[v] - B_x[B_\perp] &= 0, && (4.3)\\
m\bar{\tau}[B_\perp] + \bar{B_\perp}[u] - B_x[v] &= 0, && (4.4)\\
m[e_t] + [(p + \frac{{B_\perp}^2}{2})u - B_x B_\perp v] &= 0, && (4.5)
\end{aligned}
$$

where m is defined by $\tau m = u - s$ and s is the shock speed. Subscripts L, R denote the left state and the right state. *Here the left state and the right state represent properties behind the wave, and ahead of the wave, respectively.* Notice that we use the Lagrangian MHD equations of variables $(\tau, u, v, B_\perp, p)$. The reason is that the midpoint rule $[\mathbf{f}] = A(\bar{\mathbf{u}})[\mathbf{u}]$ is satisfied in the Lagrangian equations, but in the Eulerian equations there exists no unique average. By combining Eqs. 4.1 $\sim$ 4.5, Eq. 4.5 can be replaced by

$$
[\frac{\tau p}{\gamma - 1} + \tau\bar{p}] + \frac{1}{4}[\tau][B_\perp]^2 = 0, \qquad (4.6)
$$

which is the generalized Rankine-Hugoniot relation given first by Lüst [77]. Notice that the case $m = 0$ for non-zero B_x represents the contact discontinuity across which there is only the density jump. Thus we can assume m non-zero for shocks. Eliminating $[v]$ and m, we may obtain the Hugoniot relation for the pressure and the transverse magnetic field.

$$
\frac{\gamma - 1}{4}\bar{B_\perp}[B_\perp]^4 + \frac{\gamma - 1}{4}[p][B_\perp]^3 + \gamma\bar{p}\bar{B_\perp}[B_\perp]^2
$$

$$+(\gamma\bar{p} - {B_x}^2 - \bar{B_\perp}^2)[p][B_\perp] - \bar{B_\perp}[p]^2 \;\; = \;\; 0. \tag{4.7}$$

We believe this equation to be new. It can be factored as

$${p_L}^2(\frac{\gamma-1}{2}[B_\perp] - B_{\perp L})(Y - Y_1)(Y - Y_2) \;\; = \;\; 0, \tag{4.8}$$

where $Y = [p]/p_L$ and Y_1, Y_2 are solutions given first by Bazer and Ericson [8]. In their notation,

$$Y_{1,2} \;\; = \;\; \frac{\gamma}{s_L}\Big(-\frac{h^2}{2} + h\big(\frac{\frac{\gamma}{2}h\sin\theta_L - 1 + s_L \pm \sqrt{R}}{2\sin\theta_L - (\gamma-1)h}\big)\Big), \tag{4.9}$$

where $h, s_L, \sin\theta_L, R$ are defined by

$$h = \frac{[B_\perp]}{\sqrt{{B_x}^2 + {B_{\perp L}}^2}}, \;\; s_L = \frac{\gamma p_L}{({B_x}^2 + {B_{\perp L}}^2)}, \;\; \sin\theta_L = \frac{B_{\perp L}}{\sqrt{{B_x}^2 + {B_{\perp L}}^2}},$$

$$R = h^2(\frac{\gamma^2}{4}\sin^2\theta_L - \gamma + 1) + h\sin\theta_L(2-\gamma)(1+s_L) + 4s_L \;\sin^2\theta_L + (1-s_L)^2.$$

Even though Eq. 4.9, which treats the left state as a reference, has been the usual basis for MHD shock calculations since the late fifties, Eq. 4.7 which treats the left and right states symmetrically is also useful in the sense that it reveals more information on the Hugoniot, for example, asymptotic property, limiting shocks with zero pressure, and can be readily extended to give the complete solution. For example, given $B_{\perp L,R}$ and $p_{L,R}$ satisfying Eq. 4.7, we can derive from Eq. 4.6 the density ratio

$$\Omega \equiv \frac{\tau}{\tau_L} \;\; = \;\; \frac{2(\gamma\bar{p} + \frac{\gamma-1}{4}[B_\perp]^2) - [p]}{2(\gamma\bar{p} + \frac{\gamma-1}{4}[B_\perp]^2) + [p]}, \tag{4.10}$$

and subsequently the mass flux via Eqs. 4.1 and 4.2

$$|m| \;\; = \;\; \sqrt{\frac{[p] + \bar{B_\perp}[B_\perp]}{\tau_L(1-\Omega)}}, \tag{4.11}$$

Finally the velocity jumps follow from Eqs. 4.1 and 4.3.

4.2 Shock Types

Whichever method is adopted to find states satisfying the jump relationships, it is necessary to determine which jumps are physically admissible. Some parameters may be found to classify shock types. These play an important role in establishing the supplementary conditions, such as entropy conditions in gasdynamics. For a shock, the signs of the following four parameters $P_{1,2,3,4}$ determine which of the magnetoacoustic characteristics run into the shock:

$$\frac{c_f}{\tau} - |m|, \quad -(\frac{c_s}{\tau} - |m|), \quad \frac{c_{fL}}{\tau_L} - |m|, \quad -(\frac{c_{sL}}{\tau_L} - |m|), \tag{4.12}$$

where $c_{f,s}$ are positive propagation speeds satisfying

$$(\frac{c_{f,s}}{\tau})^2 = \frac{1}{2\tau}\Big((B_x{}^2 + B_\perp{}^2 + \gamma p) \pm \sqrt{(B_x{}^2 + B_\perp{}^2 + \gamma p)^2 - 4B_x{}^2\gamma p}\ \Big),$$

with $c_s \leq \sqrt{\tau}B_x \leq c_f$, and $|m|$ is the absolute value of the mass flow rate.

Similar to the model, there are sixteen possible sign distributions of these four parameters, but only nine can actually arise because the following relations must be satisfied.

$$c_s \leq c_f \quad \text{and} \quad c_{sL} \leq c_{fL}. \tag{4.13}$$

The classification of shock types is identical with the model explained in Section 3.3. At this stage, the classification is merely geometric in nature; we need still to decide which types are physically meaningful.

4.3 Viscosity Admissibility Condition for MHD Shocks

The evolutionary condition developed by Akhiezer *et al.* [3], Polovin [94] and Jeffrey and Taniuti [58] restricts the physically admissible shocks for planar MHD Riemann problem to regular planar slow and fast shocks in which the number of

small-amplitude outgoing waves is one, equivalent to the number of the boundary conditions minus one $(2-1)$. It turns out, however, that regular shocks alone can not ensure the uniqueness of the Riemann problem. The failure of the evolutionary condition has become more obvious after several researchers investigated the MHD Riemann problem by numerical experiments [116, 15, 63, 128, 127, 36, 17]. In the past, it was assumed by the evolutionary condition that MHD intermediate shocks are unstable because the linearized perturbation of the jump relations is overdetermined. Contrary to this belief, recently, Brio and Rosenau [17] showed that the nonlinear intermediate shocks have such characteristics, but the linearized problem cannot be characterized as incoming or outgoing since there are waves moving with the shock speed.

In the mean time, some mathematicians (Schaeffer, Shearer, Gomes, and Isaacson *et al.*), who work on the Riemann problem of non-strictly hyperbolic conservation laws with application to oil recovery, proposed the viscosity admissibility condition to overcome failure of the evolutionary condition which restricts the characteristics that enter and leave a discontinuity. The viscosity admissibility condition considers relevant discontinuities to be limits of travelling waves for an associated parabolic equation in order to take account of certain physical effects that have been neglected in the ideal equations. Global analysis of the dynamical system defined by travelling wave solutions to the associated parabolic equation plays a crucial role in this theory. For an example, by applying this criterion to the planar 2×2 model system in case I, Gomes [46] proved that there are shocks (undercompressive) which have stable viscous profiles but do not satisfy the Lax conditions. However, these undercompressive shocks are not admissible in the version of the model problem (case IV) that is analogous to MHD.

Therefore, we will adopt the viscosity admissibility condition to determine physically relevant MHD shocks.[1] The global phase portraits of the coplanar MHD problem are given in Appendix C. In the finite domain, typically, there are four singularities, two nodes and two saddles. The saddle-saddle connection cannot exist, so undercompressive shocks will be excluded from the wave curve. But, overcompressive shocks do have viscous profiles since a repelling node can be connected with an attracting node. In conclusion, the evolutionary condition excludes certain types of shocks, while the viscosity admissibility condition permits them. It will be shown in Section 4.10 that precisely those shocks admitted under the viscosity condition allow unique solutions to be found for all planar MHD Riemann problems.

4.4 Magnetoacoustic Simple Waves

MHD simple waves, which are rarefaction wave solutions to a MHD system of equations, have been studied by various researchers. Shercliff [108] and Mann [79] examined simple waves in a state space defined as $(\rho, B_\perp)$. Polovin [93] derived the Riemann invariants in a state space defined as $(a^2/{c_a}^2,\ {c_{f,s}}^2/a^2)$. Recently, Roe and Balsara [100] obtained approximate curves for magnetoacoustic simple waves in a state space $(c_a/a,\ c_{a\perp}/a)$, where $c_{a\perp} \equiv B_\perp/\sqrt{\rho}$, starting from the MHD magnetoacoustic eigensystem.

Here, we will follow the approach considered by Polovin since it yields an exact relation for MHD simple waves in a monatomic gas. Then they will be reformulated in a non-dimensional phase space which turns out to be very useful.

The system of equations for MHD simple waves can be written, starting from the

[1] This condition, too, can fail to guarantee the existence and uniqueness of the solutions of Riemann problems [56].

Eq. 2.28 in section 2.5, as

$$-\epsilon c_n d\rho + \rho du = 0, \tag{4.14}$$

$$-\epsilon c_n \rho du + B_\perp dB_\perp + a^2 d\rho = 0, \tag{4.15}$$

$$-\epsilon c_n \rho dv - B_x dB_\perp = 0, \tag{4.16}$$

$$-\epsilon c_n dB_\perp + B_\perp du - B_x dv = 0, \tag{4.17}$$

with constant B_x and entropy, where $\lambda = u + \epsilon c_n$. For right-running waves and left-running waves, ϵ is 1 and -1, respectively. Here, c_n, which is the characteristic speed of magnetoacoustic waves, is given by

$$c_n{}^2 c_{a\perp}{}^2 = (c_n{}^2 - a^2)(c_n{}^2 - c_a{}^2). \tag{4.18}$$

From Eqs. 4.14 and 4.15 we have

$$(a^2 - c_n{}^2)d\rho + B_\perp dB_\perp = 0. \tag{4.19}$$

Introducing the variables r and q through

$$r \equiv \frac{a^2}{c_a{}^2}, \quad q \equiv \frac{c_n{}^2}{a^2}, \tag{4.20}$$

we can write Eq. 4.18 as

$$B_\perp = B_x \sqrt{(q-1)(r - \frac{1}{q})}\, \mathrm{sign}(B_{\perp L}). \tag{4.21}$$

From Eq. 4.14, we have

$$du = \epsilon c_n \frac{d\rho}{\rho} = \epsilon \frac{c_n}{\rho} \frac{B_x{}^2}{\gamma a^2} dr = \epsilon \frac{c_n}{\gamma} \frac{dr}{r} = \epsilon \frac{a}{\gamma} \sqrt{q} \frac{dr}{r}, \tag{4.22}$$

where $r = \rho a^2 / B_x{}^2$ and $c_n = a\sqrt{q}$ are used. Thus we derive

$$\frac{du}{dr} = \epsilon \frac{a}{\gamma} \frac{\sqrt{q}}{r}. \tag{4.23}$$

From Eqs. 4.16, 4.17 and 4.21 we have

$$B_x{}^2(1-\frac{{c_n}^2}{{c_a}^2})dv = \frac{B_\perp}{B_x}du \tag{4.24}$$

and finally

$$\frac{dv}{dr} = -\epsilon\frac{a}{\gamma}\frac{\sqrt{(q-1)(rq-1)}}{(rq-1)}\,\mathrm{sign}(B_xB_{\perp L}). \tag{4.25}$$

Next, Eqs. 4.23 and 4.25 can be expressed as follows.

$$\Delta u = \epsilon\frac{\hat{a}}{\gamma}\int\sqrt{q_\pm}\,r^{-\frac{\gamma+1}{2\gamma}}\,dr\,, \tag{4.26}$$

$$\Delta v = -\epsilon\frac{\hat{a}}{\gamma}\int\frac{\sqrt{(q_\pm-1)(rq_\pm-1)}}{(rq_\pm-1)}\,\mathrm{sign}(B_xB_{\perp L})\,r^{-\frac{\gamma+1}{2\gamma}}\,dr\,, \tag{4.27}$$

where $\hat{a} = c_{aL}{r_L}^{\frac{1}{2\gamma}}$. Note that $a^2 = \hat{a}^2 r^{\frac{\gamma-1}{\gamma}}$ if we introduce $\hat{\rho},\hat{p},\hat{a}$ defined by $\rho = \hat{\rho}r^{\frac{1}{\gamma}}, p = \hat{p}r, \hat{a}^2 = \gamma\hat{p}/\hat{\rho}$. The relation between r and q in simple waves can be derived by inserting Eq. 4.21 and $d\rho = dp/a^2 = {B_x}^2/(\gamma a^2)\,dr$ into Eq. 4.19.

$$\frac{dq}{dr} = \frac{2-\gamma}{\gamma}\frac{q^2(q-1)}{(rq^2-1)}. \tag{4.28}$$

The direct integration of Eq. 4.28 yields the following solution.

$$J_\pm = r(q_\pm-1)^{-\alpha} + \alpha\int {q_\pm}^{-2}(q_\pm-1)^{-(\alpha+1)}\,dq_\pm, \tag{4.29}$$

where $\alpha = \gamma/(2-\gamma)$ and $J_\pm$ represents the fast and slow magnetoacoustic Riemann invariants. For a monatomic gas, it reduces to an analytic form

$$\begin{aligned} J_\pm = {} & \frac{(r-1)}{(q_\pm-1)^5} + \frac{5}{2}\frac{1}{(q_\pm-1)^4} - \frac{5}{(q_\pm-1)^3} + \frac{10}{(q_\pm-1)^2} \\ & -\frac{25}{q_\pm-1} - \frac{5}{q_\pm} + 30\ln(\frac{q_\pm}{|q_\pm-1|}). \end{aligned} \tag{4.30}$$

For slow waves, $rq-1<0$, $0\le q_-<1$, whereas $rq-1>0$, $1<q_+<\infty$ for fast waves. The final note is that there exist non-physical portions of rarefaction waves in (r,q) space; it is the region with $(q-1)(rq-1)<0$ (See Eq. 4.21), implying that r,q coordinates can not serve as the final basis for rarefaction waves. In next section, we will derive the new basis consisting of two non-dimensional parameters.

4.5 Hugoniot Curves and Integral Curves in the Reduced Plane

For a particular left state, we can use equations Eq. 4.7 or 4.9 to trace the Hugoniot curve. For each state on the curve, we can compute the parameters that describe the characteristic speeds and so identify the shock type corresponding to that point. Based on the relatively simple form Eq. 4.7 that the Hugoniot assumes for variables, $p, B_\perp$, we choose these variables to represent the phase space, and make them non-dimensional as

$$U = \frac{\gamma p}{{B_x}^2}, \quad V = \frac{B_\perp}{B_x}. \tag{4.31}$$

We argue that these variables are the ultimate phase space for non-zero B_x in which all MHD waves can be represented without any trouble in the sense that (1) they are non-dimensional parameters by which the umbilic point can be fixed (2) they are chosen from the Hugoniot condition, matching the fact that rarefaction waves are the solution of Rankine-Hugoniot relations with the limit of $|\mathbf{u}_R - \mathbf{u}_L| \to 0$ (3) they can represent the entire physical region defined by $p, \rho, T \geq 0$ and $u, v, B_\perp \in \mathbf{R}$. For special cases such as $\rho = 0, T = 0$ and $B_\perp = 0$, only the pressure p can be a basis [2]. Either ρ or a variable divided by a, for example $(\rho, B_\perp)$ by Shercliff and Mann, $(a^2/{c_a}^2,\ {c_{f,s}}^2/a^2)$ by Polovin and $(c_a/a,\ c_{a\perp}/a)$ by Roe and Balsara, can not define the absolute temperature. Also, $([p]/p_L,\ [B_\perp]/\sqrt{{B_x}^2 + {B_\perp}_L^2})$ by Bazer and Ericson and $(p, B_\perp)$ by Gogosov do not satisfy property (1). The notation in Eq. 4.9 can be expressed in terms of U, V by $(U_L = \gamma p_L/{B_x}^2,\ V_L = B_{\perp L}/B_x)$

$$Y = \frac{U}{U_L} - 1, \quad h = \frac{V - V_L}{\sqrt{1 + {V_L}^2}}, \quad s_L = \frac{U_L}{1 + {V_L}^2}, \quad \sin\theta_L = \frac{V_L}{\sqrt{1 + {V_L}^2}}. \tag{4.32}$$

[2] Even in the hydrodynamic limit, there is no trouble. The reason is that the hydrodynamic limit can be represented by $B_\perp = 0$ and $[v] = 0$, without $B_x = 0$. (See Eqs. 4.1 $\sim$ 4.5.)

In the (U, V) plane, the shape and classification of the Hugoniot curves is identical for either right-running or left-running waves. Examples of the Hugoniot curves can be found in Fig. 4.1. Note that all shocks except the transport shocks can be found in the Hugoniot loci of MHD.

Similarly, integral curves defined by Eq. 4.30 can be represented by these coordinates using the following relations.

$$r = U, \quad q_{\pm} = \frac{1}{2U}\Big(1 + U + V^2 \pm \sqrt{(1 + U + V^2)^2 - 4U}\Big). \tag{4.33}$$

Integral curves are depicted in Fig. 4.2. In Figs. 4.1 and 4.2, the point $(1, 0)$ is the umbilic point where the slow and fast wavespeeds coincide. Fig. 4.1 (a)-(c) are topologically identical to the Hugoniot curves found in Fig. 3.1 for a particular case of an 2×2 set of conservation laws designed to have a singular point where the wavespeeds coincide. The curves have the same general shape as for the model problem, and the various shock types are encountered along them in the same order. In each case, overcompressive shocks are only found if V is sufficiently small. Similar to the model, the non-convexity of MHD waves is observed, which is illustrated in Fig. 4.3.

Various critical points on the Hugoniot can be identified, where one type of shock gives way to another. The state C_L is the point where the Hugoniot locus is tangent to a fast integral curve. It may be defined as C_L satisfying

$$\frac{1}{\tau} c_f(\mathbf{U}) - |m(\mathbf{U}_L, \mathbf{U})| = 0. \tag{4.34}$$

In Table 3.1 it can be found that C_L is on the border between fast regular shocks and undercompressive shocks or on the border between slow regular shocks and overcompressive shocks. B_L, D_L may be defined as points satisfying

$$\frac{1}{\tau_L} c_s(\mathbf{U}_L) - |m(\mathbf{U}_L, \mathbf{U})| = 0. \tag{4.35}$$

Here, B_L and D_L are defined for the $+\sqrt{R}$ branch and the $-\sqrt{R}$ branch at the Hugoniot curve, respectively. B_L is on the border between fast shocks and overcompressive shocks while D_L is on the border between slow shocks and undercompressive shocks. Because the arguments in Section 3.7 are essentially topological, they apply without alteration to the MHD equations.

4.6 Compound Waves

In order to ensure the uniqueness to the solution, so-called compound waves are introduced as substitutes for undercompressive shocks which are inadmissible by the viscous stability criterion developed in Appendix C. Similar to the model, they consist of waves of one family (slow or fast) and are of three types. (See Fig. 3.7.)

A slow compound wave C_1 is a slow rarefaction wave R_1 followed by a slow shock S_1. Similarly a fast compound wave C_2 can be defined as a fast shock wave S_2 followed by a fast rarefaction wave R_2. In both cases the speed of the shock s equals the speed of the adjacent rarefaction wave $u - \text{sign}(m)c_{f,s}$. From the definition of critical points (eg. C_L, B_L, D_L), it can be seen that a slow compound wave C_1 consists of a jump to the point D_L followed by a slow rarefaction R_1, and a fast compound wave consists of a jump to the point C_L followed by a fast rarefaction R_2. Similar to the model, there is a chance of a slow rarefaction followed by a jump to a fast rarefaction. (See Fig. 3.7.)

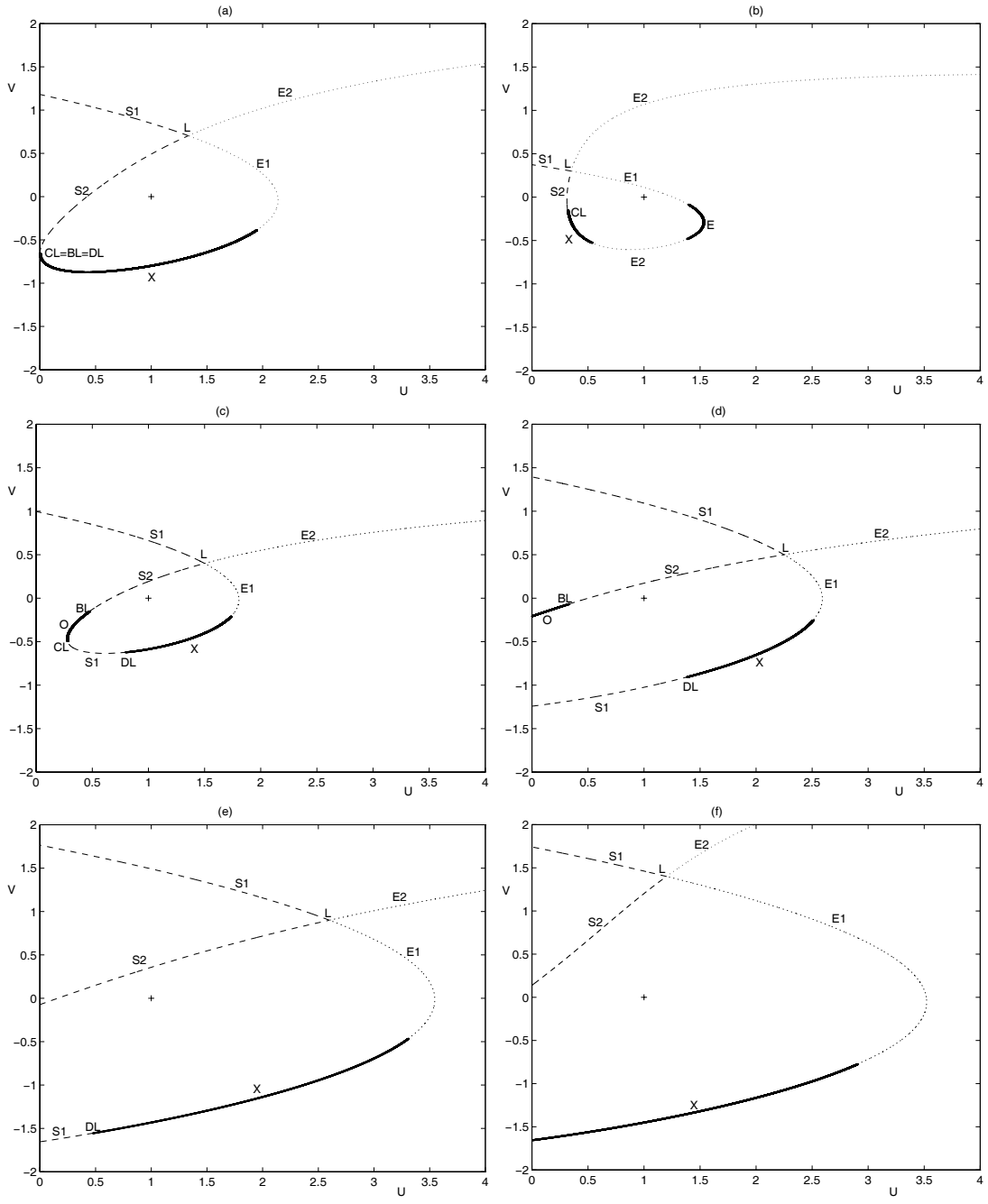

Figure 4.1: (a)-(f). Examples of MHD Hugoniot curves: S_1, S_2 - 1, 2 regular, E_1, E_2 - 1, 2 expansive, O, X - overcompressive, undercompressive, E - expansive shocks.

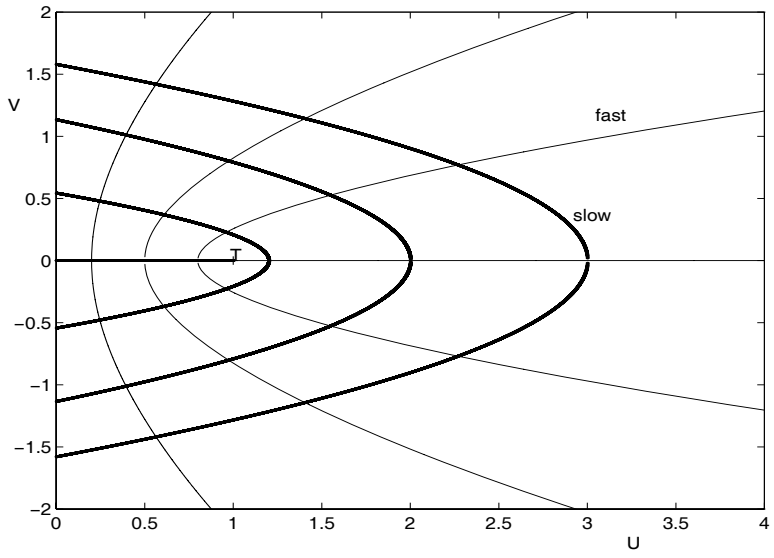

Figure 4.2: MHD integral curves. The thick solid lines indicate slow rarefaction waves, and the thin lines indicate fast rarefaction waves.

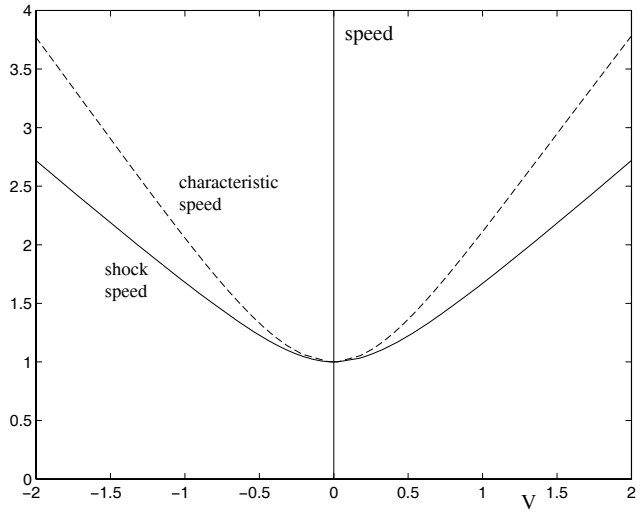

Figure 4.3: The shock speed and the characteristic speed as a function of V along a MHD fast rarefaction wave with $U_L = 0.5$, $V_L = 0$. Compare with Fig. 3.4.

4.7 Magnetoacoustic Shocks and Rarefaction Waves in Various Limits

4.7.1 Hydrodynamic Limit

In the hydrodynamic limit ($B_{\perp L} = B_{\perp R} = 0$), the Hugoniot curve can be obtained from Eqs. 4.1, 4.2, 4.3 and 4.6.

$$\frac{[\tau]}{\tau_L} = -\frac{2[p]}{(\gamma+1)[p] + 2\gamma p_L}, \text{ or } \frac{\tau}{\tau_L} = \frac{\beta + p/p_L}{1 + \beta p/p_L} \text{ where } \beta = \frac{\gamma+1}{\gamma-1}, \tag{4.36}$$

and

$$m = -\frac{[p]}{[u]} = \frac{[u]}{[\tau]},\ m^2 = -\frac{[p]}{[\tau]}. \tag{4.37}$$

Signs of four parameters $P_1,\ P_2,\ P_3,\ P_4$ can be determined by

$$\sqrt{U_L^{-1} + 1 + Y + |U_L^{-1} - (1+Y)|} - \sqrt{2 + \frac{\gamma-1}{\gamma}Y}, \tag{4.38}$$

$$-\sqrt{U_L^{-1} + 1 + Y - |U_L^{-1} - (1+Y)|} + \sqrt{2 + \frac{\gamma-1}{\gamma}Y}, \tag{4.39}$$

$$\sqrt{U_L^{-1} + 1 + |U_L^{-1} - 1|} - \sqrt{2 + \frac{\gamma+1}{\gamma}Y}, \tag{4.40}$$

$$-\sqrt{U_L^{-1} + 1 - |U_L^{-1} - 1|} + \sqrt{2 + \frac{\gamma+1}{\gamma}Y}. \tag{4.41}$$

With the help of Table 3.1, we can classify all hydrodynamic shocks.

$$S_1 - E_1 - E - E_2 \quad \text{if} \quad 0 < U_L < 1, \tag{4.42}$$

with boundary points $U_L,\ U',\ U''$, where $U' \equiv \frac{2\gamma}{\gamma+1} - \frac{\gamma-1}{\gamma+1}U_L$ and $U'' \equiv \frac{2\gamma}{\gamma-1} - \frac{\gamma+1}{\gamma-1}U_L$.

$$S_1 - O - S_2 - E_2 \quad \text{if} \quad 1 < U_L < \frac{2\gamma}{\gamma+1}, \tag{4.43}$$

with boundary points $U'',\ U',\ U_L$.

$$O - S_2 - E_2 \quad \text{if} \quad \frac{2\gamma}{\gamma+1} < U_L < \frac{2\gamma}{\gamma-1}, \tag{4.44}$$

with boundary points U', U_L.

$$S_2 - E_2 \quad \text{if} \quad \frac{2\gamma}{\gamma - 1} < U_L. \tag{4.45}$$

with a boundary point U_L. In the second case (Fig. 4.12 (b)), S_1 and O meet at a particular point defined by

$$U_{C_L} = \frac{2\gamma}{\gamma - 1} - \frac{\gamma + 1}{\gamma - 1} U_L. \tag{4.46}$$

Note that

$$\lim_{U_L \to 1} U_{C_L} = 1. \tag{4.47}$$

Also, rarefaction waves in the hydrodynamic limit can be derived from Eq. 4.14 $\sim$ 4.17. They yield

$$(a^2 - {c_n}^2) d\rho = 0, \quad du = \epsilon c_n \frac{d\rho}{\rho}, \quad \text{and} \quad dv = dB_\perp = 0, \tag{4.48}$$

and become

$$\Delta u \;=\; \epsilon \int \frac{a}{\rho}\, d\rho, \tag{4.49}$$

which is the solution of a pure gas rarefaction wave. It can be rewritten in our (U, V) space, noting that $da/a = (\gamma - 1)/2(d\rho/\rho)$,

$$J_\pm \;=\; u - \epsilon \frac{2a}{\gamma - 1}. \tag{4.50}$$

Along pure gas rarefaction waves, the velocity u is determined solely by the pressure, yielding the so-called $p - u$ diagram.

$$\Delta u \;=\; \epsilon \frac{2}{\gamma - 1} \frac{|B_x|}{\sqrt{\rho_L}} U_L{}^{-\frac{1}{\gamma}} \int U^{\frac{\gamma+1}{\gamma}}\, dU, \tag{4.51}$$

since $a = |B_x|/\sqrt{\rho_L}(U/U_L)^{1/\gamma} U$.

4.7.2 Zero Pressure Limit

Let us consider first a case $p_L = p_R = 0$. For shocks, the Rankine-Hugoniot equations in section 4.1 reduce to

$$[\tau] = [u] = \bar{B_\perp} = 0 \text{ and } [v] = \epsilon\sqrt{\tau_L}[B_\perp]. \tag{4.52}$$

Across this shock, the transverse magnetic field changes its sign without modification of its magnitude. Since $\tau_L (= \tau_R)$ can have any value, this limit is the absolute temperature limit (*i.e.* $T = 0$).

For rarefaction waves, Eqs. 4.14 $\sim$ 4.17 reduce to

$$\rho c_n = B_x^2 + B_\perp^2, \quad c_n^2 d\rho = B_\perp dB_\perp \quad \text{and} \quad T = 0. \tag{4.53}$$

Again, this case is the absolute temperature limit. These relations yield a Riemann invariant for fast rarefaction waves

$$J_+ \;=\; \frac{\rho^2}{1+V^2}. \tag{4.54}$$

Next, let us consider a case $p_R = 0$ and $p_L \neq 0$. For regular shocks, the density jump can be written as

$$\frac{\rho}{\rho_L} \;=\; \frac{(\gamma-1)p_L + \frac{\gamma-1}{2}[B_\perp]^2}{(\gamma+1)p_L + \frac{\gamma-1}{2}[B_\perp]^2} \tag{4.55}$$

and thus ρ_R can not be zero, meaning that in this case $p_R = 0$ represents the absolute temperature limit. Notice that it becomes $\rho/\rho_L = (\gamma-1)/(\gamma+1)$ in the hydrodynamic limit.

For rarefaction waves, the entropy is constant along integral curves and thus

$$\frac{\rho}{\rho_L} = \left(\frac{p}{p_L}\right)^{\frac{1}{\gamma}} \tag{4.56}$$

is enough to examine the limit. Since $p_R = 0$ means $\rho_R = 0$, this case is the vacuum limit. Therefore, the vacuum state can be reached only by slow rarefaction waves.

4.7.3 Zero B_x Limit

In this limit, the Hugoniot curves can be obtained from Eqs. 4.1∼4.6 by inserting $B_x = 0$.

For non-zero m, we obtain a Rankine-Hugoniot relation

$$\frac{\gamma - 1}{4}[B_\perp]^3 + \gamma\bar{p}[B_\perp] - \bar{B_\perp}[p] = 0. \tag{4.57}$$

The density ratio and the mass flux are

$$\Omega = \frac{B_{\perp L}}{B_\perp},\ |m| = \sqrt{\frac{[p] + \bar{B_\perp}[B_\perp]}{\tau_L(1-\Omega)}}. \tag{4.58}$$

For zero m, we obtain a Rankine-Hugoniot relation

$$[u] = 0 \ \text{ and } \ [p + \frac{{B_\perp}^2}{2}] = 0. \tag{4.59}$$

Also, rarefaction waves in this limit can be derived from Eq. 4.14 ∼ 4.17 by inserting $B_x = 0$. The characteristic speed of magnetoacoustic waves is given by

$${c_n}^2 = a^2 + {c_a}_\perp^2 \ \text{ or } \ c_n = 0. \tag{4.60}$$

But waves with the speed $c_n = 0$ will be removed since they can be replaced by shocks with zero m. For the magnetoacoustic rarefaction wave, we obtain the following relation

$$\frac{dq}{dp} = \frac{q-1}{\alpha p}, \tag{4.61}$$

$$\frac{du}{dp} = \epsilon\frac{a}{\gamma}\frac{\sqrt{q}}{p}. \tag{4.62}$$

It yields

$$J = p(q-1)^{-\alpha} \ \text{ or } \ J = p^{1+\alpha}{B_\perp}^{-2\alpha}. \tag{4.63}$$

Notice that $(p, B_\perp)$ is the ultimate phase space in this limit.

4.8 Classification of Domains by MHD Shock Type

The only structural difference between the model problem and the MHD problem is that in the latter case there is a physical significance to the value $U = 0$, that is, $p = 0$. Thus, for certain positions of the point L, some sections of the Hugoniot may be cut off, as in Fig. 4.1 (d)-(f). The solution to the MHD Riemann problem needs to account for this difference. The effect is to simplify the solution to the Riemann problem for states well away from the umbilic point, and so we will begin with the case where L is close to the umbilic point, and the complete loop to the Hugoniot curve lies in $U > 0$. Then the topology of the Hugoniot and wave curves is identical to that of the model problem.

Therefore, under the same set of hypotheses about what shock types are admissible, the *topology of the Riemann solutions is also identical.* By this phrase we mean that for a given (U_L, V_L), the (U, V) plane is divided into non-overlapping regions within each of which the resulting waves are of the same type. For the model problem, it turns out that the Riemann problem is well-posed if the waves are selected by the following modification of the evolutionary criterion:

$$P_4 \leq 0 \leq P_2 \quad \text{or} \quad P_1 \leq 0 \leq P_3. \tag{4.64}$$

By well-posed, it is meant that a unique solution to the Riemann problem exists for all pairs of left and right states, and that this solution depends continuously on these states. It is the property of continuous dependence that has to be assured by a correct choice of admissible shocks.

Specifically, the following shocks are found to be necessary.

Regular fast and slow shocks These do not change the sign of the transverse field, and are found in Fig. 4.1 (a)-(f) in the upper half-plane, labelled S_1, S_2.

Slow intermediate shocks [3] These do change the sign of the transverse field, and are found in Fig. 4.1 (c)-(e) in the lower half-plane, labelled S_1.

Fast intermediate shocks These produce a sign change, and are found in Fig. 4.1 (a)-(e), labelled S_2.

Overcompressive shocks These produce a sign change, and are found in Fig. 4.1 (c),(d), labelled O.

Transitional cases B_L, C_L and D_L These are found in Figs. 4.1 (a)-(e).

None of the shocks listed, except for the first item, would be regarded as admissible by the evolutionary criterion.

The remaining parts of the Hugoniot locus have to be discarded. Branches E_1, E_2 and E would be discarded by any criterion. The undercompressive shocks X are not required in this particular case, but are needed when solving the model quadratic problem with parameters that relate to oil recovery rather than MHD.

We claim that a special case of the Riemann problem for the full MHD equations is also well-posed in terms of such waves. This special case is one where we prescribe one of the left and right states, together with the state between the slow waves. (We defer to Section 4.11 the discussion of how this problem relates to the usual Riemann problem.) Even the solution to this restricted Riemann problem involves 17 different cases. Each wave, fast and slow, may be a regular shock, a compound wave, a rarefaction wave, or it may be absent. The seventeenth case is where the fast and slow shocks coalesce into an overcompressive shock. Which of these cases occurs will depend on where the left and right states lie with respect to certain critical curves, which will now be described.

[3] In this case, the word 'intermediate' is equivalent to 'non-classical.'

4.8.1 PC^*U^* Curve

A distinctive feature in Fig. 4.1 is that Hugoniot curves for some left states have the form of a closed loop around the umbilic point, but for other states the loop passes out of the physically meaningful range $U > 0$. Therefore, it might be useful to classify the domain by this feature (PC^*U^*). The domain can be distinguished by the following critical curve in (U_L, V_L) plane defined as

$$\left(\frac{\partial U}{\partial V}\right)_{U=0} = 0 \text{ for } V \text{ satisfying Eq. 4.7 or 4.9.} \tag{4.65}$$

An example can be found in Fig. 4.1 (a). We have from Eq. 4.7 that,

$$\frac{\gamma-1}{4}\bar{V}[V]^4 - \frac{\gamma-1}{4\gamma}U_L[V]^3 + \frac{U_L}{2}\bar{V}[V]^2 - (\frac{U_L}{2} - 1 - \bar{V}^2)\frac{U_L}{\gamma}[V] = \frac{\bar{V}}{\gamma^2}{U_L}^2, \tag{4.66}$$

and after some manipulation Eq. 4.65 becomes

$$\frac{\gamma-1}{8}[V]^3([V] + 8\bar{V}) + \frac{3-2\gamma}{4\gamma}U_L[V]^2 + \frac{\gamma+1}{\gamma}U_L\bar{V}[V] + (1+\bar{V}^2)\frac{U_L}{\gamma} = \frac{\gamma+1}{2\gamma^2}{U_L}^2. \tag{4.67}$$

From these equations we can eliminate V to give a relation between U_L, V_L. This critical curve is shown by dotted lines in Fig. 4.4. The origin and U^* given as

$$U^* = \frac{2\gamma}{\gamma+1} \tag{4.68}$$

are located on this curve. Note that hydrodynamic slow shocks disappear across U^*. Within the PC^*U^* curve, the Hugoniot curve is a closed loop, and if both states lie within this region the solution to the Riemann problem is identical to the model. If one state is outside this region then certain waves will not occur. In fact, the remaining classifications have to do with which types of wave are available to create a sign change in $B_\perp$.

4.8.2 TC^* Curve

In Fig. 4.1., it can be observed that overcompressive shocks may or may not exist for certain left states. The critical curves for the existence of overcompressive shocks can be calculated in the following way. If $\bar{B_\perp} = 0$, Eq. 4.7 reduces to

$$[p][B_\perp](\gamma\bar{p} - {B_x}^2 + \frac{\gamma-1}{4}[B_\perp]^2) = 0. \tag{4.69}$$

For finite $B_\perp$,

$$\gamma\bar{p} - {B_x}^2 + \frac{\gamma-1}{4}[B_\perp]^2 \;\; = \;\; 0. \tag{4.70}$$

Using this, the Lagrangian shock speed 4.11 can be written as

$$|m| = \frac{1}{\sqrt{\gamma\tau_L}}\Big((\gamma+1){B_x}^2 - (\gamma-1){B_\perp}_L{}^2 - \gamma p_L\Big). \tag{4.71}$$

Then, the equation $c_{sL}/\tau_L - |m| = 0$ reduces in (U,V) notation to

$$2(\gamma+1)U_L = \gamma|V_L|\sqrt{(\gamma-2)^2{V_L}^2 + 4(\gamma+1)} - \Big((\gamma^2+2\gamma-2){V_L}^2 - 2(\gamma+1)\Big). \tag{4.72}$$

From Table 3.1, it can be seen that the overcompressive shock disappears across this critical curve.

The point C^*, which is the intersection of PC^*U^* and TC^* critical curves, can be calculated by combining Eq. 4.65 and Eq. 4.70. We have C^* given as

$$\left(\frac{2\gamma(\sqrt{2\gamma(\gamma-1)}-1)}{2\gamma^2-2\gamma-1},\;\; \pm\sqrt{\frac{(2\gamma+1)-\gamma\sqrt{\frac{2\gamma}{\gamma-1}}}{2\gamma^2-2\gamma-1}}\right), \tag{4.73}$$

in (U,V) domain, which is well-defined for $1 < \gamma \leq 2$ and $\gamma \neq (1+\sqrt{3})/2$. When $\gamma = (1+\sqrt{3})/2$, C^* becomes $((1+\sqrt{3})/2,\; \pm 12^{0.25}/2)$. The Hugoniot curve at this special left state is given in Fig. 4.1 (a). The curve is tangent to the $U = 0$ axis at $C_L(= B_L = D_L)$.

4.8.3 C^*U^{**} Curve

For some left states, the right states satisfying $c_{sL}/\tau_L - |m| = 0$ may be located in the negative pressure domain. This means that TC^* is no longer critical for the existence of overcompressive shocks. Instead, overcompressive shocks will disappear if the point B_L lies to the left of $U = 0$ (see Fig. 4.1 (d),(e)). Thus, we may define the C^*U^{**} curve as

$$\frac{c_{sL}}{\tau_L} - |m| = 0, \quad p_R = 0 \quad \text{with} \quad +\sqrt{R} \text{ branch in Eq. 4.9.} \tag{4.74}$$

These two conditions can be expressed in (Y, h) notation as follows.

$$-\frac{(\gamma-1)}{4s_L}(2s_L+\gamma h^2)(h^2+2h\sin\theta_L-\frac{2s_L}{\gamma}) = 1+s_L-\sqrt{(s_L-1)^2+4s_L\sin^2\theta_L}, \tag{4.75}$$

$$-\frac{s_L}{\gamma} = -\frac{h^2}{2} + \frac{h}{2\ \sin\theta_L-(\gamma-1)h}(\frac{\gamma h\sin\theta_L}{2} - 1 + s_L + \sqrt{R}). \tag{4.76}$$

Overcompressive shocks begin to appear across this curve. The curve is calculated numerically. It is easy to show

$$U^{**} = \frac{2\gamma}{\gamma-1}, \tag{4.77}$$

by inserting $B_{\perp L} = B_{\perp R} = 0$ into $c_{sL}/\tau_L - |m| = 0$.

4.8.4 $C^*\infty$ Curve

When the point D_L crosses $U = 0$ (see Fig. 4.1 (e),(f)), slow shocks are no longer available to change the sign of $B_\perp$. The definition is the same as the C^*U^{**} curve except for the branch. Thus, it may be defined as

$$\frac{c_{sL}}{\tau_L} - |m| = 0, \quad p_R = 0 \quad \text{with} \quad -\sqrt{R} \text{ branch in Eq. 4.9.} \tag{4.78}$$

The slow-shock part can be found below the U axis across this critical curve. Note that the point satisfying $c_{sL}/\tau_L - |m| = 0$ is a starting point at which the undercompressive shock turns into the slow shock.

4.8.5 PU^{**} Curve

Fast shocks are no longer available to change the sign of $B_\perp$ across this critical curve. The PU^{**} curve can be defined as the Hugoniot passing the origin. Applying this condition to Eq. 4.7 yields

$$V_L = \pm\sqrt{\sqrt{\frac{8U_L}{\gamma(\gamma-1)}} - \frac{2U_L}{\gamma}}. \tag{4.79}$$

4.8.6 MHD Wave Mechanisms Available to Change the Sign

Five critical curves are plotted in Fig. 4.4 (a) which shows shock wave mechanisms available to change the sign of the transverse field. The PC^*U^* critical curve is shown by dotted lines, because it is not critical in shock wave mechanisms. Each region enclosed by four critical curves ($TC^*, C^*U^{**}, C^*\infty$, and PU^{**}) will have certain shocks available to change the sign. There exist five different cases: $S_1, S_2, S_1S_2, S_1S_2O$, and no shock. All properties are symmetrical about $V_L = 0$ axis. Points marked as + represent the reference states in Fig. 4.1 (a)-(f).

Compound waves can also change the sign. Slow compound waves C_1 are available everywhere, but fast compound waves C_2 are available only when the critical point C_L exists. Whether C_L exists for a particular reference state can be determined by checking C_L for intermediate states which move along the slow shock S_1 and the slow integral curve R_1 originating from the reference L. By this procedure, we can find the region in which fast compound waves C_2 are available, which is illustrated in Fig. 4.4 (b). The region is enclosed by the boundary which consists of some parts of PC^*U^* critical curve and section of the slow integral curve starting at C^*. Some curves are shown by dotted lines to explain how the boundary (indicated by solid lines) is determined. Notice that fast compound waves are available where L is close to the umbilic point.

Finally, by combining shock and compound wave mechanisms, it can be shown that MHD wave mechanisms have eight different cases, which is illustrated in Fig. 4.5.

4.9 Switch-on and Switch-off Waves

In MHD, switch-on waves are defined as shocks or rarefaction waves by which the magnetic field is generated at the expense of a decrease of pressure. Because in our formulation the left state represents properties behind the wave, such waves are those satisfying $B_R = 0$ and $B_L \neq 0$. Among slow and fast waves, slow rarefaction waves and fast shocks can produce the magnetic field. For slow rarefaction waves, the possible region in (U, V) space can be defined as any U_L on slow integral curves starting from U_R, satisfying $U_L < U_R$ and $U_R > 1$. For fast shocks, only U_L within the region enclosed by PU^{**} critical curve can have the corresponding the right state U_R restricted as $0 \leq U_R < 1$ at which $B_R = 0$.

On the other hand, switch-off waves are defined as shocks or rarefaction waves by which the magnetic field vanishes. That is, all the magnetic energy vanish, causing an increase of the thermal energy. Such waves are those satisfying $B_L = 0$ and $B_R \neq 0$. Contrary to switch-on waves, by slow shocks and fast rarefaction waves, the magnetic field can vanish in crossing over waves. For fast rarefaction waves, the possible region is defined as any U_R on fast integral curves starting from U_L, satisfying $U_L < U_R$ and $U_L < 1$. For slow shocks, U_R within the region defined by the Hugoniot curve passing the point $(U^*, 0)$ can have the corresponding switch-off state satisfying $1 < U_L < U^*$. U_R outside the region can also have the corresponding switch-off state satisfying $U^* < U_L$.

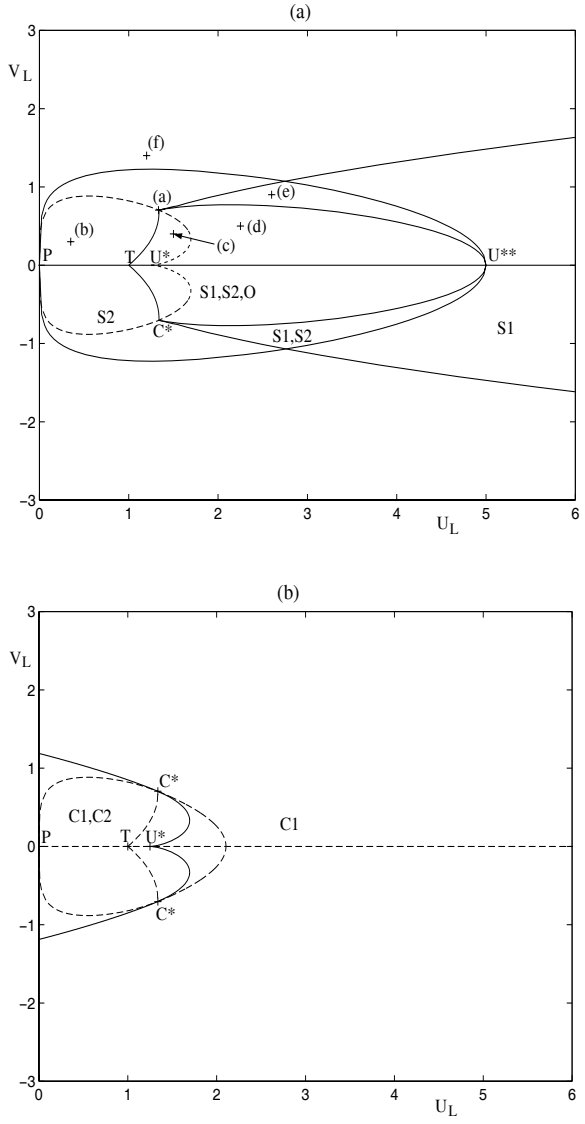

Figure 4.4: (a) Shock mechanisms available to change the sign of the transverse field: PC^*U^* critical curve is indicated by dot lines, while the other are indicated by solid lines. (b) Compound wave mechanisms available to change the sign: Fast compound waves are available within the boundary curve indicated by solid lines. T, P represent the umbilic point and the origin, respectively.

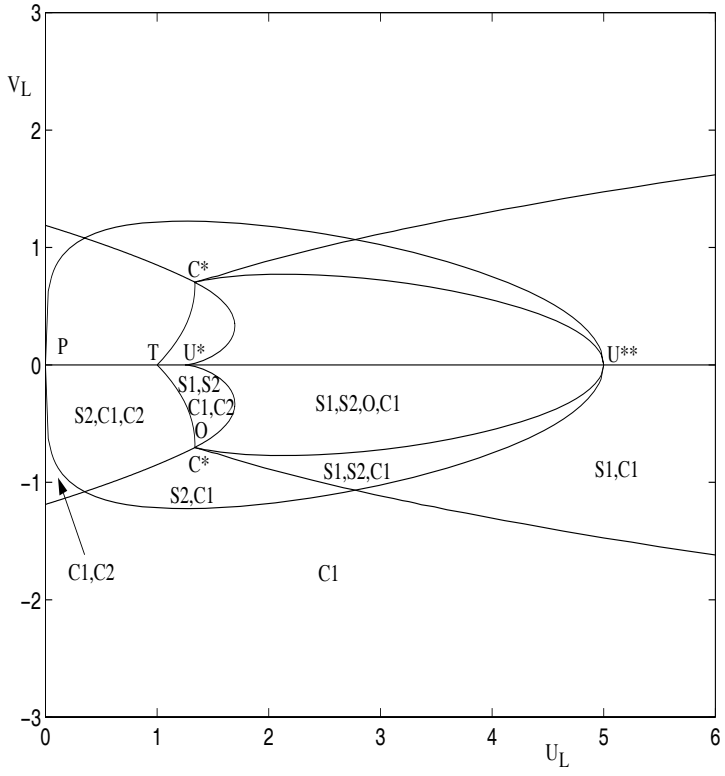

Figure 4.5: MHD Mechanisms available to change the sign of the transverse field: Critical curves are shown by thin solid lines. Waves available to change the sign are indicated in the lower half-plane. All properties are symmetrical about the U_L axis.

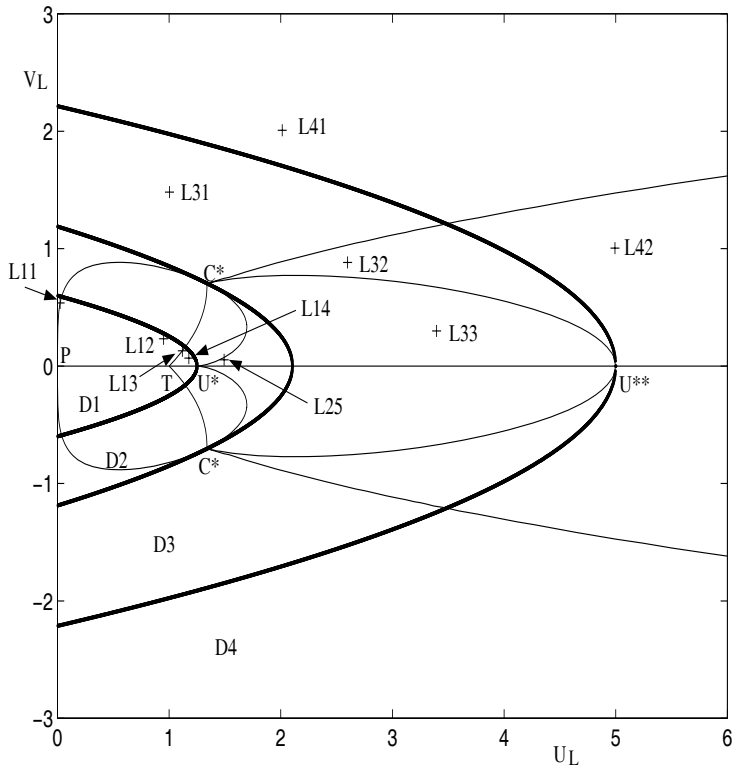

Figure 4.6: Classification of domains by wave combinations and solution patterns. Critical curves are shown by thin solid lines, while slow integral curves are shown by thick solid lines. The reference states can be classified into four subdomains $D1, D2, D3$ and $D4$. The left states ($L_{11} \sim L_{42}$) that represent the reference state in sectors are marked by $+$.

4.10 Solution of the Planar MHD Riemann Problem on One-Directional Waves

The solution of the Riemann problem in (U, V) space consists of a path LIR where L, R are the given left and right states and I is an intermediate state such that LI is a valid slow wave and IR is a valid fast wave. To facilitate this construction, we define the wave curve associated with a given left state L as the set of all points that can be reached from L by valid waves. These comprise all points on the Hugoniot through L representing valid shocks, all points on the integral curves through L representing valid rarefaction waves, and all points that can be reached from L through compound waves. Then I lies on the wave curve through L, and R lies on the wave curve through I.

For a given left state, a right state will be connected by one of 17 different wave combinations. Therefore, there may exist a large number of cases in solution patterns which will be beyond classification. However, thanks to the classification of MHD wave mechanisms available to change the sign, we can classify left states into some subdomains in which the solution patterns are qualitatively the same. In the next section, these subdomains will be defined.

4.10.1 Classification of Domains by Wave Combinations and Solution Patterns

Which MHD waves are available to change the sign, as described in Fig. 4.5, will play a crucial role in classifying domains by wave combinations. But, the PU^{**} curve in Fig. 4.5 is not critical for wave combinations, even though it is critical for wave mechanisms changing the sign. Thus, it will not be considered in classifying domains by wave combinations. The only remaining criterion of the classification of domains is the slow integral curve. The reason for this is that for a left state,

different wave combinations begin to appear as intermediate states move along the slow integral curve. Therefore, *by inserting slow integral curves passing U^*, C^* and U^{**}, four subdomains can be defined.* These subdomains are shown in Fig. 4.6. In each subdomain the solution is different in sectors 2 through 4. Note that sectors are defined by which wave combinations exist and subdomains are defined by the set of such sectors. In order to show the solution in each sector, nine cases (L_{11}[4], $L_{12}, L_{14}, L_{25}, L_{31}, L_{32}, L_{33}, L_{41}, L_{42}$) marked as + in Fig. 4.5 will be considered. A special case L_{13} will be considered to show the transition between the solution of case L_{12} and the solution of case L_{14}. Note that L_{21}, L_{22}, L_{23} and L_{24} are not considered. The reason for this is that because the critical points B_L, D_L on the Hugoniot of the left states of first three sectors in subdomain $D2$ always exist, the pattern of wave combinations is the same as that of subdomain $D1$.

Now we will construct the solution to the Riemann problem. This construction can be explained with the help of Figs. 4.7 and 4.8. Fig. 4.7 (a)-(d) shows that Hugoniot curves in the domain $D1$ may be classified into two cases. For reference states L_{11}, L_{12} which are located on the left of the critical curve TC^*, there are no overcompressive shocks nor slow shocks with negative $B_\perp$. However, both shocks can be found for L_{14}. Thus this difference in admissible shock curves has an important effect on the solution of the Riemann problem. Once integral curves and Hugoniot loci and compound waves are given for a particular left state, the wave curves are the set of waves: $1, 2$ rarefaction waves, $1, 2$ shock waves, $1, 2$ compound waves, and fast rarefaction wave originating from point C_L. These wave curves in the domain $D1$ are shown in Fig. 4.8. Points marked as + represent left state, umbilic point, the reflection points of left states including one on TC^* curve (*i.e.*, $[p] = \bar{B_\perp} = 0, \bar{B_\perp} =$

[4]It represents a left state in the first sector of subdomain $D1$.

0), and p_R from Eq. 4.70.

We now discuss all four cases including the switch-off shock solution and the hydrodynamic shock solution.

4.10.2 Solution for Subdomain $D1$

Fig. 4.9 (a)-(d) and Fig. 4.12 (a), (b) comprise the full set of solutions by which all possible cases can be represented. In Fig. 4.9 (b) the left state is located above the critical curve TC^*. The overcompressive shocks and slow shocks cannot be found below the U axis. There are three dotted curves split at the point ${C_L}^*$. The curve $\{-\infty {C_L}^*\}$ is the boundary curve on which the fast shock becomes the fast compound wave. The curve $\{{C_L}^*\infty\}$ represents fast rarefaction waves on which the solution is the limit of either C_1R_2 or R_1C_2. If the right state is on this curve, the solution is C_1C_2 or R_1R_2. This is a kind of transitional wave for the magnetic field. The configuration of this special wave in the physical space (x,t) is presented in Fig. 3.7. The curve $\{{C_L}^*T\}$ is the set of locus B_L as the intermediate state moves along the slow rarefaction wave curve. It is the boundary of R_1S_2 and C_1S_2 which represent two different paths. In fact, two solutions are identical in the physical space (x,t) due to equal shock speed and are called a *triple shock* [54]. Note that right states which are connected by compound waves always exist below the U axis. In Fig. 4.9 (c), (d) the point C_L begins to bifurcate three points B_L, D_L and C_L itself. Overcompressive shocks emerge as the triple shock region $\{B_LT\}$ shrinks. Solution S_1R_2 can be found below the axis due to the presence of slow shocks while solution R_1C_2 disappears. The configuration of solutions becomes symmetrical as the left state approaches the axis. Fig. 4.12 (a), (b) shows switch-off shocks and hydrodynamic shocks in domain $D1$. In Fig. 4.12 (b), overcompressive shocks are observed on the line $\{C_LB_L\}$. We

can clearly see the continuous dependence of solutions on the left state.

4.10.3 Solution for Subdomain $D2$

Fig. 4.10 (a) in addition to Fig. 4.9 (a)-(d) and Fig.. 4.12 (c) comprise the full set of solutions in domain $D2$. The only difference with domain $D1$ comes of opening from the closed Hugoniot loci near the $V = 0$ axis due to negative pressure. As a result, fast compound waves become lost in the domain as the left state approaches the axis. Contrary to domain $D1$, the zero pressure state can be obtained by overcompressive shocks and S_1R_2 combinations.

4.10.4 Solution for Subdomain $D3$

Fig. 4.10 (b)-(d) and Fig. 4.12 (c) comprise the full set of solutions in domain $D3$. Figure 11 (b)-(d) represent solutions in three subdomains separated by two critical curves, C^*U^{**} and $C^*\infty$. The distinctive feature is that some parts are always cut out of the Hugoniot loci loop due to the zero pressure limit. As the left state moves, slow shocks with opposite sign begin to emerge in advance of overcompressive shocks. As a result, fast compound waves disappear in domain $D3$ and a new C_1S_2 combination can make the right state reach a vacuum state.

4.10.5 Solution for Subdomain $D4$

Fig. 4.11 (a), (b) and Fig. 4.12 (c) comprise the full set of solutions in domain $D4$. The presence of a critical curve yields two cases in the pattern of solution. The solution is almost the same as that in domain $D3$. However, a case corresponding to Fig. 4.10 (d) cannot be found due to the absence of overcompressive shocks. In Fig. 4.11 (a) and (b), it can be observed that the U axis itself is a boundary line across which one wave changes character.

4.10.6 Solutions Requiring Special Waves

Fig. 4.12 (a)-(c) represent all the possible solutions for switch-off shocks and hydrodynamic shocks. Switch-off shocks can be calculated by substituting $B_{\perp L} = 0$ in Eq. 4.9 and hydrodynamic shocks are given in Section 4.7.1. When $U_L < 1$, switch-off can be accomplished only by the fast rarefaction wave. As U_L passes the umbilic point, switch-off shocks begin to emerge. Switch-off can be obtained only through the slow shock as shown in Fig. 4.12 (b), (c). From Figs. 4.9$\sim$4.12, it can be shown that switch-on and switch-off can be attained only through R_1, S_2 and S_1, R_2, respectively. For the Riemann problem with $p_{L,R} = 0$, a special slow shock and a fast simple wave given in Section 4.7.2 are the only possible self-similar solutions. That is, when $|B_{\perp L}| \geq |B_{\perp R}|$, we have always a unique solution, R_2, S, or SR_2. But, when $|B_{\perp L}| < |B_{\perp R}|$, there exists no solution so that there is no mechanism amplifying the magnetic field when there is no other energy available. One final note is that the difference in the density between the vacuum limit and the absolute temperature limit can be sustained by the presence of a contact discontinuity.

Finally, we have described all possible wave combinations and mechanisms changing the sign. It is shown that solutions in domains $D1, D2$ are most general, in other words, most complicated and are almost the same as that of the 2×2 model system described in Section 3.8. Solutions in domains $D3, D4$ have the same features, but due to the cutting off of the Hugoniot locus by the zero pressure limit they become different. From solution diagrams it is also shown that the viscosity admissibility condition has the advantage of ensuring the existence and uniqueness of solutions over the evolutionary condition. On the other hand, the evolutionary condition can not ensure the existence of solutions when all non-evolutionary solutions are strictly

excluded. This can be manifested by considering a case in the hydrodynamic limit. From Figs. 4.12 (b) and (c), it can be observed that the solutions involve overcompressive shocks and thus there does not exist any evolutionary solution. In fact, the evolutionary condition is not different from ignoring all shocks with opposite sign for $B_\perp$. Therefore, within its framework, all overcompressive shocks, compound waves, and regular S_1, S_2 shocks with opposite sign are lost.

4.11 Full Riemann Problem

4.11.1 Structure of the Riemann Problem

Until now, we consider only half of the Riemann problem. That is, instead of specifying left and right states, we specify one of them, together with an intermediate state on one side of the contact discontinuity, so that the two given states are separated only by right-running (or left-running) waves. Here, by observing that the MHD system is symmetrically hyperbolic and magnetoacoustic waves are determined by the magnetic field and the pressure, we will prove the well-posedness of full MHD planar Riemann problem.

Theorem 1 For planar MHD Riemann problem, let us denote l, r left and right states, and m intermediate states that consist of left, right states m_l, m_r separated by the contact discontinuity. *Then the following data sets are equivalent in that there exists a one-to-one mapping between $\Re$ and $\Re_m$. Also, for any Riemann problem defined by such sets, there exists the unique solution if all the slow, fast, and overcompressive shocks are taken.*

$$\Re_m = \{(\rho, p, B_\perp)_{l,r}, \quad (p, B_\perp)_m, \quad \rho \geq 0, \quad p \geq 0, \quad B_\perp \in \mathbf{R}\},$$

$$\Re = \{(\rho, p, B_\perp)_{l,r}, \quad \Delta u, \quad \Delta v, \quad \rho \geq 0, \quad p \geq 0, \quad B_\perp \in \mathbf{R}, \quad (\Delta u, \Delta v) \in \mathbf{R}_{uv}\},$$

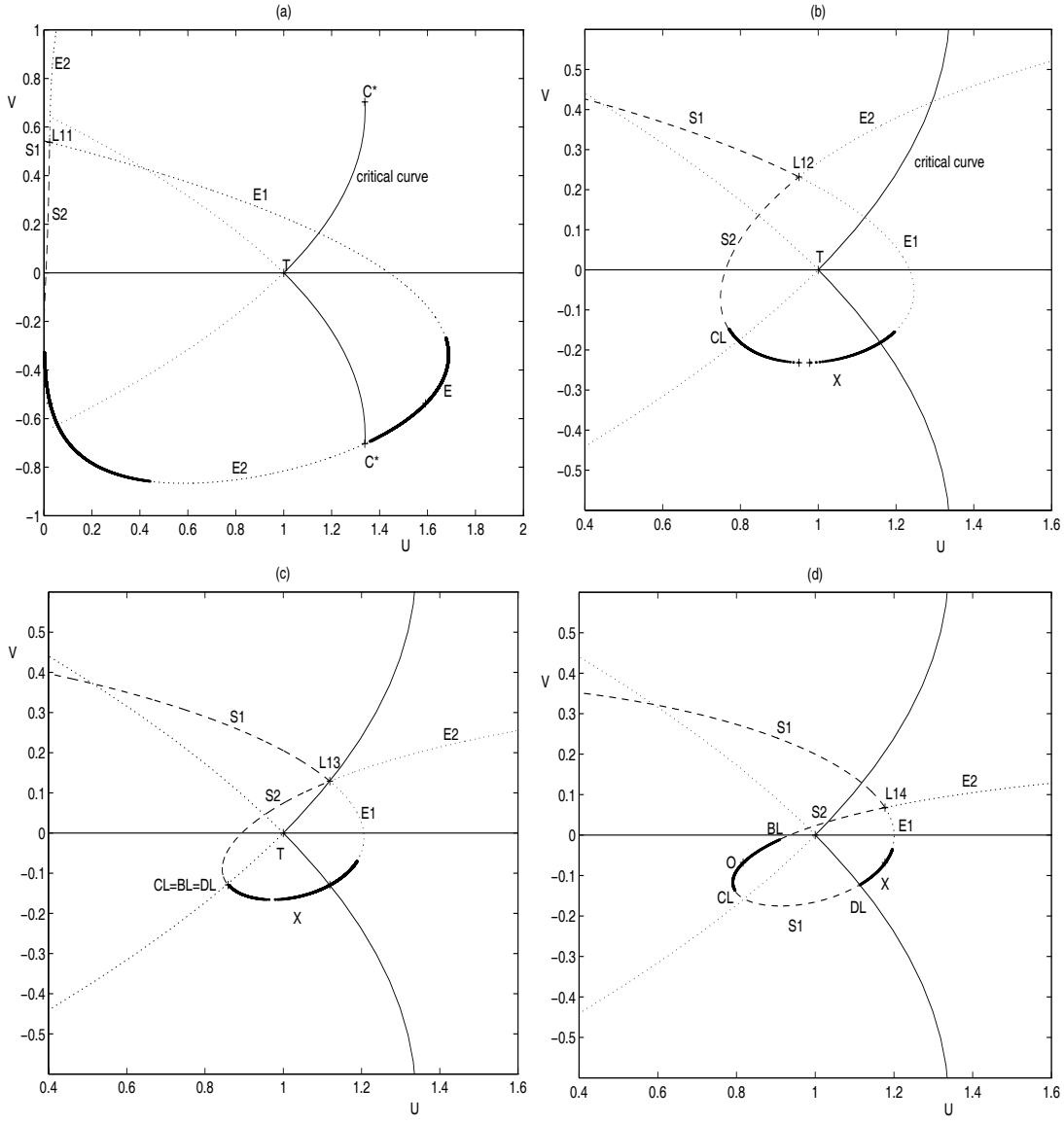

Figure 4.7: (a)-(d). MHD Hugoniot loci and shock types in the domain $D1$: $S_1, S_2 - 1, 2$ regular, $E_1, E_2 - 1, 2$ expansive, E - expansive, O - overcompressive, X - undercompressive shocks.

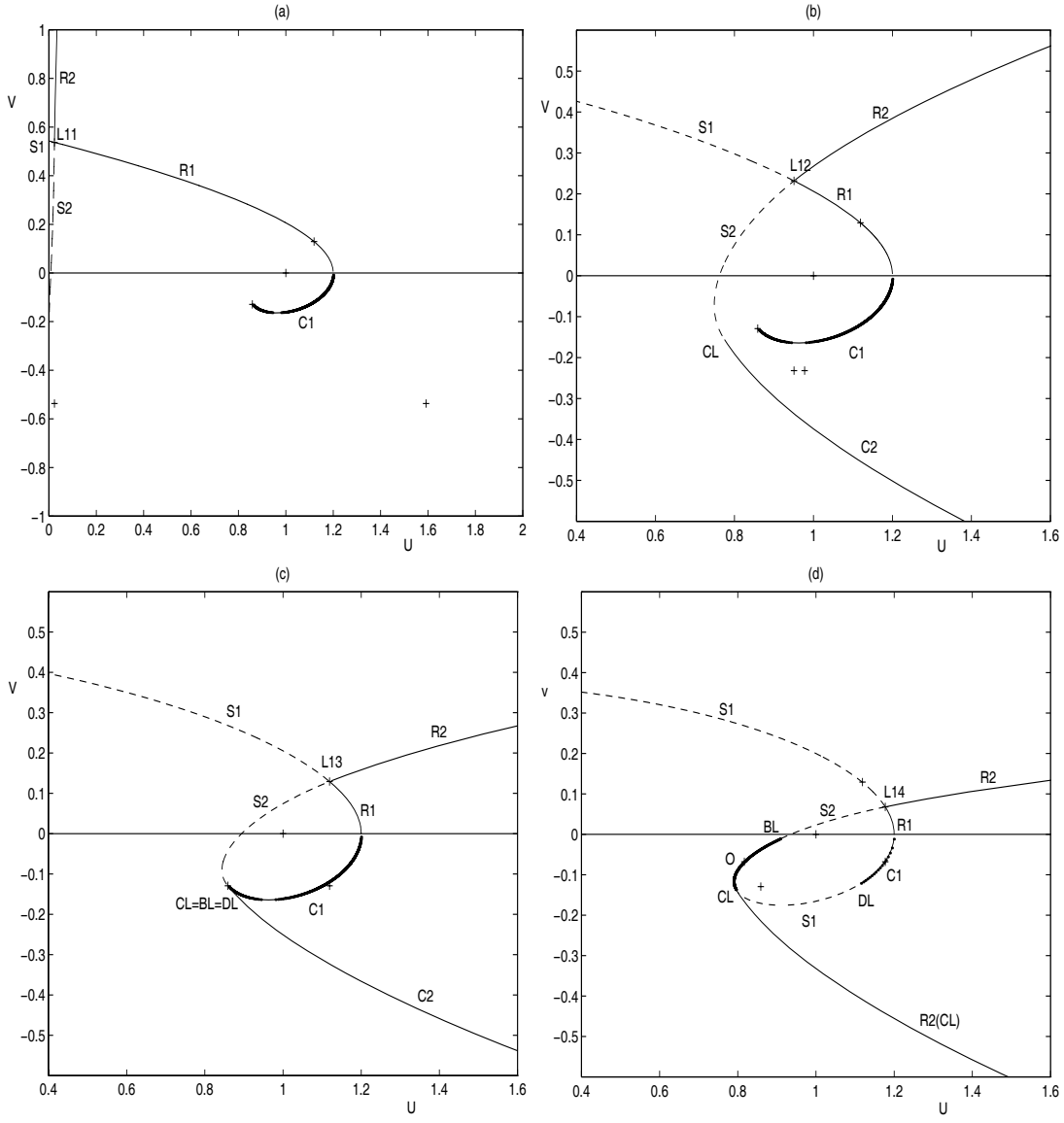

Figure 4.8: (a)-(d). MHD wave curves in the domain $D1$: C_1, C_2 - 1,2 compound waves. $R_2(C_L)$ represents a fast rarefaction wave curve originating from the point C_L.

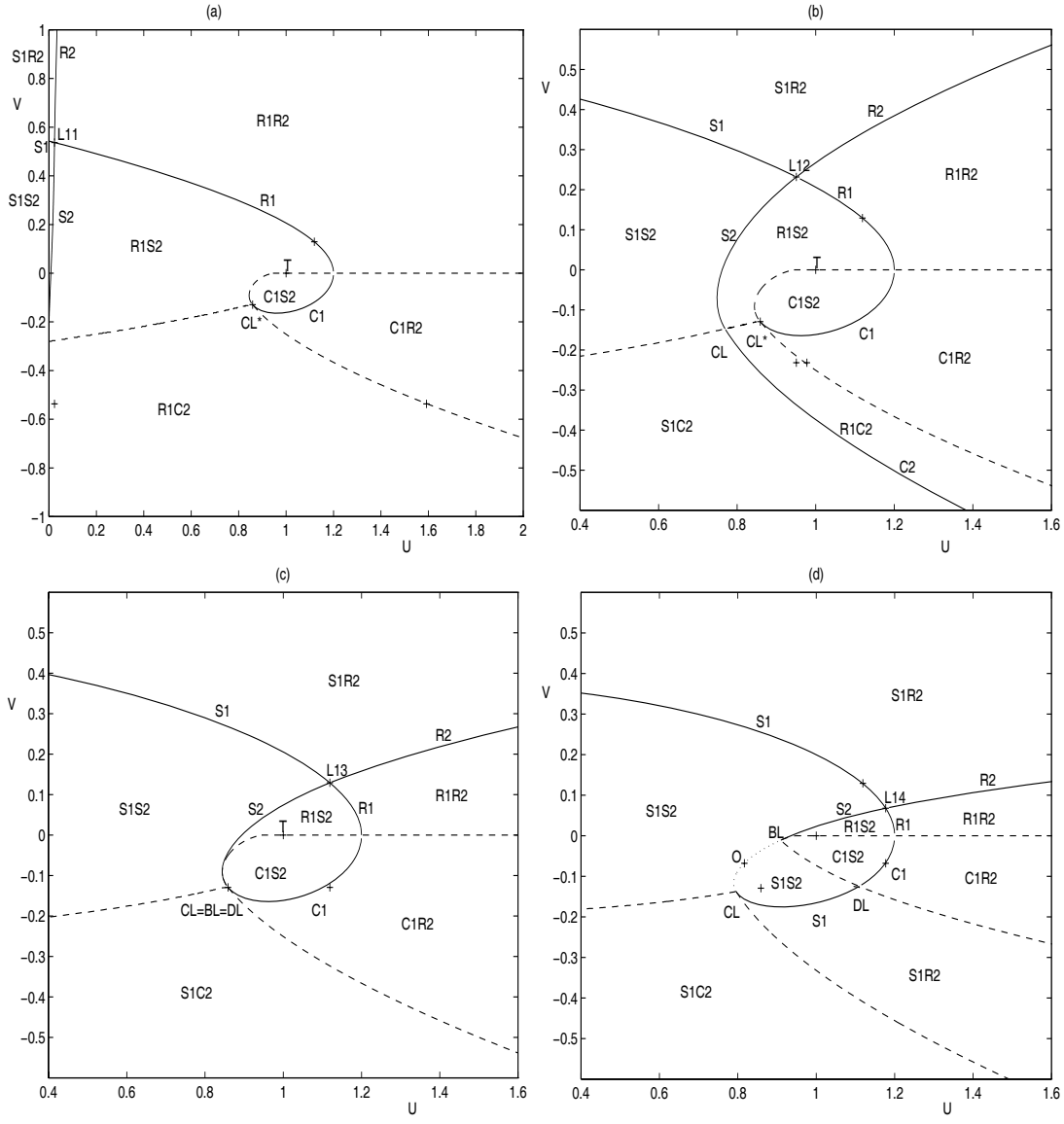

Figure 4.9: (a)-(d). MHD Riemann problem solution in the domain $D1$: solid line - boundary line across which one wave is zero, dashed line - one wave changes character, dot line - no change.

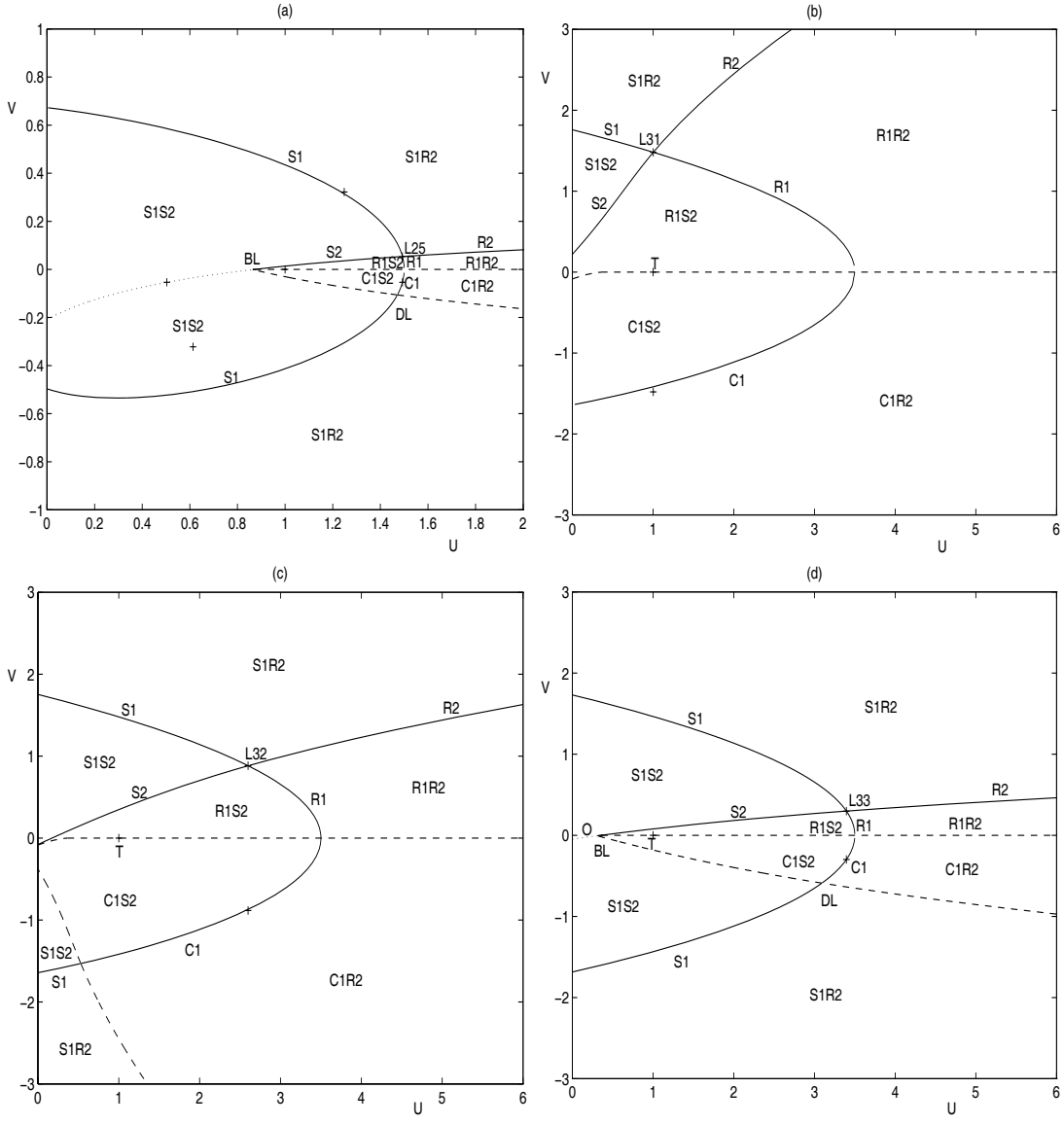

Figure 4.10: (a)-(d). MHD Riemann problem solution : (a) in the domain $D2$ and (b),(c),(d) in the domain $D3$.

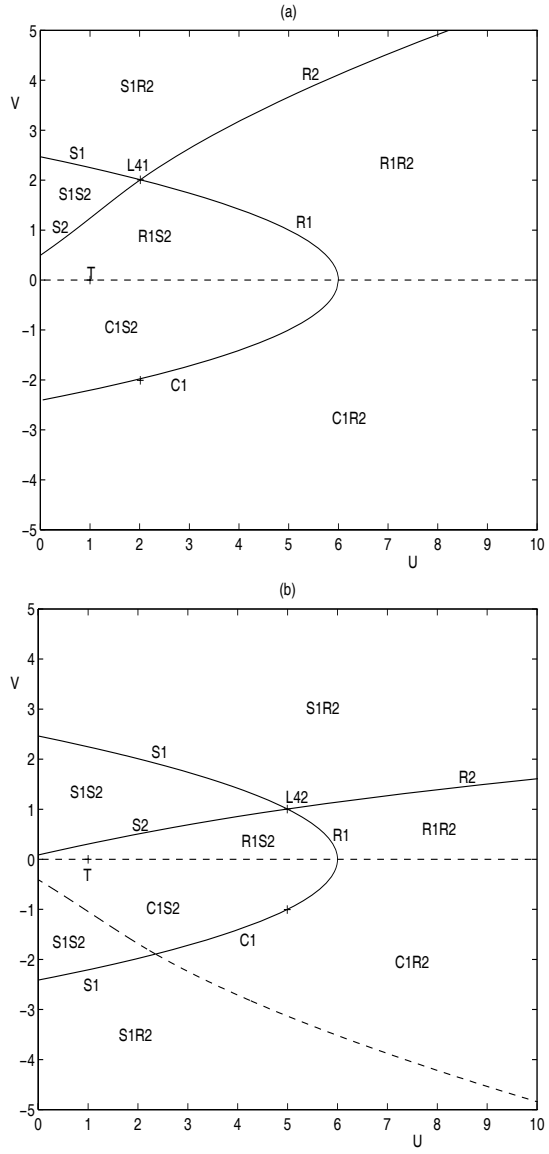

Figure 4.11: (a)-(b). MHD Riemann problem solution in the domain $D4$.

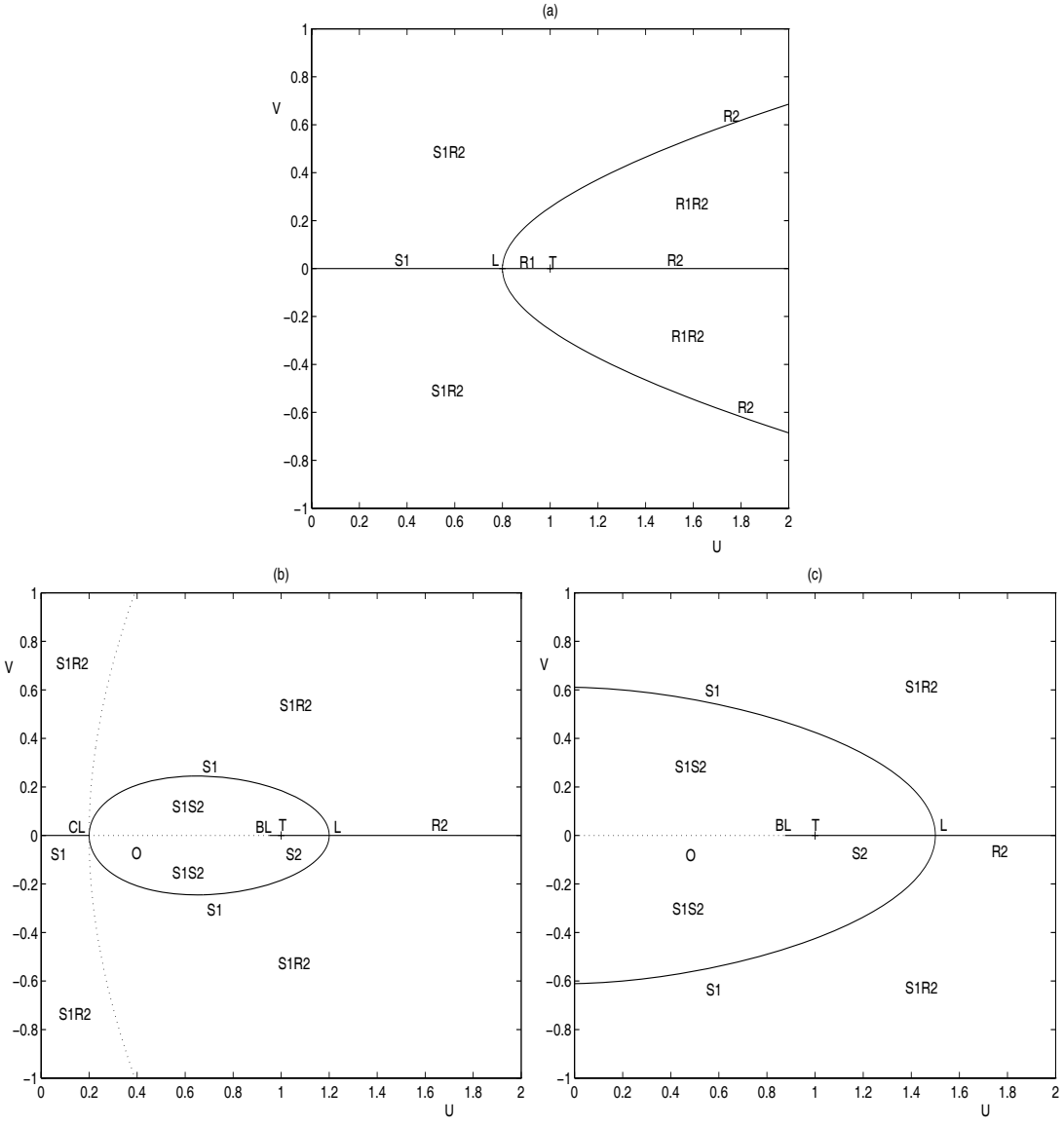

Figure 4.12: (a)-(c). MHD switch-off and hydrodynamic shock solution :(a) $U_L < 1$, (b) $1 < U_L < U^*$, (c) $U^* < U_L$.

where $\Delta \equiv (\,)_r - (\,)_l$ *and* $\mathbf{R}_{uv}$ *is defined by all combinations of* $(p, B_\perp)_{l,r}$.

Remark In the second set, $\mathbf{R}_{uv}$ denotes a certain subset of $\mathbf{R}^2$, corresponding to the fact that attempting to prescribe too large a velocity difference will lead to a vacuum behind waves, just as in hydrodynamics. The boundary of $\mathbf{R}_{uv}$ depends on the prescribed values of $(p, B_\perp)_{l,r}$.

Proof In order to show that the following mapping is one-to-one,

$$\mathcal{F} : \Re_m \to \Re, \tag{4.80}$$

let us rewrite Δu and Δv. They can be written as

$$\frac{u_r - u_l}{|B_x|} = \frac{u_r - u_m}{\sqrt{\tau_{m_r}}|B_x|}\sqrt{\tau_{m_r}} - \frac{u_l - u_m}{\sqrt{\tau_{m_l}}|B_x|}\sqrt{\tau_{m_l}}, \tag{4.81}$$

$$\frac{v_r - v_l}{|B_x|} = \frac{v_r - v_m}{\sqrt{\tau_{m_r}}|B_x|}\sqrt{\tau_{m_r}} - \frac{v_l - v_m}{\sqrt{\tau_{m_l}}|B_x|}\sqrt{\tau_{m_l}} \tag{4.82}$$

The most crucial finding is that the property of $\frac{u_{l,r}-u_m}{\sqrt{\tau_{m_{l,r}}}|B_x|}$, $\frac{v_{l,r}-v_m}{\sqrt{\tau_{m_{l,r}}}|B_x|}$ depends only on the combination of waves which are eventually determined in (U, V) state space.

Let us examine $\frac{u_r-u_m}{\sqrt{\tau_{m_r}}|B_x|}$. If we denote r_1, r_2 intermediate states between m_r and r, and l_1, l_2 intermediate states between m_l and l, then a mapping for right-running waves $\mathcal{F}_r$ can be defined by (same for $\mathcal{F}_l$)

$$\mathcal{F}_r : \Re_m{}' \to \Re', \tag{4.83}$$

where

$$\Re_m{}' = \{(p, B_\perp)_r, \quad (p, B_\perp)_m, \quad p \geq 0, \quad B_\perp \in \mathbf{R}\},$$

$$\Re' = \{(p, B_\perp)_r, \quad \delta u, \quad \delta v, \quad p \geq 0, \quad B_\perp \in \mathbf{R}, \quad (\delta u, \delta v) \in \mathbf{R}_{uv}{}'\},$$

$\delta \equiv (\,)_r - (\,)_m$ and $\mathbf{R}_{uv}{}'$ is defined by all combinations of $(p, B_\perp)_{r,m}$. This mapping can be manifested by the following relations

$$\frac{u_r - u_m}{\sqrt{\tau_{m_r}}|B_x|} = \frac{u_{r_1} - u_m}{\sqrt{\tau_{m_r}}|B_x|} + \frac{u_{r_2} - u_{r_1}}{\sqrt{\tau_{r_1}}|B_x|}\sqrt{\frac{\tau_{r_1}}{\tau_{m_r}}} + \frac{u_r - u_{r_2}}{\sqrt{\tau_{r_2}}|B_x|}\sqrt{\frac{\tau_{r_2}}{\tau_r}\frac{\tau_{r_1}}{\tau_{m_r}}} \tag{4.84}$$

$$\frac{v_r - v_m}{\sqrt{\tau_{m_r}}|B_x|} = \frac{v_{r_1} - v_m}{\sqrt{\tau_{m_r}}|B_x|} + \frac{v_{r_2} - v_{r_1}}{\sqrt{\tau_{r_1}}|B_x|}\sqrt{\frac{\tau_{r_1}}{\tau_{m_r}}} + \frac{v_r - v_{r_2}}{\sqrt{\tau_{r_2}}|B_x|}\sqrt{\frac{\tau_{r_2}}{\tau_r}\frac{\tau_{r_1}}{\tau_{m_r}}} \quad (4.85)$$

Since the Rankine-Hugoniot conditions, the density ratio Ω and m^2 are symmetric with respect to the left and right states, the following relations are satisfied for shocks.

$$\frac{[u]}{\sqrt{\tau_L}|B_x|} = \epsilon\sqrt{(1-\Omega)(\frac{[u]}{\gamma} + \bar{V}[V])}, \quad (4.86)$$

$$\frac{[v]}{\sqrt{\tau_L}|B_x|} = -\epsilon[V]\sqrt{\frac{\gamma(1-\Omega)}{[u] + \gamma\bar{V}[V]}}, \quad (4.87)$$

where

$$\Omega = (2\bar{U} + \frac{\gamma-1}{2}[V]^2 - \frac{[U]}{\gamma})(2\bar{U} + \frac{\gamma-1}{2}[V]^2 + \frac{[U]}{\gamma})^{-1}. \quad (4.88)$$

For rarefaction waves, they can be rewritten as

$$\frac{[u]}{\sqrt{\tau_L}|B_x|} = \frac{\epsilon}{\gamma}U_L{}^{\frac{1}{2\gamma}}\int_{q_L}^{q} f_u(q)\,dq, \quad (4.89)$$

$$\frac{[v]}{\sqrt{\tau_L}|B_x|} = -\frac{\epsilon}{\gamma}U_L{}^{\frac{1}{2\gamma}}\int_{q_L}^{q} f_v(q)\,dq, \quad (4.90)$$

where $r = (q-1)^2\{J_\pm - \alpha\int q^{-2}(q-1)^{-\alpha-1}\,dq\}$, $\frac{\tau}{\tau_L} = (\frac{U_L}{U})^{\frac{1}{\gamma}}$,

$$f_u(q) \equiv \sqrt{q}\,r^{-\frac{\gamma+1}{2\gamma}}\frac{dr}{dq}, \quad f_v(q) \equiv \frac{\sqrt{(q-1)(rq-1)}}{(rq-1)}\,r^{-\frac{\gamma+1}{2\gamma}}\frac{dr}{dq}.$$

Therefore, the term $\frac{u_r - u_m}{\sqrt{\tau_{m_r}}|B_x|}$ depends only on $(p, B_\perp)_{r,r_1,r_2,m_r}$. A diagram in space defined by such terms is given in Fig. 4.13. It is obtained for a solution diagram given in Fig. 4.9 (b) using Eqs. 4.86$\sim$4.90. Notice that the left boundary is defined as the zero temperature limit. The reason is that the boundary represents properties ahead of the wave. If the left and right states are defined in reverse, the boundary becomes a vacuum limit.

Next, let us examine the mapping $\mathcal{F}_r$ in detail. Since $\frac{u_r - u_m}{\sqrt{\tau_{m_r}}|B_x|}$ is monotone in shocks and rarefaction waves due to the monotonicity of $\frac{[u,v]}{\sqrt{\tau}|B_x|}$, and its direction is not changed by $\mathcal{F}_r$ which yields only bending or stretching of rubber, the

mapping $\mathcal{F}_r$ is *one-to-one* on $\mathbf{R}^2$, since it is *topology-preserving mapping*. When $(p, B_\perp)_m = (p, B_\perp)_r$ (or $(p, B_\perp)_l$), the mapping corresponds to $\mathcal{F}_r$ (or $\mathcal{F}_l$). Any deviation in $(p, B_\perp)$ will locate its counterpart in a different position in $(\frac{\Delta u}{\sqrt{\tau_{m_r}}|B_x|}, \frac{\Delta v}{\sqrt{\tau_{m_r}}|B_x|})$ coordinates (or $(\frac{\Delta u}{\sqrt{\tau_{m_l}}|B_x|}, \frac{\Delta v}{\sqrt{\tau_{m_l}}|B_x|})$). When $(p, B_\perp)_l = (p, B_\perp)_r$, any deviation from m in $(p, B_\perp)$ will yield the different position, since the patch is proper and the effect of $\mathcal{F}_r$ (or $\mathcal{F}_l$) is only bending or stretching. In general case, for given $(p, B_\perp)_{l,r}$, a particular $(p, B_\perp)_m$ will produce a diagram in space

$$\Big(\frac{u_r - u_m}{\sqrt{\tau_{m_r}}|B_x|} - \frac{u_l - u_m}{\sqrt{\tau_{m_l}}|B_x|}, \frac{v_r - v_m}{\sqrt{\tau_{m_r}}|B_x|} - \frac{v_l - v_m}{\sqrt{\tau_{m_l}}|B_x|}\Big). \tag{4.91}$$

A deviation from m will yield the different position since each $\frac{\Delta(u,v)}{\sqrt{\tau}|B_x|}$ has the different value.

Similarly, the inverse mapping is one-to-one since

$$\frac{u_r - u_l}{|B_x|} = \frac{u_m - u_l}{\sqrt{\tau_l}|B_x|}\sqrt{\tau_l} - \frac{u_m - u_r}{\sqrt{\tau_r}|B_x|}\sqrt{\tau_r}, \tag{4.92}$$

$$\frac{v_r - v_l}{|B_x|} = \frac{v_m - v_l}{\sqrt{\tau_l}|B_x|}\sqrt{\tau_l} - \frac{v_m - v_r}{\sqrt{\tau_r}|B_x|}\sqrt{\tau_r}. \tag{4.93}$$

Thus we proved that the mapping $\mathcal{F}$ is one-to-one.□

4.11.2 Solution in (x, t) Physical Space

The exact Riemann solution in phase space can be projected in (x, t) physical Space. In gasdynamics, such procedure is simple. The calculation of the evolution of variables through rarefaction waves can be done by determining the velocity profiles first. (For shocks, it is trivial.)

In MHD, the procedure becomes somewhat complicated. For shocks, the propagation velocity can be determined as follows.

$$s = u_L - \tau_L m = u_L + \epsilon\sqrt{\tau_L}|B_x|\sqrt{\frac{[U] + \gamma\bar{V}[V]}{\gamma(1-\Omega)}}, \tag{4.94}$$

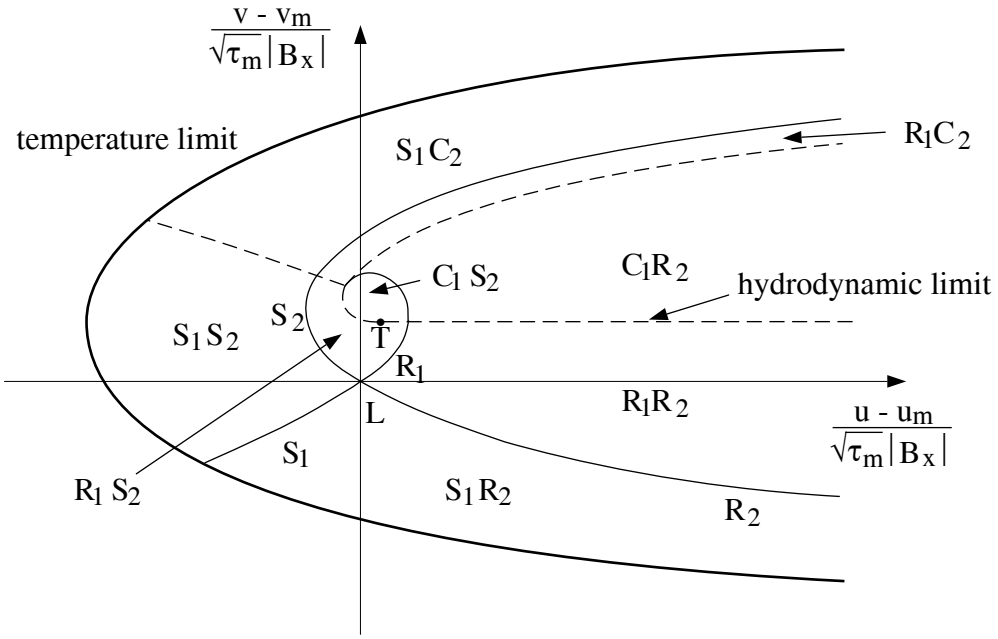

Figure 4.13: A diagram in the velocity space. Compare with Fig. 4.9 (b).

For left-running and right-running rarefaction waves, we have

$$\frac{x}{t} \;=\; \frac{dx}{dt} = u + \epsilon c_{f,s}. \tag{4.95}$$

Since r is function of q through simple waves and

$$c_{f,s}^2 = \tau_L B_x^2 r_L{}^{\frac{1}{\gamma}} r^{\frac{\gamma-1}{\gamma}} q_\pm, \quad J_{u\pm} = u - \epsilon \frac{\sqrt{\tau_L}|B_x|}{\gamma} r_L{}^{\frac{1}{2\gamma}} \int f_u(q)\, dq,$$

u and dx/dt are also function of q. By plotting u and x/t for $q_\pm$, we can obtain u profile in x at a time t. Similarly, v can be determined from

$$J_{v\pm} = v + \epsilon \frac{\sqrt{\tau_L}|B_x|}{\gamma} r_L{}^{\frac{1}{2\gamma}} \int f_v(q)\, dq. \tag{4.96}$$

On the other hand, the pressure p can be calculated by Eq. 4.29, and then it yields τ by constant entropy condition. Finally $B_\perp$ is determined by a relation 4.21.

4.12 Physical Interpretation of the Exact Riemann Solution

We have shown with mathematical rigor that the MHD Riemann problem, *in flatland*, is well-posed provided that $(\Delta u, \Delta v)$ are suitably restricted, implying that the solutions are always self-similar. The exact solution showed that the wave combinations are determined by the pressure and the magnetic field and the velocity differences. It can be checked that there are 289 different wave combinations; 256 cases where each of the four waves may be a shock, a compound wave, a rarefaction, or absent; 33 cases where two left-running waves could merge into a left-running overcompressive shock with any of the 16 configurations of right-running waves, and the mirror image of this is also possible. If we include the contact discontinuity, we have 578 different cases, which excludes the practical use of an exact MHD Riemann solver.

When $B_{\perp L} B_{\perp R} < 0$, there always exists a non-classical shock, either embedded in compound waves or corresponding to an overcompressive shock. Interestingly, even when $B_{\perp L} B_{\perp R} > 0$, the intermediate state can locate in the region with different $B_\perp$ sign, depending on given $(\Delta u, \Delta v) \in \mathbf{R}_{uv}$ values. For example, if $(p, B_\perp)_l = (p, B_\perp)_r$ and $B_{\perp m} B_{\perp l,r} < 0$, the solution is symmetric about the contact discontinuity and the magnetic field can change its sign twice. An example is given in Fig. 4.14. The Riemann data are $\rho_{L,R} = p_{L,R} = 1,\ B_{\perp L,R} = -1,\ \Delta u = \Delta v = 2.5$ with $\gamma = 5/3,\ B_x = 1$. A first-order numerical scheme with Roe's approximate Riemann solver is used[5]. The Riemann solution involves a non-evolutionary shock embedded in a fast compound wave. On the other hand, if $(\Delta u, \Delta v) \notin \mathbf{R}_{uv}$, which is a subset of $\mathbf{R}^2$, the complete solution to the Riemann problem does not exist since a vacuum will form in the flow.

[5] Note that it is built using conventional evolutionary waves.

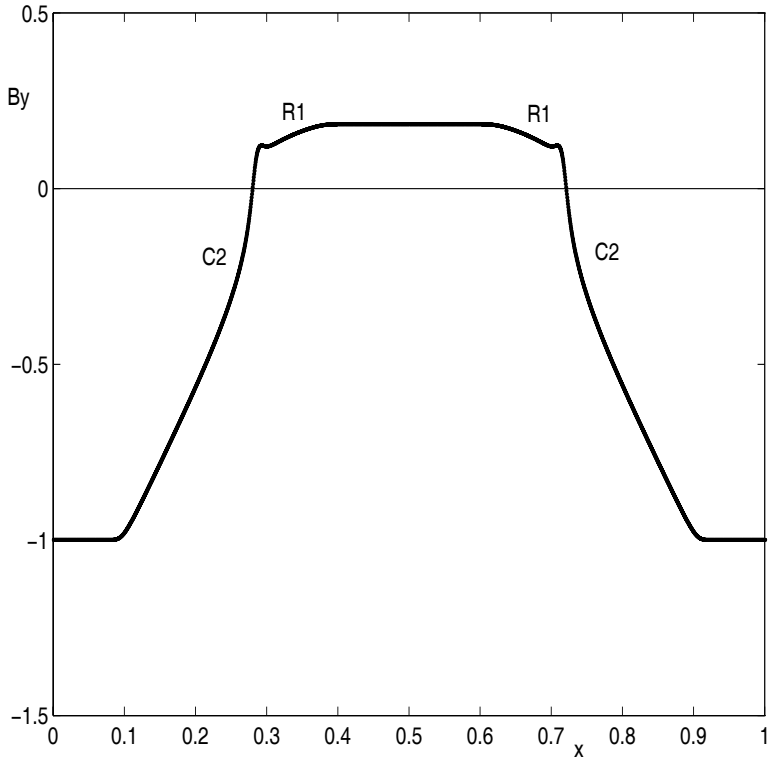

Figure 4.14: An example of the MHD Riemann problem involving the double change of $B_\perp$ sign.

However, the most important consequence of the study of the planar Riemann problem probably is the finding that all the complicated behaviors of nonlinear waves can be explained only in (U, V) domain, which will be of great help in investigating MHD processes[6].

[6] In fact, we demonstrate the direct correspondences $\Delta u \sim U$, $\Delta v \sim V$ in full MHD. In incompressible MHD, so-called Elsässer variables $z = v \pm B_\perp$ have been used that represent the dynamic alignment of v and $B_\perp$ [12, pages 193-194].

CHAPTER V

NON-PLANAR RIEMANN PROBLEM FOR 3×3 MODEL

Non-planar Riemann problems are of two types; coplanar problem with non-zero w components and non-coplanar problem. A distinction between two types can be highlighted by introducing the transverse field moment defined as

$$I_z \equiv \int_{-\infty}^{\infty} w \, dx \, . \tag{5.1}$$

Starting from Eq. 2.41 and integrating them, we can derive the relation for the transverse field moment.

$$\frac{dI_z}{dt} + 2[uw] \;\; = \;\; 0 \, . \tag{5.2}$$

When end states are coplanar, I_z is globally invariant. But once the problem becomes non-coplanar, I_z is no longer invariant and is time-dependent.

In this chapter, keeping in mind the fundamental difference of the planar and the non-planar problem, we will explore the Riemann problem of the 3×3 model [88]. Most works are related to the uniqueness of the Riemann solution: entropy, admissibility conditions, and the existence of viscous profiles. By investigating the singularity near the triple umbilic point, we will demonstrate how Glimm's concern[1]

[1] "It is likely that new phenomena will occur with $n \times n$ system, $n \geq 3$, but this case has yet to be explored." [41, page 577].

and Keyfitz's argument[2] can be applied to the non-planar MHD Riemann problem. It turns out that the index theory of dynamical system ceases to work for the model system with $n = 3$ [3].

5.1 Rankine-Hugoniot Conditions

For the system 2.41, we have the following Rankine-Hugoniot conditions.

$$s[u] = 2c\bar{u}[u] + 2\bar{v}[v] + 2\bar{w}[w], \tag{5.3}$$

$$s[v] = 2\bar{v}[u] + 2\bar{u}[v], \tag{5.4}$$

$$s[w] = 2\bar{w}[u] + 2\bar{u}[w]. \tag{5.5}$$

Therefore, the Hugoniot and wave trajectories are all either coplanar ($v/w = \text{const.}$) or purely rotational ($u = \text{const.}, v^2 + w^2 = \text{const.}$).

5.2 Shock Types

For the system 2.41, there appear three waves which can be described using MHD terminology as slow, Alfvén and fast; their speeds are given by

$$\lambda_a = 2u, \qquad \lambda_{f,s} = (c+1)u \pm \sqrt{(c-1)^2u^2 + 4(v^2+w^2)} \tag{5.6}$$

always satisfying $\lambda_s \leq \lambda_a \leq \lambda_f$, and the right eigenvectors are

$$\mathbf{r}_a = \begin{vmatrix} 0 \\ w \\ -v \end{vmatrix}, \qquad \mathbf{r}_{f,s} = \begin{vmatrix} \frac{1}{2}\lambda_{f,s} - u \\ v \\ w \end{vmatrix}. \tag{5.7}$$

[2] "One must begin with a careful statement of some physical basis for studying a Riemann problem, including a recognition that a theory centered on Riemann problems can apply only in a situation in which only self-similar solutions are to be expected. For example, this is the case if one is looking either at a very large time or a very small one." [65, page 579].

[3] All the gasdynamic waves are one-dimensional in the direction normal to the wave front, meaning that $n = 1$. But in MHD, due to intermediate shocks, the problem becomes generally $n = 3$. The reason for this can be traced to the fact that electromagnetic waves are inherently non-planar.

For a shock arising in 3×3 model system, the signs of the following six parameters determine which of the MHD characteristics run into the shock:

$$(\lambda_{f,a,s})_{L,R} - s. \tag{5.8}$$

In MHD terminology, the signs can be represented by four domains I$\sim$IV defined as

$$\text{IV} \quad \lambda_s \quad \text{III} \quad \lambda_a \quad \text{II} \quad \lambda_f \quad \text{I}.$$

There are sixteen possible combinations, but only fourteen can actually arise in the model system, since IV $\rightarrow$ IV and I $\rightarrow$ I correspond to the right and left transport shocks which turn out to be absent in the MHD Hugoniot. The fourteen shocks are:

$$S_1\,(\text{II} \rightarrow \text{IV},\ \text{III} \rightarrow \text{IV}),\ S_2\,(\text{I} \rightarrow \text{III},\ \text{I} \rightarrow \text{II}),$$

$$E_1\,(\text{IV} \rightarrow \text{II},\ \text{IV} \rightarrow \text{III}),\ E_2\,(\text{III} \rightarrow \text{I},\ \text{II} \rightarrow \text{I}),$$

$$O\,(\text{I} \rightarrow \text{IV}),\ E\,(\text{IV} \rightarrow \text{I}),$$

$$X\,(\text{II} \rightarrow \text{III},\ \text{III} \rightarrow \text{II},\ \text{III} \rightarrow \text{III},\ \text{II} \rightarrow \text{II}).$$

The relationship between the speed of a shock and waves in the fourteen types of shocks is illustrated in Fig. 5.1. IS_1, IS_2 denote intermediate slow, fast shocks. Because the classification is based only on the geometry of characteristics, we need to determine which shocks are physically meaningful.

5.3 Admissibility Conditions

In chapter III, it is shown that linear theories are inappropriate for the non-strictly hyperbolic system. Therefore, we will introduce the viscosity admissibility condition, and at the same time consider an entropy-flux condition since in $n = 3$ system all viscous profiles are not necessarily stable. Then we will show that admissible shocks of 3×3 model system are regular shocks $S_1\,(\text{III} \rightarrow \text{IV})$, $S_2\,(\text{I} \rightarrow \text{II})$ and intermediate shocks $IS_1\,(\text{II} \rightarrow \text{IV})$, $IS_2\,(\text{I} \rightarrow \text{II})$, $O\,(\text{I} \rightarrow \text{IV})$, $X\,(\text{II} \rightarrow \text{III})$.

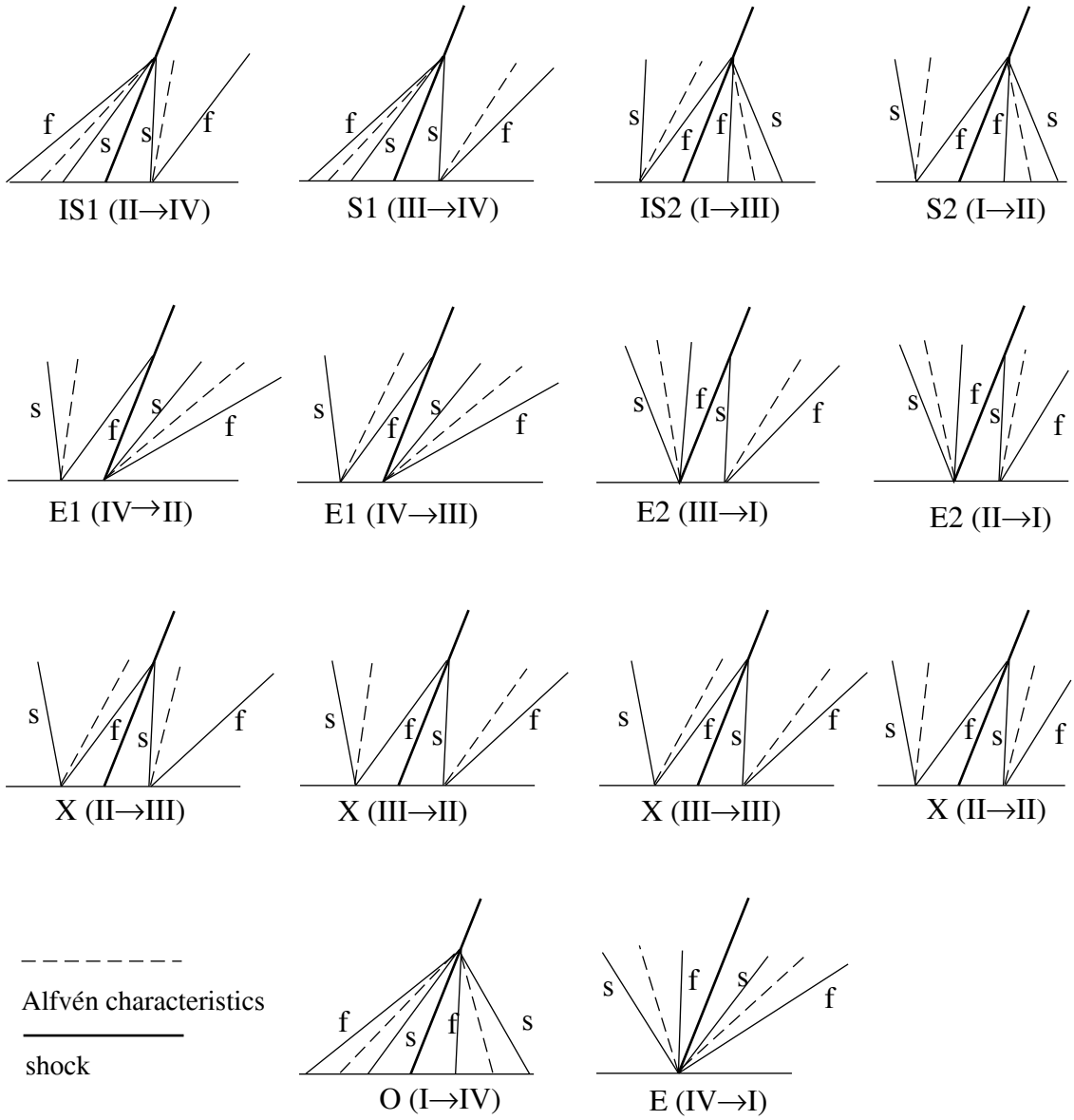

Figure 5.1: The relationship between the speed of a shock and characteristics

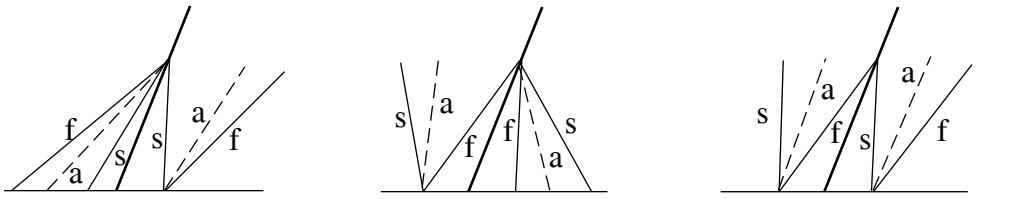

Figure 5.2: The relationship between the speed of evolutionary shocks and characteristics. In rotational discontinuity, characteristics of the same family are parallel each other.

5.3.1 Evolutionary Condition

In evolutionary theory, a discontinuity is evolutionary, in other words, physically relevant, if and only if the number of small amplitude outgoing waves diverging from the discontinuity is equal to the number of the boundary conditions minus one. Or a travelling step discontinuity is called linearly dynamically stable if the linearized Rankine-Hugoniot equation has a unique solution for $t \geq 0$ [35]. The evolutionary condition restricts the permitted shocks to those having two diverging characteristics, that is, $S_1\,(\mathrm{III} \rightarrow \mathrm{IV})$, $S_2\,(\mathrm{I} \rightarrow \mathrm{II})$ and $X\,(\mathrm{II} \rightarrow \mathrm{III})$. But, in order to ensure the uniqueness we need another condition on $X\,(\mathrm{II} \rightarrow \mathrm{III})$ shocks since they can in general change u and $(v^2 + w^2)$ as well as the angle. Thus, only possible X shock is the so-called *rotational discontinuity*. In the framework of evolutionary theory, the Riemann solutions of 3×3 model consist of regular planar shocks and a rotational discontinuity. The relationship between the speed of evolutionary shocks and characteristics is summarized in Fig. 5.2. The conclusion can be stated straightforwardly that the magnetic field can change its sign only through the rotational discontinuity.

5.3.2 An Entropy Condition

For either the 3×3 or 2×2 systems there is unique quadratic function that is conserved in smooth regions of the flow, and can serve as an entropy for the system. It is simply $e = (u^2 + r^2)/2$ and in smooth regions it satisfies the conservation law

$$e_t + h_x = 0\,, \tag{5.9}$$

with an entropy flux $h = 2u(cu^2/3 + r^2)$. Here, a vector $(v, w) = (r\cos\theta, r\sin\theta)$ is introduced. Across shocks, this entropy is dissipated, and it can be shown that

$$\frac{\partial}{\partial t}\int_{x_L}^{x_R} e\,dx = h(x_L) - h(x_R) + \frac{[u]}{2}\left\{\frac{c}{3}[u]^2 + [v]^2 + [w]^2\right\}. \tag{5.10}$$

For all compressive waves, $u_L > u_R$. Thus, all compressive waves are entropy-dissipative. Note that no entropy dissipation is predicted for Alfvén waves.

When dissipation is included in the governing equations, the entropy evolution equation becomes

$$e_t + h_x = \mu\{e_{xx} - u_x^2 - r_x^2 - r^2\theta_x^2\}. \tag{5.11}$$

Here, μ, η are assumed to be equal. In the brackets, the first term leaves entropy conserved, but the remaining terms dissipate it, including the last term which provides dissipation through rotation.

5.3.3 Viscous Profiles

By setting $\mu = \eta$ and $\chi = 0$, the dynamical system of the 3×3 model system can be written as the ordinary differential equations.

$$\begin{pmatrix} u \\ v \\ w \end{pmatrix}_\xi = \begin{pmatrix} cu^2 + v^2 + w^2 - ({cu_L}^2 + {v_L}^2 + {w_L}^2) - s(u - u_L) \\ 2(uv - u_L v_L) - s(v - v_L) \\ 2(uw - u_L w_L) - s(w - w_L) \end{pmatrix} \tag{5.12}$$

The boundary conditions are

$$\lim_{\xi\to-\infty}\mathbf{u}(\xi)=\mathbf{u}_L,\quad \lim_{\xi\to\infty}\mathbf{u}(\xi)=\mathbf{u}_R,\quad \mathbf{u}_\xi(\pm\infty)=0. \tag{5.13}$$

The travelling wave solutions can exist only if $\mathbf{u}_{L,R}$ lie on the same Hugoniot curve, in which case they are also singular points of the o.d.e. system. Therefore, for any non-coplanar Riemann problem involving changes of u and r one can not anticipate single travelling wave solution, because the Hugoniot curves are all either coplanar or purely rotational. For the coplanar problem, we can obtain the phase portrait of the 3×3 dynamical system by using the local approach. Like the planar problem, there are generally four singularities in finite domain, representing four reference state I$\sim$ IV. Since the local topology near singularities depends on the sign of $\lambda_{f,a,s}-s$ and it must be identical with the phase portrait in planar limit, shown in Fig. 3.5, four states can be determined in the topology as

$$\text{I(Na), II(S), III(S), IV(Nr).}$$

A theory centered on Riemann problems can apply only in a situation in which only self-similar solutions are to be expected. For example, this is the case if one is looking either at a very large time or a very small one. A typical phase portrait is given in Fig. 5.3. It can be found that

$$\text{regular planar shocks (III} \to \text{IV, I} \to \text{II) and}$$

$$\text{intermediate shocks (II} \to \text{IV, I} \to \text{III, I} \to \text{IV, II} \to \text{III),}$$

six in total, are physically admissible. Other shocks IV $\to$ II, IV $\to$ III, III $\to$ I, I $\to$ I, and IV $\to$ I are obviously inadmissible and III $\to$ II shock is non-physical since it violates entropy-flux condition $[u]<0$. In particular, the rotational discontinuity, which is a special case of II $\to$ III shock, III $\to$ III, and II $\to$ II shocks are

inadmissible since these shocks contradict the inadmissibility of undercompressive shocks in the planar problem.[4] The relationship between the speed of a shock and characteristics is summarized in Fig. 5.4.

On the other hand, we can obtain an exact solution for overcompressive and undercompressive shocks. It may be verified that the following solution

$$\begin{aligned} u &= -u_0 \tanh(2u_0 x/\mu), \\ v &= -v_0 \tanh(2u_0 x/\mu) + C w_0 \operatorname{sech}(2u_0 x/\mu), \\ w &= -w_0 \tanh(2u_0 x/\mu) - C v_0 \operatorname{sech}(2u_0 x/\mu) \end{aligned} \tag{5.14}$$

is a solution of the system 5.12 for a stationary shock $s = 0$, provided

$$C^2 = 1 + (c-2)\frac{u_0^2}{v_0^2 + w_0^2}$$

This represents a viscous profile for an intermediate shock with $r_0^2 > (2-c)u_0^2$. The transverse vector rotates through the wave. In the v, w-plane, it traces an ellipse whose major and minor axes are in the ration $C : 1$. Note that C can have either sign, corresponding to two senses of rotation around the ellipse. This special solution shows how the internal structure of an overcompressive shock can cause the rotation usually associated with Alfvén waves.

Without loss of generality, let $w_0 = 0$, so that the wave is polarized in the x, y plane. Then, a transverse field moment

$$I_z = -C(\mu\pi/2)v_0/u_0. \tag{5.15}$$

Initial data not satisfying this constraints must give rise to additional waves. An overcompressive shock necessarily satisfies $r_0 \leq \sqrt{c}u_0$, so that $1 < 2(c-1)/c \leq C^2$.

[4] Or these shocks are structurally unstable because they all are characterized by the saddle-saddle connection in (v, w) domain.

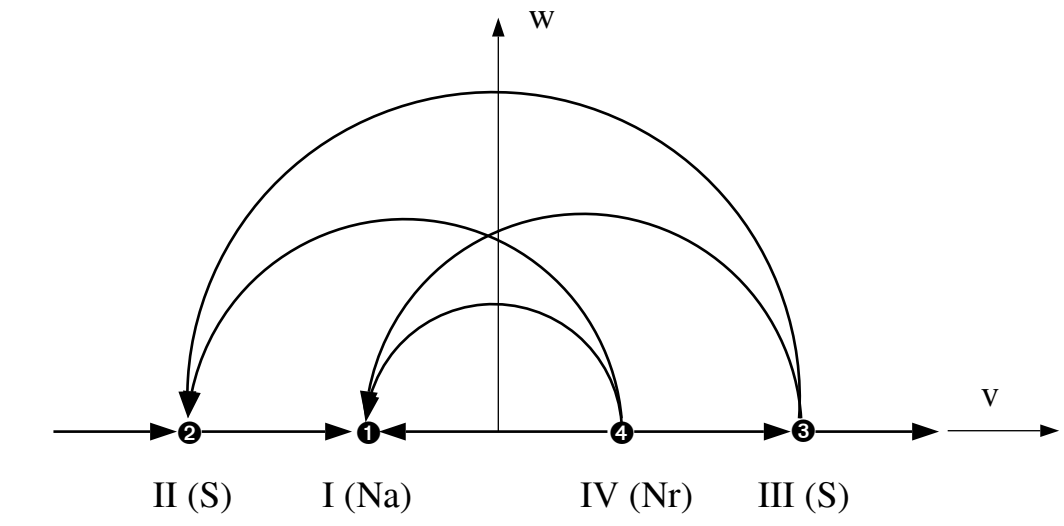

λ_f - s	+	−	+	+
λ_a - s	−	−	+	+
λ_s - s	−	−	+	−

Figure 5.3: The phase portrait of the 3×3 system in (v, w) domain. Compare with examples of the phase portraits of the planar model problem.

Note that solutions with $u_R > u_L$ must be abandoned in viscous profiles since they violate the entropy-flux condition.

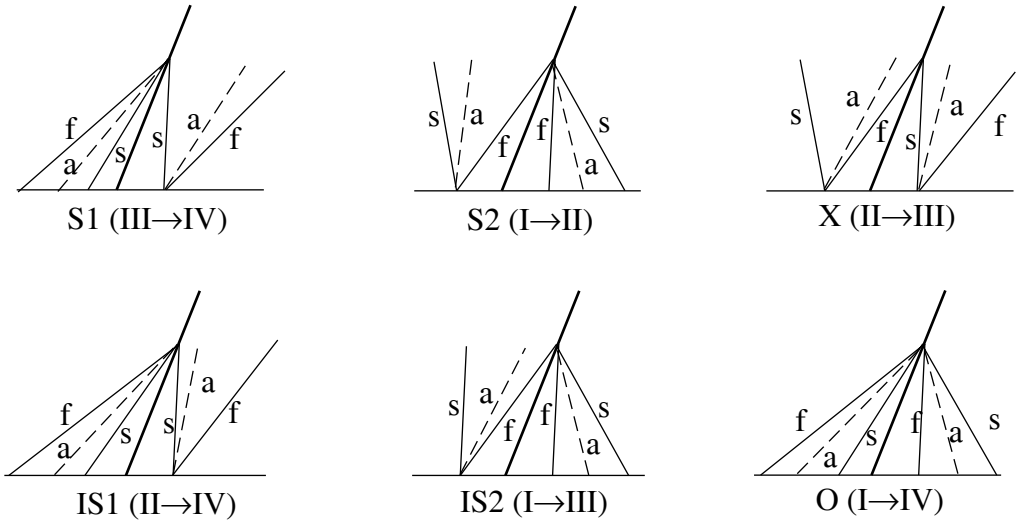

Figure 5.4: The relationship between the speed of shocks having viscous profiles and characteristics

5.4 Solution of the Riemann Problem for the 3×3 Model

We now consider in more detail the proposal [88] to generate the large time or small time Riemann problems for the 3×3 model from those for the planar problem. If we employ the *polar* form of the 3×3 model 2.41, we have

$$u_t + 2cuu_x + 2rr_x = \mu u_{xx} \tag{5.16}$$

$$r_t + 2ur_x + 2ru_x = \eta(r_{xx} - r\theta_x^2) - \chi(r\theta_{xx} + 2r_x\theta_x) \tag{5.17}$$

$$\theta_t + 2u\theta_x = \chi(r_{xx}/r - {\theta_x}^2) + \eta(\theta_{xx} + 2r_x\theta_x/r) \tag{5.18}$$

From the system 5.7, it is easy to see that the fast and slow waves have no effect on θ, and are solutions of the *reduced* coplanar problem in which

$$\mathbf{u} = \begin{vmatrix} u \\ r \end{vmatrix}, \qquad \mathbf{f} = \begin{vmatrix} cu^2 + r^2 \\ 2ur \end{vmatrix}. \tag{5.19}$$

Alfvén waves have no effect on u or r, and in the absence of dissipation are governed by the scalar advection equation

$$\theta_t + 2u\theta_x = 0. \tag{5.20}$$

We might therefore suppose that a Riemann problem for the system 2.41, with data $\mathbf{u}_L = (u_L, v_L, w_L), \mathbf{u}_R = (u_R, v_R, w_R)$ could be solved by the following procedure. Re-express the data as $\mathbf{u}_L = (u_L, r_L, \theta_L), \mathbf{u}_R = (u_R, r_R, \theta_R)$, and for given (u_L, r_L) and (u_R, r_R), solve the coplanar Riemann problem with this data and then insert an Alfvén wave of strength $\theta_R - \theta_L$. There is ambiguity in this procedure because we can represent either given state in one of two polar representations $(r \to -r, \theta \to \theta + \pi)$. Thus we can choose to solve the coplanar problem with r_L, r_R either of the same sign or opposite signs. The Riemann solutions that result never coincide unless one or both of $r_{L,R}$ vanish.

To eliminate this ambiguity we impose the very simple requirement that the solution can be mapped into physical space. Thus, the coplanar solution will define u as a function of the similarity variable $x' = x/t$, and the Alfvén wave needs to be inserted where

$$F(x') = 2u(x') - x' = 0. \tag{5.21}$$

We assert that Eq. 5.21 always has precisely one root, which occurs either in the uniform region between the waves (if $r_L r_R \geq 0$) or else inside a shock that reverse the sign of r (if $r_L r_R < 0$). If the Alfvén wave coincides with a shock, the combined jump does not satisfy the Hugoniot relations unless the data are coplanar, *i.e.*

$$\frac{v_L}{w_L} = -\frac{v_R}{w_R}. \tag{5.22}$$

Therefore, for non-coplanar data, the solution to the 3×3 Riemann problem at large times is given by inserting a Alfvén wave into the reduced 2×2 problem. For coplanar data there are two solutions, one of which effects the rotation by a π Alfvén wave, the other through a non-classical shock. We argue that the non-classical solutions are relevant in particular at the small time, and an Alfvén wave[5] is needed

[5]It is not necessarily the rotational discontinuity. Also, it can not be self-similar, since such

in the large-time solution. The plausibility of this argument will be given in the next section by considering canonical cases.

5.5 Canonical Cases

For the coplanar problem, there is a jump across which $u \to -u, v \to -v$ and $w_{L,R} = 0$. Since $\bar{u} = \bar{v} = 0$, the Hugoniot relationships give $s = 0$. The wavespeeds change according to

$$\lambda_{sR} = -\lambda_{fL}, \quad \lambda_{fR} = -\lambda_{sL} \tag{5.23}$$

The wave is overcompressive if $\lambda_{sL} > 0$; this happens if $\sqrt{c}u_L > v_L > 0$. Otherwise it is an undercompressive shock. Although such a jump satisfies the Hugoniot relationships, it decays into a pair of rarefaction waves, followed by a reversal shock along the line $\sqrt{c}u_L = v_L$ in planar limit. This special case of a reversal shock is called a *triple shock* [54]. It can be regarded as a stationary slow shock from $\mathbf{u} = \mathbf{u}_L$ to $\mathbf{u} = 0$, followed by a stationary fast shock from $\mathbf{u} = 0$ to $\mathbf{u} = \mathbf{u}_R$. Both of the component shocks and the overall jump satisfy the Hugoniot conditions. If the same data is presented to the restricted coplanar problem, u changes sign, but v does not. The solution is then a slow regular shock, followed by an Alfvén wave, and then a fast regular shock. The value of v in the Alfvén wave can be calculated from the Hugoniot relations as

$$v_m = \frac{1}{3}\left[2\sqrt{3cu_L^2 + 4v_L^2}\cos\frac{\delta}{3} + v_L\right], \quad \delta = \cos^{-1}\left[\frac{v_L((27-9c)u_L^2 - 8v_L^2)}{(3cu_L^2 + 4v_L^2)^{\frac{3}{2}}}\right] \tag{5.24}$$

The solutions in canonical cases are illustrated in Fig. 5.5. Introducing a non-dimensional parameter

$$I_z{}^* \equiv \frac{I_z}{(\pi/2)\mu} \tag{5.25}$$

waves violates a constraint $\frac{\partial}{\partial t}(\frac{x}{t}) < 0$ [94, page 85].

we can compare I_z^* for three different solutions. By using Eqs. 5.15 and 5.25, the following relation is always satisfied.

$$I_z{}^*{}_{planar}(=0) \;<\; I_z{}^*{}_{O,X} \;<\; I_z{}^*{}_{S_1AS_2} \tag{5.26}$$

In addition, we can calculate the rate that the entropy is dissipated across the discontinuity. For the first case,

$$\sum_{S_1,S_2} \frac{\partial E}{\partial t} \;<\; \frac{\partial E}{\partial t}\Big)_O, \tag{5.27}$$

and for the second case,

$$\sum_{S_1,S_2} \frac{\partial E}{\partial t} \;<\; \frac{\partial E}{\partial t}\Big)_X \;<\; \sum_{C_1,C_2} \frac{\partial E}{\partial t}, \tag{5.28}$$

where $E \equiv \int_{-\infty}^{\infty} e\, dx$. Notice that non-classical shocks experience a relatively high entropy dissipation rate.

5.6 The Effect of Non-Coplanarity and Dispersive Coefficient

In Section 5.4, we showed how Riemann solutions for the 3×3 model are generated from those for the coplanar subproblem. By imposing the simple requirement, we proved that an Alfvén wave must either be within a shock, which reverses the sign for v, or else in the central uniform region. In order to see how Alfvén waves in two different situations (one within a shock and the other in the central uniform region) are related, we will consider the following problems.

First, starting from an stationary coplanar overcompressive shock with $I_z^* = \sqrt{c-1}$, we apply a very small non-coplanar variation on the upstream state. (But this variation has an infinite I_z^*.) Here, since we are interested in a global picture of the non-coplanar solution, we will not consider finite I_z^* disturbances.

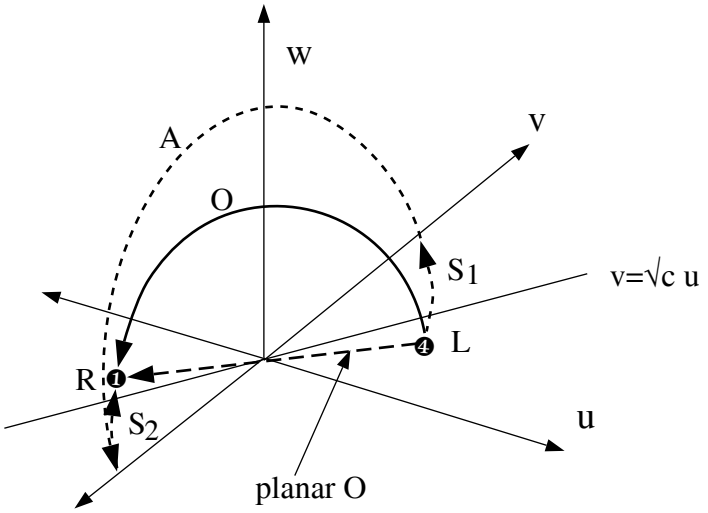

(a) $0 < v_L < \sqrt{c}\, u_L$

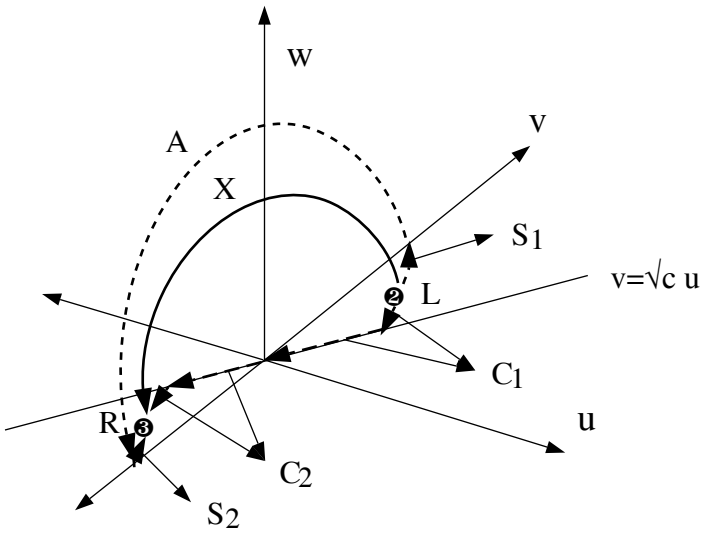

(b) $0 < \sqrt{c}\, u_L < v_L$

Figure 5.5: Riemann solutions in two canonical cases.

Next, starting from the shock profile, we apply the dispersive coefficient. This will enable us to examine the effect of the non-dissipation coefficient on exotic shocks. For numerical calculations, a conventional two-step Lax-Wendroff scheme is used [97]. To reduce numerical dissipation, we used a large number of grid points (*e.g.* 2000).

5.6.1 Non-Coplanarity

In the beginning of this chapter, we showed that once the problem becomes non-coplanar, I_z is no longer invariant and is time-dependent. In fact, the exact solution of coplanar Riemann problem given in Section 3.8 is valid only for sufficiently small I_z and thus can be regarded as the neighboring solution of the coplanar problem with large I_z and the non-coplanar problem near π rotation. Therefore, we can deduce that intermediate shocks in the coplanar situation become time-dependent by any non-coplanar variation in the left and right states. This can be confirmed by numerical results described in Fig. 5.6 (a). This numerical code has dissipation but no dispersion. Solutions are shown at regular time intervals. As seen in Fig. 5.6 (a), an overcompressive shock is broken up into three waves, two regular shocks and an intermediate shock, and eventually the intermediate shock becomes an Alfvén wave. From this analysis, we propose a hypothesis,

Proposition 1. *Intermediate shocks are unstable under any non-coplanar variation on the upstream and downstream states, so that the large-time solution contains only regular shocks, but that all exotic shocks are needed to explain small-time behavior.*

This hypothesis can be also supported by observing that for very small non-coplanar variations, $dI_z/dt \approx 2\mu$, explaining that the solutions evolves in the direction of increasing I_z.

5.6.2 Dispersive Coefficient

Under the dispersive coefficient intermediate shocks persist in the large-time solution. This situation is shown in Fig. 5.6 (b). Even though the initial overcompressive shock is broken up into three waves as the previous case, the time-dependent intermediate shock (undercompressive) does not turn into an Alfvén wave. Therefore, we may conclude that the intermediate shock with π rotation angle can be sustained by dispersive effects. This conclusion can be confirmed by considering a dynamical system including the dispersive effects. Let us introduce $(\eta, \chi) = \mu' e^{i\psi}$, $\sigma = \mu'/\mu$ where $-\pi/2 \le \psi \le \pi/2$. Then a dynamical system of the 3×3 model can be written as

$$D \begin{pmatrix} u \\ v \\ w \end{pmatrix}_{\xi} = \begin{pmatrix} [cu^2 + v^2 + w^2] - s[u] \\ [2uv]\cos\psi + [2uw]\sin\psi - s([v]\cos\psi + [w]\sin\psi) \\ -[2uv]\sin\psi + [2uw]\cos\psi - s(-[v]\sin\psi + [w]\cos\psi) \end{pmatrix} \quad (5.29)$$

where $[Q] = Q - Q_L$ and $D = \left((1,0,0)^T, (0,\sigma,0)^T, (0,0,\sigma)^T\right)$. It can be shown that a class of data such that $\mathbf{u}_R = -\mathbf{u}_L$, $s = 0$ is the singularity of the dynamical system. However, once non-coplanar variations are applied to the upstream and downstream states, intermediate shocks can not persist as in the purely dissipation case.

5.7 Well-posedness of the Riemann Problem

In chapter III and IV, we proved that the Riemann problem of planar model and MHD system is well-posed and all admissible shocks are time-independent. In this chapter, however, we found totally different results for the non-coplanar Riemann problem. In the coplanar problem, the solutions of the Riemann problem depend not only on $\mathbf{u}_{L,R}$ but also on I_z, though all shocks are still time-independent. By considering canonical cases, it is demonstrated that the Riemann solutions exist

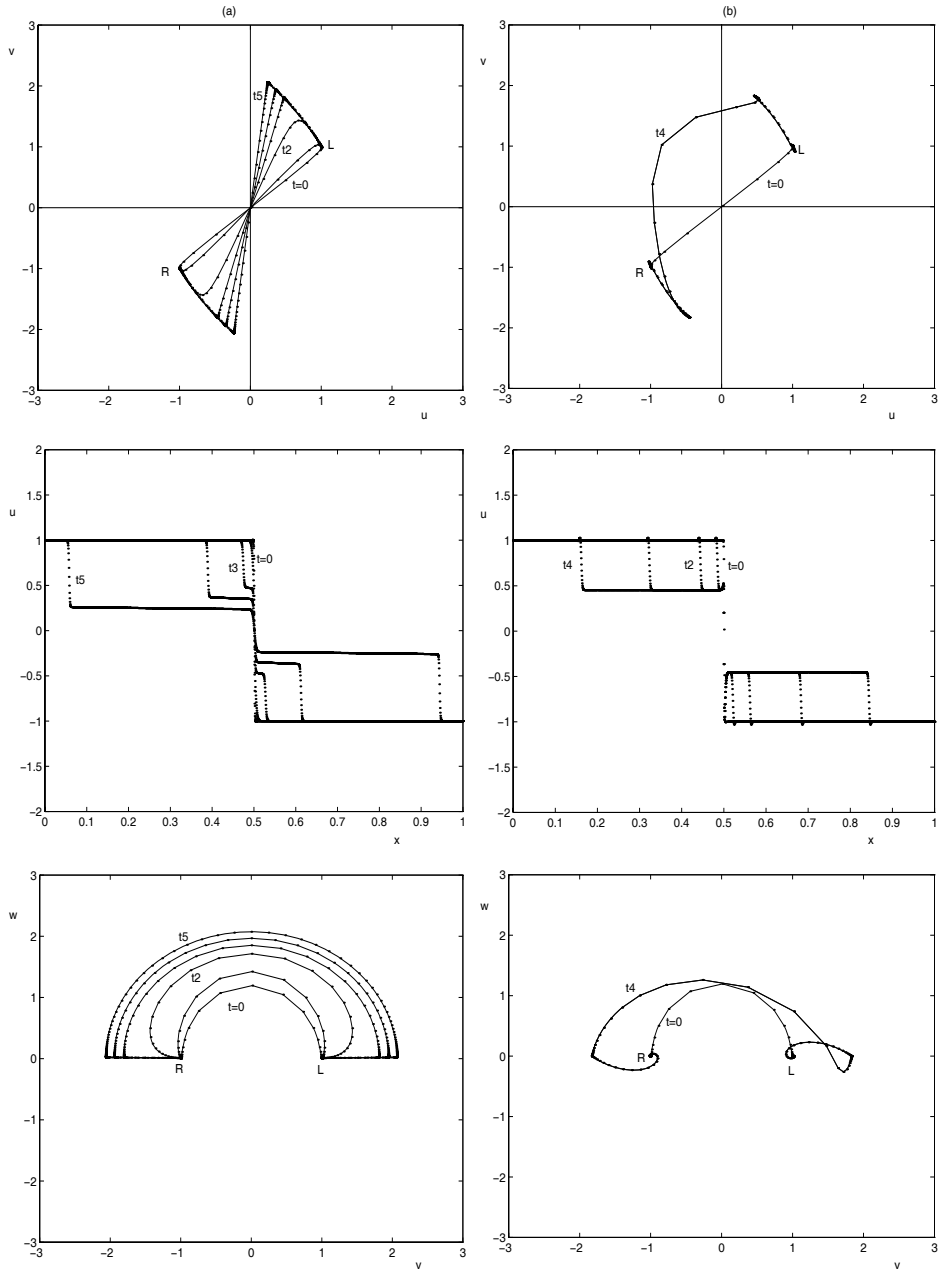

Figure 5.6: (a)-(b). Evolution of overcompressive shock structure under non-coplanar variation on downstream states and dispersive coefficient: (a) very small non-coplanar variation ($\mu = \eta = 0.002, \chi = 0$), (b) dispersive effect ($\mu = \eta = 0.001, \chi = 0.002$). t_2, t_4 and t_5 indicate the time at two, four and five intervals, respectively.

but they are not necessarily unique. In non-coplanar problem, we can anticipate the self-similar Riemann solution only at the very small time (regular planar and intermediate shocks) and the very large time (only regular planar shocks), implying that the Riemann problems have a meaning only at a very small or large time.

CHAPTER VI

NONLINEAR EVOLUTION OF MHD SHOCK WAVES

One of the important consequence of the study of 3×3 non-planar Riemann problem is that for given left and right states the evolution of waves is highly nonlinear and sometimes may undergo an abrupt change in configuration, depending on the transverse field moment, even though all such time-dependent phenomena will disappear at the very large time. Since many interesting phenomena arising in plasmas, for example, magnetic substorm, and disruptive processes in thermonuclear fusion reactor, are inherently time-dependent problem, we expect that the investigation of nonlinear evolution of finite amplitude waves is of critical importance.

In general, there are several effects which may add essential modification to the nonlinear evolution of waves. All are related to the modification of $\int_{-\infty}^{\infty} \mathbf{u}\, dx$. These are of two types: self-consistent driving mechanism and external disturbances. In this chapter, we discuss how finite amplitude waves develop nonlinearly when they are subject to drivers and disturbances. We consider the 3×3 model system and extract information on the nonlinear evolution of MHD waves, by showing the relationship between the model and MHD. The analysis tools are numerical experiments and the analytical results on the 3×3 Riemann problem given in the previous chap-

ter. Among the 17 cases in the planar limit and several effects, only a few have been actually tested numerically since we restrict our interests to the general understanding of nonlinear evolution of waves. More details will be available only after through investigations are made.

6.1 Relationship between 3×3 Model and MHD

The physical and mathematical reasoning for approximating 7×7 MHD system by 3×3 model system rests on the surprising simplicity of MHD system that MHD waves are symmetric about the contact discontinuity which always moves with the fluid particle. Therefore, when $c = \gamma + 1$ and the reference states of MHD Riemann problem lie near the umbilic point[1], the behavior of waves found in model system and MHD system is identical. The correspondence of two systems can be summarized as

$$\text{variable} \qquad u \qquad U-1 \quad \text{or} \quad \sqrt{U}-1 \tag{6.1}$$

$$\text{variable} \qquad v \qquad \frac{B_y}{B_x} \tag{6.2}$$

$$\text{variable} \qquad w \qquad \frac{B_z}{B_x} \tag{6.3}$$

$$\text{energy} \qquad \tfrac{1}{2}(u^2+v^2+w^2) \qquad \frac{p}{\gamma-1} + \frac{{B_y}^2+{B_z}^2}{2} \tag{6.4}$$

$$\text{entropy} - \text{flux condition} \qquad [u] < 0 \qquad [p] < 0 \tag{6.5}$$

$$\text{shock speed} \qquad s \qquad m \tag{6.6}$$

$$\text{parameters} \qquad \lambda_{f,a,s} - s \qquad \frac{c_{f,a,s}}{\tau} - \epsilon m \tag{6.7}$$

$$\text{critical curves} \qquad v = \pm\sqrt{c}u \qquad TC^* \tag{6.8}$$

Notice that $\frac{p}{\gamma-1} + \frac{{B_y}^2+{B_z}^2}{2}$ is an essential energy since the velocity and the density profiles in the Riemann problem depend on the pressure and the magnetic field profiles.

[1] Exactly, within PC^*U^* critical curve in Fig. 4.6.

In conclusion, all the properties (Hugoniot curve, integral curve, critical curve and point, shock types, eigensystem, solution patterns) are the same. Differences are found only in limiting cases: vacuum, absolute temperature and hydrodynamic limits.

6.2 Mathematical Formulation of Shock Evolution Under External Disturbances

6.2.1 Self-Consistent Driving Mechanism

There may exist a non-equilibrium distribution of plasma which supplies free energy to plasma waves. This problem can be described as the evolution of waves under a driver modeling a micro-instability. In our framework, the resulting equations can be obtained by adding source terms to equations of the magnetic field. That is,

$$u_t + (cu^2 + v^2 + w^2)_x = \mu u_{xx}, \tag{6.9}$$

$$v_t + (2uv)_x = \eta v_{xx} - \chi w_{xx} + \int G(x - x')v(x')\,dx', \tag{6.10}$$

$$w_t + (2uw)_x = \chi v_{xx} + \eta w_{xx} + \int G(x - x')w(x')\,dx', \tag{6.11}$$

where $G(x)$ is related to the source such that its Fourier transform corresponds to the growth rate. In the field of space plasma physics, many studies have been done for a model problem consisting of the second and third equations together with $u = (v^2 + w^2)/2$ [47, 78].

6.2.2 External Disturbances

In many circumstances, there exist external disturbances which add various forms of energy to plasma waves. For example, in astrophysical problems, thermal and kinetic energy can be added to galaxy system by the explosion of stars [85]. Also, inflow of an unsteady solar wind into the magnetosphere can be regarded as such

disturbance. As we can see from the definition of total energy, there are three types of energy: internal, kinetic and magnetic energy. Since the kinetic energy is determined by the distribution of $p, B_\perp$, the problem reduces to the study of disturbances on the pressure and the magnetic field. Therefore, in this case, the resulting equations may be written as

$$\mathbf{u}_t + \mathbf{f}_x = D\mathbf{u}_{xx} + \mathbf{S}\,, \tag{6.12}$$

where $\mathbf{S}$ represents the external disturbances[2] to u, v, w applied instantly at a certain time which are a form,

$$\sum_i \mathbf{A}_i \mathrm{sech}\left(\mathbf{B}_i(x - x_i)\right), \tag{6.13}$$

not affecting left and right states. The equations will give interesting information on how under such disturbances the global solutions change and how thermal and magnetic energies are redistributed.

6.3 Patterns of Nonlinear Evolution

In this study, we consider only the nonlinear evolution of waves under the disturbance of w in two canonical cases explained in Section 5.5. (The dispersive Hall effect is neglected.) Starting from stationary coplanar exotic shocks with $I_z^* = \sqrt{c-1}$, we apply instantly a disturbance of w at time t_o expressed as $A\,\mathrm{sech}\left(B(x - st_o)\right)$.

In Fig. 6.1, the nonlinear evolution of stationary overcompressive and undercompressive shocks are summarized. In an overcompressive shock, the solution becomes planar O, coplanar O, and S_1XS_2 in order of increasing I_z. When non-coplanar variations are applied, all have the same asymptotic solution S_1AS_2, which confirms the proposition I given in Section 5.6. In an undercompressive shock, the pattern becomes

[2] In general, they can be any function of x and t.

more complicated. The solution becomes planar C_1C_2, coplanar X, R_1XR_2, ${C_1}^*X{C_2}^*$ in order of increasing I_z, where ${C_1}^*, {C_2}^*$ represent reversed slow, fast compound waves. Finally, combining these results with the decrease of $\partial E/\partial t$ in order of increasing I_z and positive dI_z/dt for non-coplanar situation, we may summarize the complicated pictures on nonlinear evolution of waves in a framework illustrated in Fig. 6.2.

In the planar problem, the evolution of waves can be described by the Riemann solutions which are always self-similar. The associated shocks are time-independent and yield the maximum entropy dissipation rate. In the coplanar problem, the evolution of waves becomes more complicated, since it depends on I_z. Like the planar problem, all shocks are time-independent. In the non-coplanar problem, the feature of evolution of nonlinear waves can be distinguished largely in time: very small, intermediate and very large. At a very small time, that is, before the viscosity works, associated waves are planar shocks and Alfvén waves when $v_Lv_R > 0$, and are planar shocks and intermediate shocks when $v_Lv_R < 0$. At an intermediate time, that is, during which the viscosity works actively, the Riemann solutions are not self-similar, so that time-dependent intermediate shocks evolve continuously. Therefore, in this region, the evolution and structure of nonlinear shocks are highly coupled. At a very large time, that is, after the effect of the viscosity is almost gone, only planar shocks survive, and all the complicated phenomena related to time-dependent intermediate shocks are gone, leaving a broad Alfvén wave.

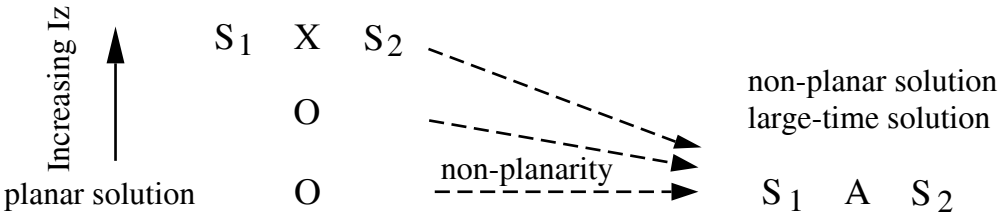

(a) Stability of a steady-state overcompressive shock (O)

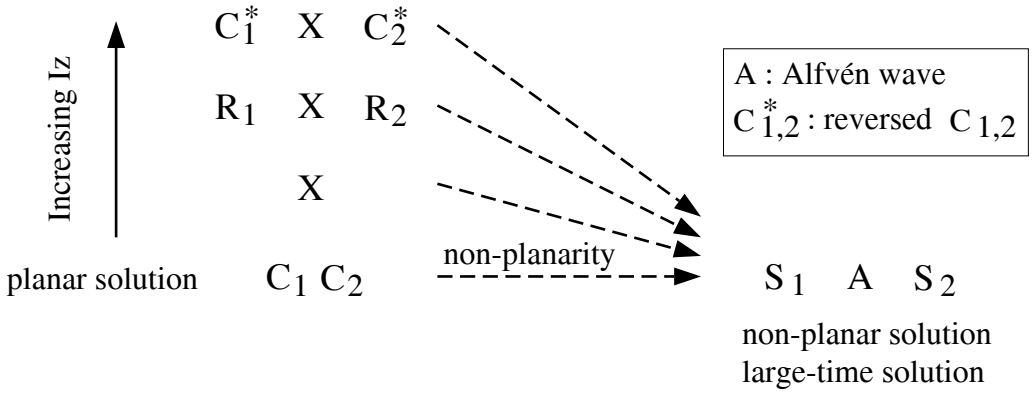

(b) Stability of a steady-state undercompressive shock (X)

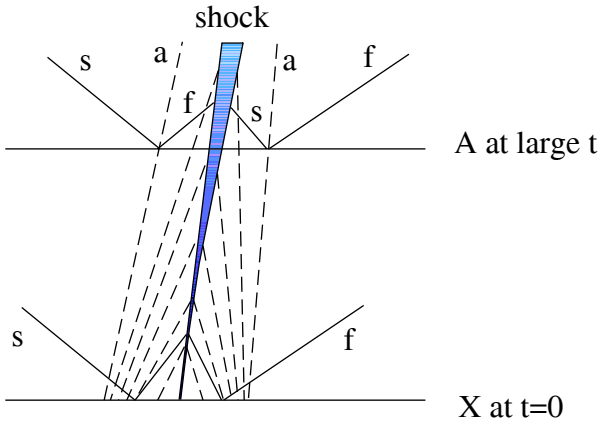

(c) Relationship between X & A and characteristics

Figure 6.1: The evolution of stationary overcompressive and undercompressive shocks under external disturbances.

property / problem	Iz	$\frac{\partial E}{\partial t}$	evolution pattern		
planar	zero	maximum	Riemann problem is well-posed. All shocks are time-independent self-similar.		
coplanar	finite	medium	Riemann solutions depend on the left and the right states, and also on Iz. All shocks are time-independent and self-similar.		
non-coplanar	infinite	minimum	small t	intermediate t	large t
			Planar shocks (same v sign). Intermediate shocks (opposite v sign). Before viscosity works.	Planar shocks. Not self-similar, time-dependent Intermediate shocks (opposite v sign). Viscosity is acting.	Planar shocks (self-similar) + Broad Alfvén wave. After the effect of viscosity is gone.

Figure 6.2: The patterns of nonlinear evolution of waves.

CHAPTER VII

NUMERICAL METHODS FOR MHD

Non-ideal MHD, which can be expressed as a set of equations which generalizes the Navier-Stokes equations by introducing the magnetic field, with the divergence-free condition on the magnetic field, contains advective, diffusive and dispersive terms. Like for the N-S equations, numerical methods for MHD which are developed from the viewpoint of continuum description, may be classified by two groups: conventional methods (for example, Lax-Friedrichs, Lax-Wendroff) and Godunov-type methods. Central to a wide variety of conventional methods is the use of different finite-difference approximations. For example, the Lax-Wendroff method is based on the Taylor series expansion. Therefore, it is assumed implicitly in all conventional methods that continuous solutions are always expected. In contrast, Godunov-type methods are based on the Riemann problem which describes the evolution of elementary waves such as shocks, contact discontinuity, and rarefaction waves. By the conservation property, the basic building blocks for the solution of Riemann problems in one dimension can be easily adapted to problems in higher space dimensions. Contrary to conventional methods, the discontinuity is included from the formulation.

Both methods have advantages and drawbacks, depending on the problem. In

particular, for high magnetic and kinetic Reynolds number flows which are of importance in many plasmas problems, Godunov-type methods show superb capability. Godunov-type methods have also a nontrivial problem: how to guarantee that numerical solutions converge to the correct solution, and that only physically relevant discontinuities are allowed in numerical solutions. In gasdynamics, it turns out that it is not difficult. An implementation of a simple geometric condition of shock admissibility works well. However, for MHD in which geometric conditions fail and the well-posedness of the Riemann problem is questioned, devising an accurate numerical method becomes a difficult task. For this reason, Wu [125] argued that numerical schemes based on the Riemann problem might be inappropriate for the MHD problem.

In this chapter, we consider some problems arising in developing Godunov-type methods for MHD, and then, using an extensive theoretical study on the MHD Riemann problem described in Chapters III$\sim$VI, we present a new approximate Riemann solver, which is remarkably simple and follows exactly the way to generate the large-time Riemann solution for the non-planar system from the well-posed planar problem.

7.1 An Eigensystem of the MHD System

The Eulerian conservative variables in MHD equations are

$$\mathbf{U}^T = (\rho,\, \rho u,\, \rho v,\, \rho w,\, B_y,\, B_z, E) \tag{7.1}$$

It is simpler to work in the primitive variables.

$$\mathbf{W}^T = (\rho,\, u,\, v,\, w,\, B_y,\, B_z,\, p) \tag{7.2}$$

Then right and left eigenvectors are

$$\mathbf{r}_c = \mathbf{M}\mathbf{r}_p, \quad \mathbf{l}_c = \mathbf{l}_p\mathbf{M}^{-1}, \tag{7.3}$$

where $\mathbf{M}$ is defined as $\Delta\mathbf{U}/\Delta\mathbf{W}$ and p, c denote primitive, conservative variables. $\mathbf{l}_p, \mathbf{r}_p$ are usually normalized such that $\mathbf{l}_p \cdot \mathbf{r}_p = \mathbf{I}$.

The eigenvectors can have some degeneracies:

(1) $B_x = 0$; (2) $B_y^2 + B_z^2 = 0$ with $c_a \neq a$; and (3) $B_y^2 + B_z^2 = 0$ with $c_a = a$.

In the first case, both c_a and c_s vanish, leading to degenerate left and right eigenvectors for the slow waves. In the second case, $c_f = a$, $c_s = c_a$, leading to degenerate eigenvectors for the Alfvén waves. In the last case, $c_f = c_a = c_s = a$, leading to degenerate eigenvectors for the slow and fast waves. In order to handle these degeneracies, a normalization is introduced by Roe and Balsara [100].

$$\alpha_f \equiv \frac{\sqrt{a^2 - {c_s}^2}}{\sqrt{{c_f}^2 - {c_s}^2}}, \quad \alpha_s \equiv \frac{\sqrt{{c_f}^2 - a^2}}{\sqrt{{c_f}^2 - {c_s}^2}}, \quad \beta_{y,z} \equiv \frac{B_{y,z}}{\sqrt{{B_y}^2 + {B_z}^2}}. \tag{7.4}$$

Using the identities,

$$c_f c_s = a\frac{|B_x|}{\sqrt{\rho}}, \quad \sqrt{{c_f}^2 - a^2}\sqrt{{c_f}^2 - {c_s}^2} = \frac{c_f}{\sqrt{\rho}}\sqrt{{B_y}^2 + {B_z}^2}, \tag{7.5}$$

$$\alpha_f^2 a^2 + \alpha_s^2 c_f^2 = c_f^2, \quad \alpha_s^2 c_s^2 + \alpha_f^2 a^2 = a^2, \tag{7.6}$$

left eigenvectors $\mathbf{l}_p$ are, in order of entropy, Alfvén, slow and fast waves,

$$\frac{1}{a^2}\Big(a^2,\ 0,\ 0,\ 0,\ 0,\ 0,\ -1\Big), \tag{7.7}$$

$$\frac{1}{2}\Big(0,\ 0,\ \mp\beta_z,\ \pm\beta_y,\ \beta_z/\sqrt{\rho},\ -\beta_y/\sqrt{\rho},\ 0\Big), \tag{7.8}$$

$$\frac{1}{2a^2}\Big(0,\ \pm\alpha_s c_s,\ \pm\alpha_f c_f \beta_y S,\ \pm\alpha_f c_f \beta_z S,\ -\alpha_f a\beta_y/\sqrt{\rho},\ -\alpha_f a\beta_z/\sqrt{\rho},\ \alpha_s/\rho\Big), \tag{7.9}$$

$$\frac{1}{2a^2}\Big(0,\ \pm\alpha_f c_f,\ \mp\alpha_s c_s \beta_y S,\ \mp\alpha_s c_s \beta_z S,\ \alpha_s a\beta_y/\sqrt{\rho},\ \alpha_s a\beta_z/\sqrt{\rho},\ \alpha_f/\rho\Big), \tag{7.10}$$

with $S \equiv \text{sign}(B_x)$. Right eigenvectors $\mathbf{r}_p^T$ are in same order

$$\Big(1,\ 0,\ 0,\ 0,\ 0,\ 0,\ 0\Big), \tag{7.11}$$

$$\Big(0,\ 0,\ \mp\beta_z,\ \pm\beta_y,\ \beta_z\sqrt{\rho},\ -\beta_y\sqrt{\rho},\ 0\Big), \tag{7.12}$$

$$\Big(\rho\alpha_s,\ \pm\alpha_s c_s,\ \pm\alpha_f c_f\beta_y S,\ \pm\alpha_f c_f\beta_z S,\ -\alpha_f a\beta_y\sqrt{\rho},\ -\alpha_f a\beta_z\sqrt{\rho},\ \alpha_s a^2\rho\Big), \tag{7.13}$$

$$\Big(\rho\alpha_f,\ \pm\alpha_f c_f,\ \mp\alpha_s c_s\beta_y S,\ \mp\alpha_s c_s\beta_z S,\ \alpha_s a\beta_y\sqrt{\rho},\ \alpha_s a\beta_z\sqrt{\rho},\ \alpha_f a^2\rho\Big). \tag{7.14}$$

7.2 A Divergence-Free Numerical Method

The problem of preserving $\nabla \cdot \mathbf{B} = 0$ condition has been considered crucial in developing numerical methods for MHD [14]. When we are trying to construct the one-dimensional Riemann solver for three dimensional flow, we can not assume a constant magnetic field in the direction of wave propagation. As a result, the Jacobian becomes an 8×8 matrix for eight variables including the magnetic field component in the direction of wave propagation. Unfortunately, it has been found that this 8×8 Jacobian has a messy eigensystem which makes it impossible to implement in numerical codes. This is due to the appearance of an 8th wave related to the behavior of $\nabla \cdot \mathbf{B}$ [95]. Furthermore, it turns out that there exist nonlinear resonances which makes the problem more difficult. For the 8×8 matrix, the eigenvalues are

$$0, \quad u, \quad u \pm c_a, \quad u \pm c_{f,s} \tag{7.15}$$

When u is 0 or $\mp c_a$, the speed of divergence wave coincides with that of entropy wave or Alfvén wave, but these coincidences do not affect the hyperbolic feature since all waves are linearly degenerate. In the case of magnetoacoustic waves, however, the nonlinear interaction rises in trans-magnetoacoustic flow, leading to a mathematical difficulty similar to the resonance occurring in nozzle flow of ordinary gasdynamics

[80, 75]. But this is a wrong approach to solve a wrong problem. Because varying magnetic field in the direction of wave propagation means that the divergence-free condition can not be satisfied locally in one-dimensional framework, we must include terms relating to $\nabla \cdot \mathbf{B}$ in fully three-dimensional flow. This was first noticed from numerical viewpoint by Powell [95, 96] by finding that the eigensystem can be remarkably simplified by adding terms relating to $\nabla \cdot \mathbf{B}$. From the complete set of equations for ideal MHD 2.14, which is valid for the non-zero $\nabla \cdot \mathbf{B}$ case, has a source term relating to $\nabla \cdot \mathbf{B}$. By taking this term into account, we can obtain the eigenvalues

$$u, \quad u, \quad u \pm c_a, \quad u \pm c_{f,s} \tag{7.16}$$

and the same eigenvectors as those of 7×7 matrix, except for the divergence wave

$$\mathbf{l}_p = \mathbf{r}_p^T = (0,\, 0,\, 0,\, 0,\, 1,\, 0,\, 0,\, 0) \tag{7.17}$$

Note that there exists no such coincidence considered in the previous system. Thus this eigensystem is preferable in implementing the divergence-free condition, since any $\nabla \cdot \mathbf{B}$ (that may be created locally due to truncation errors even if the initial data is divergence-free) will be convected away.

7.3 Lagrangian Eigensystem

When developing numerical methods for the equations of fluid flow, the common practice is to formulate the equation in a Eulerian frame. The reason is the advantage of Eulerian form over Lagrangian form in multidimensional extensions. But, one point that is often overlooked is that the Lagrangian description yields a simpler eigensystem and the Lagrangian method shows better performance in low density flow for which the Riemann solution in the Eulerian description is not linearizable.

Thus, at least for one-dimensional problem, the Lagrangian description has good ground[1]. (cf. [122, 86, 98])

Another interesting point, which becomes more important in MHD, is that Eulerian and Lagrangian equations have different averagings satisfying the conservation property. It was known in the late sixties that the arithmetic averaging of $\tau, \mathbf{u}, p$ in the Lagrangian equations for ideal gases satisfies the mean-value property [1]. In the beginning of eighties, Roe [99] found that the corresponding averaging in the Euler equation is the $\sqrt{\rho}-$weighted average for $1/\rho, \mathbf{u}$, and enthalpy h[2]. In MHD, it is observed by Brio and Wu [15] that the Eulerian form does not yield a unique Roe averaging except for $\gamma = 2$. In order to overcome this difficulty, introducing two mean states are suggested by Powell *et al.* [96]. But, as implied in Chapter IV, we can show that the arithmetic averaging of Lagrangian variables $\mathcal{W} = (\tau, \mathbf{u}, \mathbf{B}, p)$ satisfies the mean property for any γ in Lagrangian MHD, which is also known as the midpoint rule. The arithmetic averaging in Lagrangian MHD are

$$\bar{\mathcal{W}} = \frac{\mathcal{W}_L + \mathcal{W}_R}{2}, \tag{7.18}$$

$$\bar{e_t} = \frac{\bar{\tau}\bar{p}}{\gamma - 1} + \frac{\bar{u}^2 + \bar{v}^2 + \bar{w}^2}{2} + \frac{\bar{\tau}(\bar{B_y}^2 + \bar{B_z}^2)}{2}, \tag{7.19}$$

$$\bar{a'^2} = \frac{\gamma\bar{p}}{\bar{\tau}} = \frac{\tau_L a'^2_L + \tau_R a'^2_R}{\tau_L + \tau_R} \tag{7.20}$$

where $a'^2 = \gamma p/\tau = (a/\tau)^2$, and a' is the Lagrangian sound speed.

The Lagrangian conservative variables are

$$\mathcal{U}^T = (\tau,\ u,\ v,\ w,\ \tau B_y,\ \tau B_z,\ e_t). \tag{7.21}$$

The primitive variables are

$$\mathcal{W}^T = (\tau,\ u,\ v,\ w,\ B_y,\ B_z,\ p). \tag{7.22}$$

[1] Interestingly, the original Godunov method was developed in the Lagrangian form [43]. One might choose to find the solution to the Lagrangian system and remap it to a Eulerian grid [24].

[2] $\rho h = E + p + \frac{\mathbf{B}\cdot\mathbf{B}}{2}$.

Then right and left eigenvectors are

$$\mathbf{r}_c = \mathbf{N}\mathbf{r}_p, \quad \mathbf{l}_c = \mathbf{l}_p\mathbf{N}^{-1}, \tag{7.23}$$

where $\mathbf{N}$ is defined as $\Delta\mathcal{U}/\Delta\mathcal{W}$. The Lagrangian left eigenvectors are, in order of entropy, Alfvén, slow and fast waves,

$$\frac{1}{a^2}\Big(a^2,\ 0,\ 0,\ 0,\ 0,\ 0,\ \tau^2\Big), \tag{7.24}$$

$$\frac{1}{2}\Big(0,\ 0,\ \beta_z,\ -\beta_y,\ \mp\sqrt{\tau}\beta_z,\ \pm\sqrt{\tau}\beta_y,\ 0\Big), \tag{7.25}$$

$$\frac{1}{2a^2}\Big(0,\ \alpha_s c_s,\ -\alpha_f c_f \beta_y,\ -\alpha_f c_f \beta_z,\ \mp\alpha_f a\sqrt{\tau}\beta_y S,\ \mp\alpha_f a\sqrt{\tau}\beta_z S,\ \pm\tau\alpha_s\Big), \tag{7.26}$$

$$\frac{1}{2a^2}\Big(0,\ \alpha_f c_f,\ -\alpha_s c_s \beta_y,\ -\alpha_s c_s \beta_z,\ \pm\alpha_s a\sqrt{\tau}\beta_y S,\ \pm\alpha_s a\sqrt{\tau}\beta_z S,\ \pm\tau\alpha_f\Big). \tag{7.27}$$

Right eigenvectors $\mathbf{r}_p^T$ are in same order

$$\Big(1,\ 0,\ 0,\ 0,\ 0,\ 0,\ 0\Big), \tag{7.28}$$

$$\Big(0,\ 0,\ \beta_z,\ -\beta_y,\ \mp\beta_z/\sqrt{\tau},\ \pm\beta_y/\sqrt{\tau},\ 0\Big), \tag{7.29}$$

$$\Big(-\tau\alpha_s,\ \pm\alpha_s c_s,\ \pm\alpha_f c_f \beta_y,\ \pm\alpha_f c_f \beta_z,\ -\alpha_f a\beta_y S/\sqrt{\tau},\ -\alpha_f a\beta_z S/\sqrt{\tau},\ \alpha_s a^2/\tau\Big), \tag{7.30}$$

$$\Big(-\tau\alpha_f,\ \pm\alpha_f c_f,\ \mp\alpha_s c_s\beta_y,\ \mp\alpha_s c_s\beta_z,\ \alpha_s a\beta_y S/\sqrt{\tau},\ \alpha_s a\beta_z S/\sqrt{\tau},\ \alpha_f a^2/\tau\Big). \tag{7.31}$$

7.4 Flux-Difference Splitting with Fluctuation Approach

Let us consider a hyperbolic conservation law

$$\mathbf{u}_t + \mathbf{f}_x \ = \ 0. \tag{7.32}$$

There are two possible approaches to solve equations with Godunov-type methods: finite-volume formulation and fluctuation formulation. In Godunov-type methods, we start with the Godunov flux

$$F(u_L, u_R) \ = \ f\Big(u^*(u_L, u_R)\Big) \tag{7.33}$$

where $u^*(u_L, u_R)$ is the intermediate state $w(0)$ arising in the similarity solution $u(x,t) = w(x/t)$ of the Riemann problem. Replacing $u^*(u_L, u_R)$ by some approximation $\hat{u}^*(u_L, u_R)$ yields the approximate Godunov method in finite volume formulation.

$$U_j^{n+1} = U_j^n - \frac{\Delta t}{\Delta x}\Big(f(\hat{u}^*(u_j^n, u_{j+1}^n)) - f(\hat{u}^*(u_{j-1}^n, u_j^n))\Big) \tag{7.34}$$

where U_j is the cell average. Since

$$f(\hat{u}^*(u_j^n, u_{j+1}^n)) = f(U_j^n) + \sum_{left} \Delta f)_{j+\frac{1}{2}}, \tag{7.35}$$

$$f(\hat{u}^*(u_{j-1}^n, u_j^n)) = f(U_j^n) - \sum_{right} \Delta f)_{j-\frac{1}{2}} \tag{7.36}$$

it can be written in fluctuation formulation.

$$U_j^{n+1} = U_j^n - \frac{\Delta t}{\Delta x}\Big(\sum_{left} \Delta f)_{j+\frac{1}{2}} + \sum_{right} \Delta f)_{j-\frac{1}{2}}\Big) \tag{7.37}$$

The contribution to left and right states is obtained from waves, depending on the direction of propagation, whereas it is obtained from the numerical flux at their interface in finite volume formulation. In Roe's approximate Riemann solver, $\hat{u}(x,t)$ is determined by solving a constant coefficient linear system of conservation laws.

$$\hat{u}_t + \hat{A}(u_L, u_R)\hat{u}_x = 0 \tag{7.38}$$

If $\hat{A}$ has eigenvalues $\hat{\lambda}_i$ and right eigenvectors $\hat{r_i}$, and if we decompose $[u] = \sum \hat{\alpha}_i \hat{r_i}$, then we have

$$\hat{w}(\xi) = u_L + \sum_{\hat{\lambda}_i < \xi} \hat{\alpha}_i \hat{r_i}, \tag{7.39}$$

$$\hat{w}(\xi) = u_R - \sum_{\hat{\lambda}_i > \xi} \hat{\alpha}_i \hat{r_i} \tag{7.40}$$

Here, the following conditions are imposed on $\hat{A}$:

A. $\hat{A}(u_L, u_R)(u_R - u_L) = f(u_R) - f(u_L)$.

B. $\hat{A}(u_L, u_R)$is diagonalizable with real eigenvalues.

C. $\hat{A}(u_L, u_R) \to f'(\bar{u})$ smoothly as $u_L, u_R \to \bar{u}$.

From now on, the hat represents an averaging satisfying A. Eqs. 7.35 and 7.36 becomes

$$F_{j+\frac{1}{2}} = f(U_j) + \sum_{\lambda_i<0} (\hat{\lambda_i^-}\hat{\alpha}_i\hat{r}_i)_{j+\frac{1}{2}}, \tag{7.41}$$

$$F_{j+\frac{1}{2}} = f(U_{j+1}) - \sum_{\lambda_i>0} (\hat{\lambda_i^+}\hat{\alpha}_i\hat{r}_i)_{j+\frac{1}{2}}, \tag{7.42}$$

where $\lambda_i^- = \min(\lambda_i, 0)$ and $\lambda_i^+ = \max(\lambda_i, 0)$. If we average the two expressions, we obtain

$$F_{j+\frac{1}{2}} = \frac{1}{2}\Big(f(U_j) + f(U_{j+1})\Big) - \frac{1}{2}\sum_{all\,\lambda_i} (|\hat{\lambda}_i|\hat{\alpha}_i\hat{r}_i)_{j+\frac{1}{2}} \tag{7.43}$$

Or, we have the following equation in fluctuation formulation.

$$U_j^{n+1} = U_j^n - \frac{\Delta t}{\Delta x}\Big(\sum_{\lambda_i<0} (\hat{\lambda_i^-}\hat{\alpha}_i\hat{r}_i)_{j+\frac{1}{2}} + \sum_{\lambda_i>0} (\hat{\lambda_i^+}\hat{\alpha}_i\hat{r}_i)_{j-\frac{1}{2}}\Big). \tag{7.44}$$

Interestingly, no explicit information of physical flux function is needed in this equation. In gasdynamics, this point draws no special attention, but in MHD the situation become different. In MHD, the equations we are trying to solve is not perfectly conservative form for two reasons: (1) as explained in Section 7.2, the 8×8 matrix which yields a simple eigensystem is not equal to the Jacobian; and (2) in Lagrangian MHD which satisfies the mean property, the resulting system of conservation laws $\mathcal{U}_{t'} + \mathcal{F}_\xi = 0$ becomes non-conservative after transformation to the Euler frame,

$$\mathcal{U}_t + (u\mathbf{I} + \tau\frac{\partial \mathcal{F}}{\partial \mathcal{U}})\mathcal{U}_x = 0. \tag{7.45}$$

Therefore, the fluctuation formulation is preferable in Godunov-type method for MHD.

7.5 Numerical Issues in Non-strictly Hyperbolic, Rotationally Degenerate Conservation Laws for MHD

So far, we have considered problems that arise in developing approximate Riemann solvers: (1) implementing divergence-free condition; (2) defining the averaging satisfying $[\mathbf{f}] = \mathbf{A}[\mathbf{u}]$; and (3) devising a numerical method for the linearized Riemann problem. For these problems, the solutions are given: (1) adding source terms relating to $\nabla \cdot \mathbf{B}$; (2) introducing two mean states or adopting the Lagrangian description; and (3) formulating Roe's approximate Riemann solver by the fluctuation approach.

But, another numerical difficulty relevant to defining the eigensystem has not been identified. Four non-dimensional parameters appearing in eigensystem, $\beta_{y,z}$, $\alpha_{f,s}$ are ill-defined; $\beta_{y,z}$ in the limit of $\hat{B_y}^2 + \hat{B_z}^2 = 0$ and $\alpha_{f,s}$ at the umbilic point. Common practice is to choose $\beta_{y,z} = 1/\sqrt{2}$, but it is hard to justify it because a large class of Riemann data such that $\mathbf{B}_L = -\mathbf{B}_R$ will result in the same value.

Now, it is time to raise the most fundamental issue in developing Godunov-type numerical methods for MHD. The heart of Godunov-type methods is the Riemann problem. Thus when we are trying to apply them to other physical system, the necessary condition for such attempt is the well-posedness of the Riemann problem. Furthermore, there remains a question of accuracy of dissipative numerical schemes in solving the well-posed Riemann problem involving undercompressive shocks, since undercompressive shocks are sensitive to the precise form of the diffusion term and thus their asymptotic states depend on the relative ratio of the viscosity. (Lax shocks are affected only by the overall magnitude of the viscosity.) Dissipative numerical schemes on coarse grids will calculate undercompressive shock that corresponds to the numerical viscosity, rather than the physical viscosity.

Therefore, the important numerical issues that may arise in the non-strictly hyperbolic, rotationally degenerate MHD system are:

(1) how to apply the Godunov-type methods to MHD which turns out to be ill-posed except for the planar case;

(2) whether the well-posed MHD planar Riemann problem involves undercompressive shocks which may make standard numerical schemes inaccurate; and

(3) how to ensure the entropy condition.

Let us consider the second issue first. Fortunately, the answer is no for planar MHD Riemann problem. For the oil-recovery problem, however, the Riemann solution involves the undercompressive shocks and thus more careful treatment will be needed. The third issue is a current research issue. For the first issue, the theoretical results given in Chapters V and VI may serve as the solution to resolve the non-uniqueness that a specification of transverse magnetic field moments to the Riemann problem, and not just $\mathbf{u}_{L,R}$ are required. The key idea is to separate Alfvén wave from the evolution of magnitude of the magnetic field. The new method is not only based on the well-posed Riemann problem, but it also deals better with the magnetic moment. Furthermore, it can solve the indeterminacy of $\beta_{y,z}$, $\alpha_{f,s}$.

7.6 An Approximate Riemann Solver

The Hugoniot and wave trajectories for the system 2.41 are all either coplanar (v/w= const.) or purely rotational (u= const., v^2+w^2 = const.). There are precisely two solutions to the Riemann problem for 2.41, with data (u_L, v_L, w_L), (u_R, v_R, w_R). We begin by solving the Riemann problem for 5.19 with data (u_L, r_L), (u_R, r_R) where

$$r_L{}^2 = v_L{}^2 + w_L{}^2, \tag{7.46}$$

$$r_R{}^2 = v_R{}^2 + w_R{}^2. \tag{7.47}$$

We can either choose to solve the problem in which r_L, r_R have the same sign, or else the problem in which they have opposite sign. In either case, the two planar trajectories have to be connected either by a rotational discontinuity or by a Alfvén wave.

Consider now a set of Riemann problems in which the left state is kept constant, but the right state is chosen from the set $(u_R, r_R \cos\phi, r_R \sin\phi)$. As ϕ varies, it is possible that we ought to change from one of the above strategies to the other. However, in that case, we violate the principle that neighboring data have neighboring solutions. We are compelled to choose one strategy and stick with it. Taking $r_L r_R > 0$ is the simpler of the two.

There is one remaining ambiguity. The sense of the rotational discontinuity (clockwise or anti-clockwise) is unresolved, and even its magnitude contains an arbitrary multiple of 2π. However, for the ideal problem, the representation in physical space is unaffected. If a numerical flux is sought by solving a linearized Riemann problem, where should the mean state be taken? A formal Roe average suggests

$$\bar{u} = \frac{1}{2}(u_L + u_R), \quad \bar{v} = \frac{1}{2}(v_L + v_R), \quad \bar{w} = \frac{1}{2}(w_L + w_R). \tag{7.48}$$

However, to solve the coplanar problem correctly, we should take

$$\bar{r} = \frac{1}{2}(r_L + r_R), \tag{7.49}$$

which would put $(\bar{v}\,, \bar{w}\,)$ somewhere on the circle.

We propose the following scheme for calculating the intermediate state $\mathbf{u}^*$, hence $\mathbf{f}^* = \mathbf{f}(\mathbf{u}^*)$[88].

First, u^*, r^* are computed by solving the linear Riemann problem for the coplanar problem. Next,

$$\phi^* \;=\; \phi_L \text{ if the Alfvén wave has positive speed,}$$

$$\begin{aligned} \phi^* &= \phi_R \text{ if the Alfvén wave has negative speed, } i.e., \\ \phi^* &= \frac{1}{2}(1+\text{sgn}(u^*))\phi_L + \frac{1}{2}(1-\text{sgn}(u^*))\phi_R. \end{aligned} \tag{7.50}$$

ϕ^* is undetermined if $u^* = 0$, but in that case the fluxes in 2.41 do not depend on ϕ^*. The intermediate state is either L' or R' which is the projection on a circle defined by L and R.

This procedure can be applied directly to MHD problem with conserved quantities $(\rho, \rho u, \rho v, B, E)$ by introducing

$$(B_y,\, B_z) = (B\cos\phi,\, B\sin\phi),\ \phi^* = \frac{1}{2}(1+\text{sgn}(a-c_a))\phi_L + \frac{1}{2}(1-\text{sgn}(a-c_a))\phi_R. \tag{7.51}$$

In this process, the pressure and the magnetic field play an important part in calculating an intermediate state since they are essential elements to determine the shock waves.

CHAPTER VIII

CONCLUSIONS

8.1 Summary

In this thesis, we study the MHD Riemann problem theoretically and computationally for the purpose of developing a basic theory of the nonlinear evolution of MHD waves. In doing this, a model system preserving the MHD singularity is considered in advance of the full MHD system.

One of the major contribution of this thesis is to identify the isolated MHD singularity and to derive the MHD Rankine-Hugoniot conditions and simple waves relations in a useful form, and finally to connect them with recent mathematical theories of non-strictly hyperbolic conservation laws. In addition, conditions for selecting shocks, which are the most important element in constructing the weak solution to the Riemann problem, are extensively examined, and the viscosity admissibility condition which ensures the uniqueness of the planar MHD Riemann solutions is proposed[1]. As a result, we find that the MHD system is symmetrically hyperbolic and then prove that the planar MHD Riemann problem is well-posed[2].

[1] It means that we give a general proof of the results, which have been considered *not yet available*. "As a consequence, time-dependent intermediate shocks are needed in non-coplanar situations. ... Our approach in the paper is largely based on numerical examples. General proofs of the results are not yet available." [128, page 8174].

[2] See Theorem 1.

Another contribution is to demonstrate that non-planar waves are fundamentally different from planar waves by finding that the non-planar Riemann problem is not well-posed in general[3]. As a result, the finite-amplitude non-planar waves develop continuously and their behavior depend heavily on time, magnetic resistivity and associated magnetic field moments.

Finally, we identify several numerical issues in developing Godunov-type numerical methods for MHD and suggest solutions.

8.2 Future Works

Since our works are mostly mathematical in nature, they can be extended for problems in which complicated effects–relativity, anisotropic pressure, and two-fluid model–are taken into account. From a theoretical point of view, there are several issues which need the further study:

1. The relation between various entropy conditions [65].

2. The nonlinear evolution and stability of MHD waves under various drivers, external disturbances and viscosity matrices.

3. Nonlinear interaction of MHD shock waves.

4. Magnetic field reconnection.

5. The study on the turbulent dynamo problem in the form of a statistical initial-value problem [114, 85, 67]. This problem, which is concerned with the growth or decay of an initial weak magnetic field in a field of fully developed turbulence in a conducting fluid, is of considerable importance in astrophysics. A conventional viewpoint concerns in the redistribution of kinetic energy and magnetic

[3]See Proposition 1.

energy, and is based on the argument that the dynamic alignment of **u** and **B** is a direct consequence of the MHD equations. However, our study on how the Riemann solutions are constructed yields an evidence that in addition to the exchange of kinetic energy and magnetic energy, there is a possibility of the exchange of thermal energy and magnetic energy.

6. Shock geometry in relativistic MHD [73]. The classification of MHD shock waves in curved space-time will be an interesting subject since we anticipate a new kind of shock geometry. Even though some numerical results have been obtained for planar problems [120], based on our analysis of non-relativistic MHD, we are cautious in drawing conclusions from simulations taking no account of non-planarity.

7. Propagation of MHD waves through an anisotropic plasma [61, 2, 21, 109]. In contrast to an isotropic plasma, the Alfvén wave speed does not necessarily lie between the fast magnetoacoustic wave speed and the slow magnetoacoustic wave speed, yielding that the eigenvalues may have imaginary parts[4].

From a numerical point of view, the following problems might be considered in future studies:

1. Extensive test of a proposed MHD Riemann solver.

2. Investigation of accuracy of dissipative numerical schemes in solving the problem involving non-classical shocks.

3. Two-dimensional and three-dimensional numerical simulations. Of primary interest is how the shock stability theory applies to explaining the complicated

[4]The system becomes a mixed type conservation law [52].

phenomena of real problems such as the magnetosphere and magnetic field reconnection.

APPENDICES

APPENDIX A

PROOF OF $c = \gamma + 1$

The system we consider is

$$\begin{pmatrix} u \\ v \end{pmatrix}_t + \begin{pmatrix} cu^2 + v^2 \\ 2uv \end{pmatrix}_x = 0. \tag{A.1}$$

As shown by Schaeffer and Shearer [104], the parameter c controls the behavior of the system, that is, the wave structure of the system. The properties which distinguish the system by four different cases are the Hugoniot locus of the umbilic point and the $\lambda = 0$ curves. Both properties characterizes the general configuration of the Hugoniot. The Hugoniot of the umbilic point can be determined by a cubic equation (Eq. 3.7)

$$(2 - c)u^2 v - v^3 = 0. \tag{A.2}$$

And, the $\lambda = 0$ curves satisfy the quadratic equation (Eq. 3.3)

$$v^2 - cu^2 = 0. \tag{A.3}$$

Then, it can be found that there exist four different cases[1]:

I ($c < 0$, three Hugoniot lines and a $\lambda = 0$ point),

II ($0 < c < 1$, three Hugoniot lines and two $\lambda = 0$ lines),

[1] There might exist the detached Hugoniot curves.

III ($1 < c < 2$, three Hugoniot lines and two $\lambda = 0$ lines with $\sqrt{2-c} < \sqrt{c}$),
IV ($2 < c$, a Hugoniot line and two $\lambda = 0$ lines). Now, the question is whether there exist similar properties in MHD.

From the MHD Hugoniot equation 4.7, the locus of the MHD umbilic point ($U_L = 1,\ V_L = 0$) is determined by

$$V\left(V^4 + \frac{4}{\gamma(\gamma-1)}\Big(1+(\gamma-1)U\Big)V^2 + \frac{4}{\gamma^2}(U-1)^2\right) = 0, \tag{A.4}$$

with $U \geq 0$. Since the term in the bracket can not vanish, there exists only one line, that is, $V = 0$. In addition, from the Hugoniots 3.7 and 4.8, we can find horizontal asymptotes given as

$$\frac{v_{\max}}{v_L} = \frac{c}{c-2}, \quad \frac{V_{\max}}{V_L} = \frac{\gamma+1}{\gamma-1}. \tag{A.5}$$

Therefore, c must be $\gamma + 1$.

On the other hand, the comparison of the $\lambda = 0$ curves with the $c_{f,s} = 0$ curves of MHD is not straightforward due to $c_{f,s} \neq 0$ for any $(U,\ V)$. But we can solve this dilemma by redefining $\lambda = 0$ curves as follows.

$$\bar{v} = 0 \quad \text{and} \quad s = \lambda_{sL} \quad \text{with} \quad [u] \neq 0. \tag{A.6}$$

It becomes equal to Eq. A.3 since $\bar{u} = s = 0$. By this definition, the $\lambda = 0$ curves represent the boundary which separates the domain by the existence of overcompressive or expansive shocks. Thus, in MHD, it can be defined as

$$\bar{V} = 0 \quad \text{and} \quad |m| = \frac{c_{sL}}{\tau_L} \quad \text{with} \quad [U] \neq 0, \tag{A.7}$$

and are given in Eq. 4.72. As shown in Figs. 4.4$\sim$4.6, they consist of two curves passing the umbilic point.

In case of rarefaction waves, we also find that the model and the MHD system are identical in topology, as expected from the fact that the information of rarefaction waves is hidden in Rankine-Hugoniot conditions. (See Figs. 3.3 and 4.2.)

Finally, we prove $c = \gamma + 1$.

APPENDIX B

THEORY OF DYNAMICAL SYSTEM

B.1 Dynamical System

A dynamical system is determined by travelling wave solutions to the associated viscosity equation. The dynamical system can be characterized by configurations in the phase space of ordinary differential equations because the configuration is related to the existence of shock. Therefore, the analysis of the configuration is the essential tool for selecting shocks which admit a viscous profile.

The analysis of a system can be done in the following steps. To derive a dynamical system, we start from the viscosity equation associated with conservation laws

$$\mathbf{u}_t + \mathbf{f}_x = D\mathbf{u}_{xx}, \tag{B.1}$$

where we assume $\mathbf{u} = (u, v)$, $\mathbf{f} = (f(\mathbf{u}), g(\mathbf{u}))$, $D = \mu\mathbf{I}$. Let $\mathbf{u}_L$ and $\mathbf{u}_R$ be two constant states connected by a shock with speed s. The travelling wave solution of the form $\mathbf{u} = \mathbf{u}\Big((x - st)/\mu = \xi\Big)$ will converge to the weak solution of the given conservation laws. Then, by inserting $\mathbf{u} = \mathbf{u}(\xi)$, the viscosity equation reduces to

$$-s\mathbf{u}_\xi + \mathbf{f}_\xi = \mathbf{u}_{\xi\xi} \tag{B.2}$$

and can be integrated once to yield

$$\mathbf{f}(\mathbf{u}) - \mathbf{f}(\mathbf{u}_L) - s(\mathbf{u} - \mathbf{u}_L) = \mathbf{u}_\xi. \tag{B.3}$$

In this process the following boundary conditions must be satisfied:

$$\lim_{\xi \to -\infty} \mathbf{u}(\xi) = \mathbf{u}_L, \ \lim_{\xi \to +\infty} \mathbf{u}(\xi) = \mathbf{u}_R. \tag{B.4}$$

This dynamical system may be regarded as a vector field X_s which consists of

$$u_\xi \ = \ f(\mathbf{u}) - f(\mathbf{u}_L) - s(u - u_L) \equiv \Theta(\mathbf{u}), \tag{B.5}$$

$$v_\xi \ = \ g(\mathbf{u}) - g(\mathbf{u}_L) - s(v - v_L) \equiv \Phi(\mathbf{u}). \tag{B.6}$$

Notice that $\mathbf{u}_L, \mathbf{u}_R$ are also singularities and that all singularities lie on the Hugoniot locus which is defined as

$$\Big(f(\mathbf{u}) - f(\mathbf{u}_L)\Big)(v - v_L) - \Big(g(\mathbf{u}) - g(\mathbf{u}_L)\Big)(u - u_L) = 0. \tag{B.7}$$

In general, singularities are determined by solving $\Theta = 0$ and $\Phi = 0$ for given s and $\mathbf{u}_L$. For instance, singularities on the finite domain are the intersection of two curves defined by $\Theta = 0$ and $\Phi = 0$. However, there is a special case in which $\mathbf{u}_L$ is the umbilic point, so that eigenvalues become equal. In this case, the Hugoniot locus is straight lines satisfying

$$\frac{f(u,v)}{u} \ = \ \frac{g(u,v)}{v}, \tag{B.8}$$

if we assume $u_L = v_L = 0$. Singularities in this special case can be revealed by the Poincaré transform which is very useful for the analysis of unlimited orbits.

B.2 Poincaré Transformation

An approach to examining the asymptotic behavior of the unlimited orbits of a vector field is to use the so-called Poincaré transformation described below [91, pages 248-253]. Consider the Poincaré sphere where we project from the center of the unit

sphere $S^2 = \{(X,Y,Z) \in \mathbf{R}^3 \,|X^2+Y^2+Z^2 = 1\}$ onto the (x,y)-plane tangent to S^2 at either the north or south pole. This projection has the advantage that the singular points at infinity are spread out along the equator of the sphere. If we project the upper hemisphere of the sphere onto the (x,y)-plane, it follows that the equations defining (x,y) in terms of (X,Y,Z) are given by

$$x = \frac{X}{Z}, \quad y = \frac{Y}{Z}, \tag{B.9}$$

whereas the equations defining (X,Y,Z) in terms of (x,y) are given by

$$X = \frac{x}{\sqrt{1+x^2+y^2}}, \quad Y = \frac{y}{\sqrt{1+x^2+y^2}}, \quad Z = \frac{1}{\sqrt{1+x^2+y^2}} \tag{B.10}$$

These equations define a one-to-one correspondence.

A system $(\dot{x},\dot{y}) = \Big(P(x,y), Q(x,y)\Big)$ can be written in differential form as

$$Q(x,y)\,dx \; - P(x,y)\,dy \;\; = \;\; 0. \tag{B.11}$$

Let n denote the maximum degree of the terms in P and Q. Using the relations B.9 and multiplying Eq. B.11 by Z^n, the differential equation can be written as

$$\begin{vmatrix} dX & dY & dZ \\ X & Y & Z \\ P^* & Q^* & 0 \end{vmatrix} \; = \; 0, \tag{B.12}$$

where $P^*(X,Y,Z) = Z^n P(X/Z, Y/Z)$ and $Q^*(X,Y,Z) = Z^n Q(X/Z, Y/Z)$. Then, after some calculations, this leads a theorem summarized as; the flow in a neighborhood of any singular point of B.12 on the equator of the sphere, except the points $(1,\pm 1,0)$, is topologically equivalent to the flow defined by the system

$$\dot{y} = yz^n P(1/z, y/z) - z^n Q(1/z, y/z), \quad \dot{z} = z^{n+1} P(1/z, y/z). \tag{B.13}$$

Let $u \neq 0$. Applying $u = 1/z$ and $v = y/z$ to the vector field X_s and making the substitution $\zeta = z^n \xi$, we get

$$\begin{aligned} \frac{dy}{d\zeta} &= -y\Big(-sz(1-zu_L) + f(1,y) - z^2 f(u_L, v_L)\Big) \\ &\quad + g(1,y) - z^2 g(u_L, v_L) - sz(y - zv_L), \qquad \text{(B.14)} \\ \frac{dz}{d\zeta} &= -y\Big(-sz(1-zu_L) + f(1,y) - z^2 f(u_L, v_L)\Big). \qquad \text{(B.15)} \end{aligned}$$

The points on the equator represent the points at infinity of the plane. So the singularities at infinity $(y, z = 0)$, if exist, satisfy $-yf(1,y) + g(1,y) = 0$.

B.3 Local Approach

Once we determine singularities in the finite domain, we can try to deal numerically with the dynamical system B.5 and B.6. The configuration of a dynamical system enables us to select admissible viscous profiles from all possible connections of singularities, since a viscous profile is a solution of the system subject to boundary conditions $\Theta = \Phi = 0$ at each end point. But solving the dynamical system is a difficult and inefficient method because it usually requires numerical integrations.

Instead, two alternatives may be used for the purpose of determining the type of singularity. The first approach is the local approach in which the local topology is defined by the sign of eigenvalues $\lambda_{f,s} - s$ of the matrix $(\mathbf{A} - s\mathbf{I})$, where $\mathbf{A}$ is defined by $\partial \mathbf{f}/\partial \mathbf{u}$. This approach can be justified by the fact that the matrix is a tensor that relates the direction of the vector field u_ξ, v_ξ to a position within it. Thus, a singularity can be classified as a repelling node if $\lambda_{f,s} > s$, an attracting node if $\lambda_{f,s} < s$, and a saddle if $\lambda_s < s < \lambda_f$.

B.4 Global Approach (Index Theory)

The second approach is the index theory [91, pages 273-290]. This is a more rigorous, global analysis from the view-point of taking into account singularities at infinity. For a given vector field X_s on a two-dimensional surface, the index of a singularity can be defined as

$$I_{X_s}(C) = \frac{1}{2\pi} \oint_C d\tan^{-1} \frac{dv}{du}, \tag{B.16}$$

where C is a piecewise-smooth simple, closed curve centered at the singularity. Thus the index is 1 in node and -1 in saddle, since a node can be represented by a vector field (u, v) or $(-u, -v)$, while a saddle can be described by $(u, -v)$. Furthermore, by the Poincaré index theorem[1] , the sum of the indices of singularities on a two-dimensional surface is 2. Therefore, we can easily determine the type of all singularities without resolving the orbits in detail.

[1]Suppose that X_s is an analytic vector field on an analytic two-dimensional surface S of genus g and that X_s has only hyperbolic singular points; *i.e.*, isolated saddles, nodes and foci, on S. Then, $n + f - s = 2(1 - g)$. Here, the genus g is equal to the number of holes in the surface. For example, $g = 0$ for the two-dimensional sphere, $g = 1$ for the two-dimensional torus [91, pages 282-286].

APPENDIX C

ANALYSIS OF MHD DYNAMICAL SYSTEM

C.1 MHD Dynamical System

The MHD dynamical system can be derived from the non-ideal MHD equations, which are obtained by adding viscous terms to ideal MHD equations, *i.e.*, Eq. 2.27.

$$\begin{pmatrix} \tau \\ u \\ v \\ \tau B_\perp \\ e_t \end{pmatrix}_{t'} + \begin{pmatrix} -u \\ p + \frac{{B_\perp}^2}{2} \\ -B_x B_\perp \\ -B_x v \\ (p + \frac{{B_\perp}^2}{2})u - B_x B_\perp v \end{pmatrix}_{\xi} = \begin{pmatrix} 0 \\ \mu u_x \\ \nu v_x \\ \eta B_{\perp x} \\ (\Sigma + \kappa T)_x \end{pmatrix}_{\xi} \tag{C.1}$$

Σ denotes $(\mu u^2 + \nu v^2 + \eta {B_\perp}^2)/2$. For the sake of simplicity, the Hall effect has been neglected and $\mu = \nu = \eta = \kappa$ will be assumed. Inserting $\mathbf{U} = \mathbf{U}((\xi + mt')/\mu = \zeta)$ and integrating once yields the following MHD dynamical system:

$$u_x = m[u] + [p] + \bar{B_\perp}[B_\perp] \equiv \Theta, \tag{C.2}$$

$$v_x = m[v] - B_x[B_\perp] \equiv \Pi, \tag{C.3}$$

$$B_{\perp x} = m[\tau B_\perp] - B_x[v] \equiv \Phi, \tag{C.4}$$

$$\Big((u^2 + v^2 + {B_\perp}^2)/2 + T\Big)_x = m[e_t] + [(p + {B_\perp}^2/2)u - B_x B_\perp v] \equiv \Psi \tag{C.5}$$

with $m[\tau] = [u]$ and $\tau p = RT$. In doing this, the following boundary conditions must be satisfied:

$$\lim_{\zeta \to -\infty} \mathbf{U}(\zeta) = \mathbf{U}_L, \quad \lim_{\zeta \to +\infty} \mathbf{U}(\zeta) = \mathbf{U}_R. \tag{C.6}$$

This is a five dimensional autonomous system of ordinary differential equations for $\mathbf{U} = \mathbf{U}(\tau, u, v, B_\perp, T)$ with a parameter m.

In general, it is very difficult to understand the complicated dynamics of higher dimensional system. In MHD, a possible method might be a numerical study using an approximating scheme such as Runge-Kutta algorithm. For given m and a left state $(\tau, u, v, B_\perp, T)$ at a x, numerical integrations of Eqs. C.2$\sim$C.5 will reveal the phase portrait of the MHD dynamical system. However, this method requires tedious calculations and is inefficient in the sense that we are interested only in profiles connecting singularities. For this reason, we will adopt the local approach and the global approach based on the index theory.

C.2 Singularities

Singularities are determined by $\Theta = \Pi = \Phi = \Psi = 0$ for given m and a reference state.

When $m = 0$, two singularities (including the reference state) can be found and they represent neighboring states separated by the contact discontinuity.

When $m \neq 0$, the elimination of $[u]$ and $[v]$ yields the following equations:

$$m^2[\tau] + [p] + \bar{B_\perp}[B_\perp] = 0, \tag{C.7}$$

$$m^2[\tau B_\perp] - {B_x}^2[B_\perp] = 0 \tag{C.8}$$

with $[\tau] = \tau_L(\Omega - 1)$. Here $\Psi = 0$ is incorporated into the density ratio 4.88. These

can be rewritten as in (U, V) notation as

$$\sigma(\Omega - 1) + \frac{1}{\gamma}[U] + \bar{V}[V] = 0, \quad \text{(C.9)}$$

$$\sigma\Big(\Omega[V] + V_L(\Omega - 1)\Big) - [V] = 0, \quad \text{(C.10)}$$

where $\sigma = \tau_L m^2 / {B_x}^2$ and Ω is given in Eq. 4.88. Notice that all the singularities can be wholly determined in the reduced (U, V) plane and two running waves represented by $\pm m$ are united in a σ.

In conclusion, for given non-zero σ, the MHD vector field can have at most eight singularities which are projected into four singularities in (U, V) plane because C.9 and C.10 can be replaced by a quartic polynomial equation. Examples are given in Fig. C.1 (a)-(d). It can be observed that singularities are the intersection of the loop centered at the umbilic point and the detached curves similar to hyperbola.

C.3 Local Approach

Singularities in the finite domain can be classified by the sign of eigenvalues:

$$\frac{c_{f,s}}{\tau} - |m| = \frac{B_x}{\sqrt{\tau_L}}\left(S\left(\frac{1 + U + V^2 \pm \sqrt{(1 + U + V^2)^2 - 4U}}{2\Omega}\right)^{1/2} - \sqrt{\sigma}\right). \quad \text{(C.11)}$$

Notice that the vector field is symmetrical with respect to the contact discontinuity and its topology depends on only U, V values of singularities.

C.4 Global Approach

The global approach requires the information of singularities at infinity in addition to singularities in the finite domain. Singularities at infinity can be obtained by considering the Hugoniot locus, *i.e.*, Eq. 4.7, at the umbilic point $(U_L = 1, V_L = 0)$. From Eq. A.4, it is shown that singularities are on $V = 0$ axis since the term in the bracket cannot vanish. Hence there are two singularities at infinity independent of σ.

Moreover, they can be classified as nodes because singularities on $V = 0$ are nothing but singularities in the hydrodynamic limit.

On the other hand, it was not answered whether or not the index theory based on the planar system can be applied to only a section of the phase space with higher dimension. Here we presume that it is possible. A justification is that *the MHD dynamical system is invariant under a symmetric transformation*

$$x \leftrightarrow -x, m \leftrightarrow -m, [u] \leftrightarrow -[u], [v] \leftrightarrow -[v],$$

$$[p] \leftrightarrow [p], [B_\perp] \leftrightarrow [B_\perp], [\tau] \leftrightarrow [\tau]. \tag{C.12}$$

Furthermore, the local analysis also confirms it.

Finally, we demonstrate that the MHD system in U, V plane has at most four singularities in the finite domain and has two nodes at infinity. The phase portrait of the system consists of two nodes and two saddles in the finite domain. In the case of two singularities one is node and another is saddle. The configuration with three singularities occurs as the degenerate case or after the attracting node singularity reaches zero pressure. Examples of the global phase portrait for the MHD system can be seen in Fig. C.2. The saddle-saddle connection does not exist, but the node-node connection (which is related to overcompressive shocks) exists.

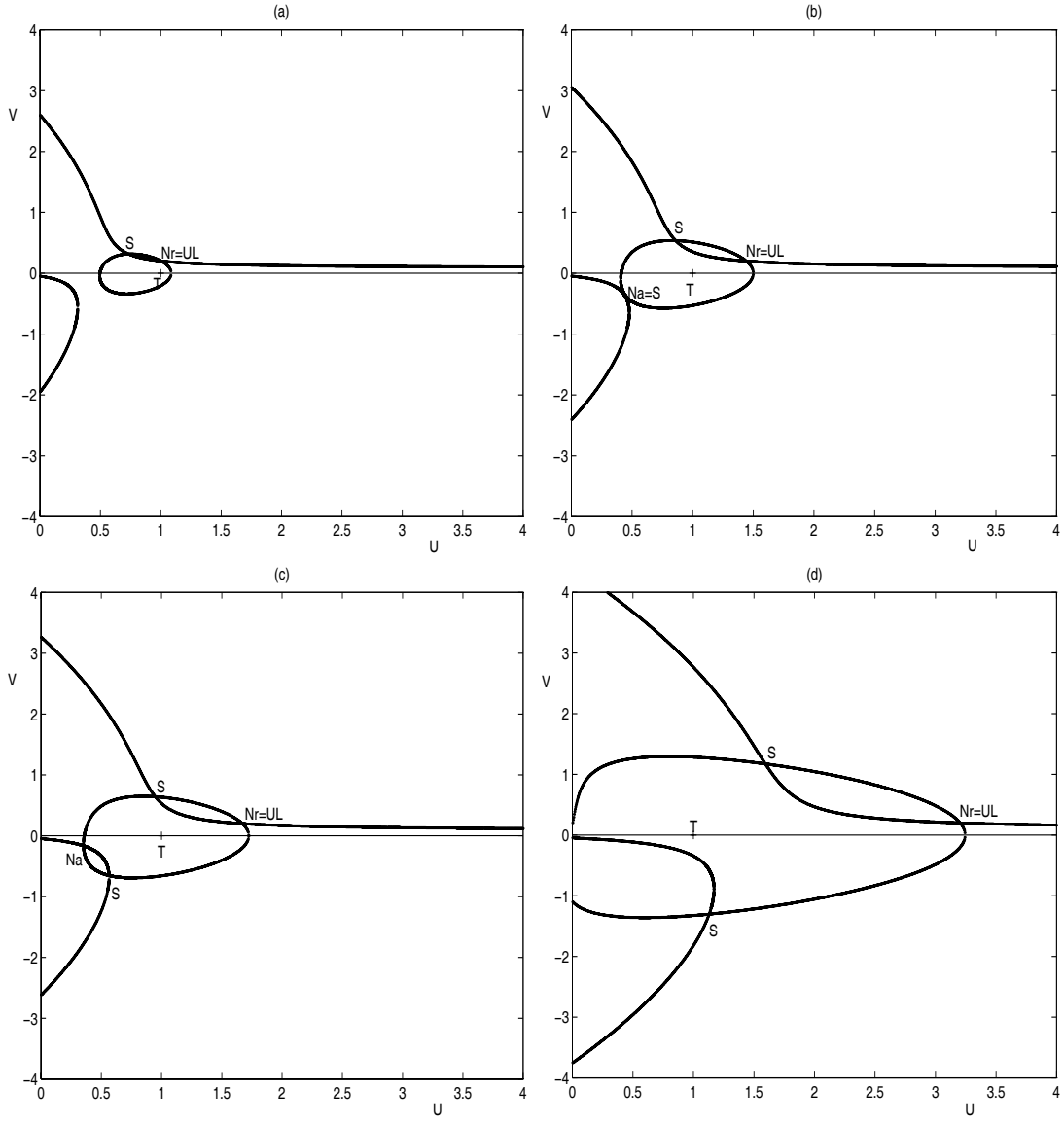

Figure C.1: (a)-(d). Singularities of MHD shocks : (a) $U_L = 1.0$, (b) $U_L = 1.4383$, (c) $U_L = 1.667$, (d) $U_L = 3.2$. $\sigma = 0.64, V_L = 0.2$. Nr,Na,S denote repelling node, attracting node and saddle,respectively.

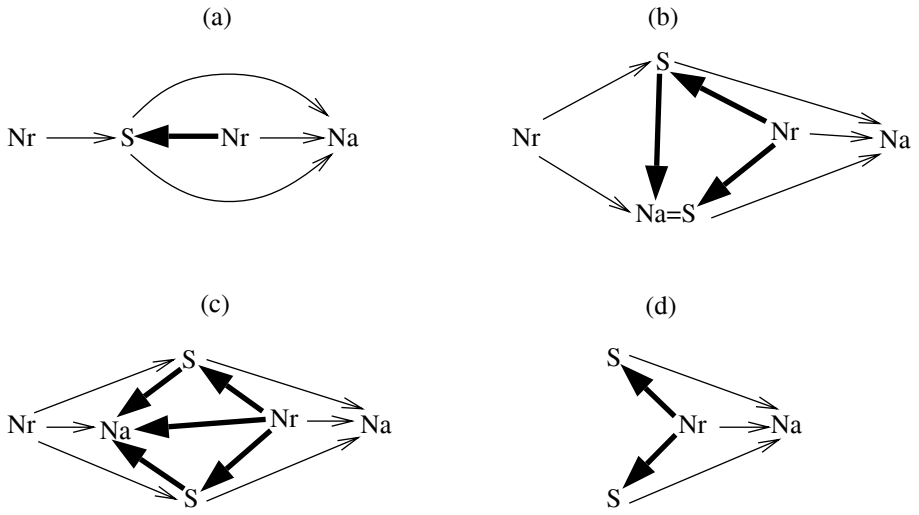

Figure C.2: (a)-(d). Examples of the global phase portrait for the planar MHD system. Case (d) cannot be found in case IV of 2×2 model system[20]. Nr,Na,S denote repelling node, attracting node and saddle,respectively. The connections from singularities at infinity are indicated by thin solid lines.

BIBLIOGRAPHY

BIBLIOGRAPHY

[1] Abarbanel, S. and Zwas, G., "An Iterative Finite-Difference Method for Hyperbolic Systems," *Math. Comp.*, vol. 23, pp. 549-566, 1969.

[2] Abraham-Shrauner, B., "Propagation of Hydromagnetic Waves through an Anisotropic Plasma," *J. Plasma Physics*, vol. 1, part 3, pp. 361-378, 1967.

[3] Akhiezer, A. I., Lubarski, G. J. and Polovin, R. V., "The Stability of Shock Waves in Magnetohydrodynamics," *Soviet Phys.-JETP*, vol. 8, pp. 507-511, 1959.

[4] Akhiezer, A. I. and Polovin, R. V., "The Motion of a Conducting Piston in a Magnetohydrodynamic Medium," *Soviet Phys.-JETP*, vol. 11, pp. 383-386, 1960.

[5] Alfvén, H., "Existence of Electromagnetic-Hydrodynamic Waves," *Nature*, vol. 150, no. 3805, p. 405, Oct., 1942.

[6] Anderson, J. E., *Magnetohydrodynamic Shock Waves*, M. I. T. Press, 1963.

[7] Aslan, N., *Computational Investigations of Ideal Magnetohydrodynamic Plasmas with Discontinuities*, Ph. D. Thesis, Dept. of Nuclear Engineering, University of Michigan, 1994.

[8] Bazer, J. and Ericson, W. B., "Hydromagnetic Shocks," *Astrophys. J.*, vol. 129, pp. 758-785, 1958.

[9] Bell, J. B., Trangenstein, J. A. and Shubin, G. R., "Conservation Laws of Mixed Type Describing Three-Phase Flow in Porous Media," *SIAM J. Appl. Math.*, vol. 46, pp. 1000-1017, 1986.

[10] Bell, J. B., Colella, P. and Trangenstein, J. A., "Higher Order Godunov Methods for General Systems of Hyperbolic Conservation Laws," *J. of Computational Physics*, vol. 82, pp. 362-397, 1989.

[11] Bickerton, R. J., Lenamon, L. and Murphy, R. V. W., "The Structure of Hydromagnetic Shock Waves," *J. Plasma Physics*, vol. 5, part 2, pp. 177-197, 1071.

[12] Biskamp, D., *Nonlinear Magnetohydrodynamics*, Cambridge University Press, 1993.

[13] Blokhin, A. M., *Strong Discontinuities in Magnetohydrodynamics*, NOVA, 1994.

[14] Brackbill, J. U. and Barnes, D. C., "The Effect of Nonzero $\nabla \cdot \mathbf{B}$ on the Numerical Solution of the Magnetohydrodynamic Equations,", *J. of Computational Physics*, vol. 35, pp. 426-430, 1980.

[15] Brio, M. and Wu, C. C., "An Upwind Differencing Scheme for the Equations of Ideal Magnetohydrodynamics," *J. of Computational Physics*, vol. 75, pp. 400-422, 1988.

[16] Brio,M. and Hunter, J. K., "Rotationally Invariant Hyperbolic Waves," *Comm. Pure Appl. Math.*, vol. XLIII, pp. 1037-1053, 1990.

[17] Brio, M. and Rosenau, P., "Evolution and Stability of the MHD Fast-Intermediate Shock Wave," *preprint*, 1994.

[18] Cable, S. and Steinolfson, R. S., "Three-Dimensional MHD Simulations of the Interaction between Venus and the Solar Wind," *J. of Geophysical Research*, vol. 100, no. A11, pp. 21,645-21,658, 1995.

[19] Cambel, A. B., *Plasma Physics and Magnetofluidmechanics*, McGraw-Hill, 1963.

[20] Chen, S., Chen, H., Martinez, D. and Matthaeus, W., "Lattice Boltzmann Model for Simulation of Magnetohydrodynamics," *Physical Review Letters*, vol. 67, no. 27, pp. 3776-3779, 1991.

[21] Chew, G. F., Goldberger, M. L. and Low, F. E., "The Boltzmann Equation and the One-Fluid Hydromagnetic Equations in the Absence of Particle Collisions," *Proc. Roy. Soc.*, vol. A236, pp. 112-118, 1956.

[22] Clauser, F. H., *Symposium of Plasma Dynamics*, Addison-Wesley, 1960.

[23] Cohen, R. H. and Kulsrud, R. M., "Nonlinear Evolution of Parallel-Propagating Hydromagnetic Waves," *Physics of Fluids*, vol. 17, no. 12, pp. 2215-2225, 1974.

[24] Colella, P. and Woodward, P. R., "The Piecewise-Parabolic Method (PPM) for Gasdynamical Simulations," *J. of Computational Physics*, vol. 54, pp. 174-201, 1984.

[25] Coroniti, F. V., "Laminar Wave-Train Structure of Collisionless Magnetic Slow Shocks," *Nuclear Fusion*, vol. 11, pp. 261-283, 1971.

[26] Dai, W. and Woodward, P. R., "An Approximate Riemann Solver for Ideal Magnetohydrodynamics," *J. of Computational Physics*, vol. 111, pp. 354-372, 1994.

[27] Dai, W. and Woodward, P. R., "A Simple Riemann Solver and High-Order Godunov Scheme for Hyperbolic Systems of Conservation Laws," *J. of Computational Physics*, vol. 121, pp. 51-65, 1995.

[28] De Hoffman, F. and Teller, E., "Magneto-hydrodynamic Shocks," *Phys. Rev.*, vol. 80, no. 2, pp. 692-703, 1950.

[29] Duhau, S., "Hydromagnetic Equations for Collisionless Plasmas in Strong Magnetic Fields," *J. Plasma Physics*, vol. 32, part 1, pp. 23-34, 1984.

[30] Duhau, S. and Torre, A. De La, "Hydromagnetic Waves for a Collisionless Plasma in Strong Magnetic Fields," *J. Plasma Physics*, vol. 34, part 1, pp. 67-76, 1985.

[31] Ericson, W. B. and Bazer, J., "On Certain Properties of Hydromagnetic Shocks," *Physics of Fluids*, vol. 3, no. 4, pp. 631-640, 1960.

[32] Freistühler, H., "Rotationally Equivariant Flux," *Workshop on Hyperbolic Problems: Theory, Computation and Applications*, IMPA, pp. 168-187, 1989.

[33] Freistühler, H., "Some Remarks on the Structure of Intermediate Magnetohydrodynamic Shocks," *J. of Geophysical Research*, vol. 96, no. A3, pp. 3825-3827, 1991.

[34] Freistühler, H., "Rotational Degeneracy of Hyperbolic Systems of Conservation Laws," *Arch. Rat. Mech. Anal.*, vol. 113, pp. 39-64, 1991.

[35] Freistühler, H., "Dynamical Stability and Vanishing Viscosity: A Case Study of a Non-Strictly Hyperbolic System," *Comm. Pure Appl. Math.*, vol. XLV, pp. 561-582, 1992.

[36] Freistühler, H. and Pitmann, E. B., "A Numerical Study of a Rotationally Degenerate Hyperbolic System. Part I, the Riemann Problem," *J. of Computational Physics*, vol. 100, pp. 306-321, 1993.

[37] Freistühler, H. and Liu, T. P., "Nonlinear Stability of Overcompressive Shock Waves in a Rotationally Invariant System of Viscous Conservation Laws," *Comm. Math. Phys.*, vol. 153, pp. 147-158, 1993.

[38] Furth, H. P., "Fusion," *Scientific American*, Sept., pp. 174-176, 1995.

[39] Gardner, C. S. and Kruskal, M. D., "Stability of Plane Magnetohydrodynamic Shocks," *Physics of Fluids*, vol. 7, no. 5, pp. 700-706, 1964.

[40] Germain, P., "Shock Waves and Shock-Wave Structure in Magneto-Fluid Dynamics," *Rev. of Mod. Phys.*, vol. 32, no. 4, pp. 951-958, 1960.

[41] Glimm, J., "The Interaction of Nonlinear Hyperbolic Waves," *Comm. Pure Appl. Math.*, vol. XLI, pp. 569-590, 1988.

[42] Glimm, J., "Nonlinear and Stochastic Phenomena: The Grand Challenge for Partial Differential Equations," *SIAM Review*, vol. 33, no. 4, pp. 626-643, 1991.

[43] Godunov, S. K., "Finite Difference Method for Numerical Computation of Discontinuous Solutions of the Equations of Fluid Dynamics," *Mat. Sbornik*, vol. 47, pp. 271-306, 1959.

[44] Gogosov, V. V., "Resolution of an Arbitrary Discontinuity in Magnetohydrodynamics," *J. Appl. Math. and Mech.*, vol. 25, pp. 148-170, 1961.

[45] Gombosi, T., *Space Plasma Physics*, Lecture Notes, University of Michigan, Ann Arbor, 1994.

[46] Gomes, M. E. S., "Riemann Problem Requiring a Viscous Profile Entropy Condition," *Adv. in Appl. Math.*, vol. 10, pp. 285-323, 1989.

[47] Hada, T., Mambu, M., Terasawa, T., Kennel, C. F. and Mjølhus, E., "Evolution of Finite Amplitude Alfvén Waves in Space Plasmas," *Nonlinear Space Plasma Physics* edited by R. Z. Sagdeev, AIP, pp. 275-283, 1993.

[48] Harten, A. and Osher, S., "Uniformly High-Order Accurate Nonoscillatory Schemes. I," *SIAM J. Num. Anal.*, vol. 24, pp. 279-309, 1987.

[49] Hau, L.-N. and Sonnerup, B. U. Ö, "On the Structure of Resistive MHD Intermediate Shocks," *J. of Geophysical Research*, vol. 94, no. A6, pp. 6539-6551, 1989.

[50] Helfer, H. L., "Magneto-hydrodynamic Shock Waves," *Astrophys. J.*, vol. 117, pp. 177-199, 1953.

[51] Hirch, C., *Numerical Computation of Internal and External Flows*, Wiley, 1988.

[52] Holden, H., "On the Riemann Problem for a Prototype of a Mixed Type Conservation Law," *Comm. Pure Appl. Math.*, vol. XL, pp. 229-264, 1987.

[53] Isaacson, E., Marchesin, D., Plohr, B., and Temple, B., "The Riemann Problem near a Hyperbolic Singularity: The Classification of Solutions of Quadratic Riemann Problems I," *SIAM J. Appl. Math.*, vol. 48, no. 5, pp. 1009-1031, 1988.

[54] Isaacson, E. and Temple, B., "The Riemann Problem near a Hyperbolic Singularity II," *SIAM J. Appl. Math.*, vol. 48, no. 6, pp. 1287-1301, 1988.

[55] Isaacson, E. and Temple, B., "The Riemann Problem near a Hyperbolic Singularity III," *SIAM J. Appl. Math.*, vol. 48, no. 6, pp. 1302-1312, 1988.

[56] Isaacson, E., Marchesin, D. and Plohr, B., "Transitional Waves for Conservation Laws," *SIAM J. Math. Anal.*, vol. 21, pp. 837-866, 1990.

[57] Isaacson, E., Marchesin, D., Palmeira, C. F. and Plohr, B. J., "A Global Formalism for Nonlinear Waves in Conservation Laws," *Comm. Math. Phys.*, vol. 146, pp. 505-552, 1992.

[58] Jeffrey, A. and Taniuti, A., *Non-Linear Wave Propagation*, Academic Press, New York, 1964.

[59] Kaku, M., *Hyperspace*, Anchor Books, 1994.

[60] Karamcheti, K., *Principles of Ideal-Fluid Aerodynamics*, John Wiley and Sons, 1966.

[61] Kato, Y. and Taniuti, T., "Propagation of Hydromagnetic Waves in Collisionless Plasma. I," *J. of the Physical Society of Japan*, vol. 21, no. 4, pp. 765-777, 1966.

[62] Kennel, C. F., Blandford, R. D. and Coppi, P., "MHD Intermediate Shock Discontinuities. Part 1. Rankine-Hugoniot Conditions," *J. Plasma Physics*, vol. 42, part 2, pp. 299-319, 1989.

[63] Kennel, C. F., Blandford, R. D. and Wu, C. C., "Structure and Evolution of Small-Amplitude Intermediate Shock Waves," *Phys. Fluids B*, vol. 2, no. 2, pp. 253-269, 1990.

[64] Keyfitz, B. L. and Kranzer, H. C., "A System of Hyperbolic Conservation Laws Arising in Elasticity Theory," *Arch. Rat. Mech. Anal.*, vol. 72, pp. 219-241, 1980.

[65] Keyfitz, B. L., "A Geometric Theory of Conservation Laws which Change Type," *ZAMM Z. angew. Math. Mech.*, vol. 75, no. 8, pp. 571-581, 1995.

[66] Kulikovskii, A. G. S. and Liubimov, G. A., "On the Structure of an Inclined Magnetohydrodynamic Shock Wave," *J. Appl. Math. and Mech.*, vol. 25, no. 1, p. 171, 1961.

[67] Ladbury, R., "Geodynamo Turns Toward a Stable Magnetic Field," *Physics Today*, Jan., pp. 17-18, 1996.

[68] Lax, P., "Hyperbolic System of Conservation Laws II," *Comm. Pure. Appl. Math.*, vol. 10, pp. 537-566, 1957.

[69] Lee, L. C. and Yan, M., "Generation of Slow-Mode Waves by the Interaction between the Bow Shock and Interplanetary MHD Waves," *Geophysical Institute Biennial Report 1993-94*, pp. 24-25, University of Alaska Fairbanks, 1994.

[70] Leonard, B. P., "Magnetic Structure of Ionizing Shock Waves. Part 1. Skew Shocks," *J. Plasma Physics*, vol. 7, part 1, pp. 135-155, 1972.

[71] Lessen, M. and Deshpande, N. V., "Stability of Magnetohydrodynamic Shock Waves," *J. Plasma Physics*, vol. 1, part 4, pp. 463-472, 1967.

[72] LeVeque, R. J., *Numerical Methods for Conservation Laws*, Birkhäuser, 1990.

[73] Lichnerowicz, A., *Magnetohydrodynamics: Waves and Shock Waves in Curved Space-Time*, Kluwer Academic Publishers, 1994.

[74] Lin, Y. and Lee, L. C., "Simulation Study of the Riemann Problem Associated with the Magnetic Reconnection," *J. of Geophysical Research*, vol. 100, no. A10, pp. 19,227-19,237, 1995.

[75] Liu, T. P., "Nonlinear Resonance for Quasilinear Hyperbolic Equation," *J. Math. Phys.*, vol. 28, no. 11, pp. 2593-2602, 1987.

[76] Liu, H., "The Interactions of Shock Waves of Nonstrictly Hyperbolic Systems," *Mathematica Acta Scientia*, vol. 12, no. 3, pp. 312-336, 1992.

[77] Lüst, R., "Stationary Magnetohydrodynamic Shock Waves of Arbitrary Strength," *Z. Naturforsch*, vol. 10a, pp. 125-128, 1955.

[78] Malkov, M. A., Kennel, C. F., Pellat, R. and Shapiro, V. D., "Alfvén Shock Trains," *Phys. Fluids B*, vol. 3, no. 6, pp. 1407-1419, 1991.

[79] Mann, G., "Simple Magnetohydrodynamic Waves," *J. Plasma Physics*, vol. 53, part 1, pp. 109-125, 1995.

[80] Marchesin, D. and Paes-Leme, P. J., "A Riemann Problem in Gas Dynamics with Bifurcation," *Comp. and Maths. with Appls.*, vol. 12A, no. 4/5, pp. 433-455, 1986.

[81] Marshall, W., "The Structure of Magnetohydrodynamic Wave in a Plasma of Infinite Conductivity," *Phys. Rev.*, vol. 103, no. 6, p. 1900, 1956.

[82] Mischailkow, K. and Hattori, H., "On the Existence of Intermediate Magnetohydrodynamic Shock Waves," *J. of Dynamics and Differential Equations*, vol. 2, no. 2, 1990.

[83] Mjølhus, E., "A Note on the Modulational Instability of Long Alfvén Waves Parallel to the Magnetic Field," *J. Plasma Physics*, vol. 19, part 3, pp. 437-447, 1978.

[84] Morioka, S. and Spreiter, J. R., "Evolutionary Conditions for Shock Waves in Collisionless Plasma and Stability of the Associated Flow," *J. Plasma Physics*, vol. 2, part 3, pp. 449-463, 1968.

[85] Mukerjee, M., "Mystery of the Missing Dynamo," *Scientific American*, Jan., pp. 24-26, 1995.

[86] Munz, C. D., "On Godunov-Type Schemes for Lagrangian Gas Dynamics," *SIAM J. Numer. Anal.*, vol. 31, no. 1, pp. 17-42, 1994.

[87] Myong, R. S. and Roe, P. L., "Solution of the Coplanar Riemann Problem on One-Directional Waves in Magnetohydrodynamics," *preprint*, 1995.

[88] Myong, R. S. and Roe, P. L., "On the Riemann Problem for Magnetohydrodynamics," *preprint*, 1995.

[89] Ogawa, H. and Hayashi, A. K., "Numerical Study on Magnetohydrodynamic Equations: A Comparison among Upwind, Centered Difference, and FCT Schemes," *Proc. of the 5th Int. Symp. on CFD-Sendai*, vol. II, pp. 387-392, JSCFD, 1993.

[90] Ogawa, H., Fujiwara, T. and Hayashi, A. K., "Shock Polar Analyses of Regular Reflections in Magnetohydrodynamics," *Phys. Plasmas*, vol. 2, no. 9, pp. 3282-3295, 1995.

[91] Perko, L., *Differential Equations and Dynamical System*, Springer-Verlag, 1993.

[92] Polovin, R. V., "The Motion of Shock Waves along a Magnetic Field," *Soviet Phys.-JETP*, vol. 12, no. 4, pp. 699-700, 1961.

[93] Polovin, R. V., "Contribution to the Theory of Simple Magnetohydrodynamic Waves," *Soviet Phys.-JETP*, vol. 12, pp. 326-330, 1961.

[94] Polovin, R. V. and Demutskii, V. P., *Fundamentals of Magnetohydrodynamics*, Consultants Bureau, 1990.

[95] Powell, K. G., "An Approximate Riemann Solver for Magnetohydrodynamics (that works in more than one dimension)," *ICASE Report 94-24*, 1994.

[96] Powell, K. G., Roe, P. L., Myong, R. S., Gombosi, T. and De Zeeuw, D., "An Upwind Scheme for Magnetohydrodynamics," *AIAA-95-1704-CP.*

[97] Richtmyer, R. D. and Morton, K. W., *Difference Methods for Initial-Value Problems*, Wiley-Interscience, 1967.

[98] Rider, W. J., "A Review of Approximate Riemann Solvers with Godunov's Method in Lagrangian Coordinates," *Computers Fluids*, vol. 23, no. 2, pp. 397-413, 1994.

[99] Roe, P. L., "Approximate Riemann Solvers, Parameter Vectors, and Difference Schemes," *J. of Computational Physics*, vol. 43, pp. 357-372, 1981.

[100] Roe, P. L. and Balsara, D. S., "Notes on the Eigensystem of Magnetohydrodynamics," *SIAM J. Appl. Math.*, vol. 56, no. 1, 1996.

[101] Rogister, A., "Parallel Propagation of Nonlinear Low-Frequency Waves in High-β Plasma," *Physics of Fluids*, vol. 14, no. 12, pp. 2733-2739, 1971.

[102] Sagdeev, R. Z., "The 1976 Oppenheimer Lectures: Critical Problems in Plasma Astrophysics. II. Singular Layers and Reconnection," *Reviews of Modern Physics*, vol. 51, no. 1, pp. 11-20, 1979.

[103] Sasoh, A. and Arakawa, Y., "Thrust Formula for Applied-Field Magnetoplasmadynamic Thrusters Derived From Energy Conservation Equation," *J. of Propulsion and Power*, vol. 11, no. 2, p. 351, 1995.

[104] Schaeffer, D. G. and Shearer, M., "The Classification of 2×2 Systems of Non-Strictly Hyperbolic Conservation Laws, with Application to Oil Recovery," *Comm. Pure Appl. Math.*, vol. XL, pp. 141-178, 1987.

[105] Schaeffer, D. G. and Shearer, M., "Riemann Problems for Nonstrictly Hyperbolic 2×2 Systems of Conservation Laws," *Trans. Am. Math. Soc.*, vol. 304, pp. 267-306, 1987.

[106] Sen, H. K., "Structure of Magnetohydrodynamic Wave in a Plasma of Infinite Conductivity," *Phys. Rev.*, vol. 102, no. 1, pp. 5-11, 1956.

[107] Shearer, M., Schaeffer, D. G., Marchesin, D. and Paes-Leme, P. J., "Solution of the Riemann Problem for a Prototype 2×2 System of Non-Strictly Hyperbolic Conservation Laws," *Arch. Rat. Mech. Anal.*, vol. 97, pp. 299-320, 1987.

[108] Shercliff, J. A., "One-Dimensional Magnetogasdynamics in Oblique Fields," *J. Fluid Mech.*, vol. 9, pp.481, 1960.

[109] Sielawa, J. T., *Simple Waves in Collisionless Interplanetary Plasma Governed by Chew-Goldberger-Low Equations*, Ph. D. Thesis, Dept. of Aerospace Engineering, University of Michigan, 1970.

[110] Tajima, T., *Computational Plasma Physics: With Applications to Fusion and Astrophysics*, Addison-Wesley, 1989.

[111] Tanaka, T., "Finite Volume TVD Scheme on an Unstructured Grid System for Three-Dimensional MHD Simulation of Inhomogeneous Systems Including Strong Background Potential Fields," *J. of Computational Physics*, vol. 111, pp. 381-389, 1994.

[112] Taniuti, T., "Reductive Perturbation Method for Quasi One-Dimensional Nonlinear Propagation II: Applications to Magnetosonic Waves," *Wave Motion*, vol. 13, pp. 133-146, 1991.

[113] Teske, M. E., *The Hydromagnetic Structure of the Annihilation between Two Oppositely-Directed Magnetic Fields*, Ph. D. Thesis, Dept. of Aerospace Engineering, University of Michigan, 1970.

[114] Thomas, J. H., "Numerical Experiments on a Model System for Magnetohydrodynamic Turbulence," *Physics of Fluids*, vol. 11, no. 6, pp. 1245-1250, 1968.

[115] Ugai, M., "Computer Studies on the Fast Reconnection Mechanism in a Shear Field Geometry," *Phys. Fluids B*, vol. 5, no. 8, pp. 3021-3031, 1993.

[116] Ugai, M. and Shimizu, T., "Computer Studies on Noncoplanar Slow and Intermediate Shocks Associated with the Sheared Fast Reconnection Mechanism," *Phys. Plasmas*, vol. 1, no. 2, pp. 296-307, 1994.

[117] Vanajakshi, T. C., Thompson, K. W. and Black, D. C., "Boundary Value Problems in Magnetohydrodynamics (and Fluid Dynamics). I. Radiation Boundary Condition," *J. of Computational Physics*, vol. 84, pp. 343-359, 1989.

[118] van Leer, B., "Towards the Ultimate Conservative Difference Scheme V. A Second Order Sequel to Godunov's Method," *J. of Computational Physics*, vol. 32, pp. 101-136, 1979.

[119] van Putten, M. H. P. M., "A Numerical Implementation of MHD in Divergence Form," *J. of Computational Physics*, vol. 105, pp. 339-353, 1993.

[120] van Putten, M. H. P. M., "A Two-Dimensional Numerical Implementation of Magnetohydrodynamics in Divergence Form," *SIAM J. Numer. Anal.*, vol. 32, no. 5, pp. 1504-1518, 1995.

[121] Vasyliunas, V. M., "Theoretical Models of Magnetic Field Line Merging, 1," *Reviews of Geophysics and Space Physics*, vol. 1, no. 1, pp. 303-336, 1975.

[122] Wagner, D. H., "Equivalence of the Euler and Lagrangian Equations of Gas Dynamics for Weak Solutions," *J. of Differential Equations*, vol. 68, pp. 118-136, 1987.

[123] Web, G. M., Brio, M. and Zank, G. P., "Symmetries of the Triple Degenerate DNLS Equations for Weakly Nonlinear Dispersive MHD Waves," *J. Plasma Physics*, vol. 54, part 2, pp. 201-244, 1995.

[124] Whang, Y. C., "Merging of Slow-Mode Compressive Waves in Low-β Plasma," *J. of Geophysical Research*, Vol. 101, No. A2, pp. 2529-2534, 1996.

[125] Wu, C. C., "On MHD Intermediate Shocks," *Geophysical Research Letters*, vol. 14, no. 6, pp. 668-671, 1987.

[126] Wu, C. C., "The MHD Intermediate Shock Interaction with an Intermediate Wave: Are Intermediate Shocks Physical?," *J. of Geophysical Research*, vol. 93, no.A2, pp. 987-999, 1988.

[127] Wu, C. C., "Effects of Dissipation on Rotational Discontinuities," *J. of Geophysical Research*, vol. 93, no.A5, pp. 3969-3982, 1988.

[128] Wu, C. C., "Formation, Structure, and Stability of MHD Intermediate Shocks," *J. of Geophysical Research*, vol. 95, no. A6, pp. 8149-8175, 1990.

[129] Wu, C. C. and Kennel, C. F., "Evolution of Small-Amplitude Intermediate Shocks in a Dissipative and Dispersive System," *J. Plasma Physics*, vol. 47, part 1, pp. 85-109, 1992.

[130] Wu, C. C. and Kennel, C. F., "The Small Amplitude Magnetohydrodynamic Riemann Problem," *Phys. Fluids B*, vol. 5, no. 8, pp. 2877-2886, 1993.

[131] Wu, C. C., "The Magnetohydrodynamic Riemann Problem and the Structure of the Magnetic Reconnection Layer," *preprint*, 1994.

[132] Yeh, T. and Axford, W. I., "On the Re-Connexion of Magnetic Field Lines in Conducting Fluids," *J. Plasma Physics*, Vol. 4, part 2, pp. 2-7-229, 1970.

[133] Zachary, A. L. and Colella, P., "A Higher-Order Godunov Method for the Equations of Ideal Magnetohydrodynamics," *J. of Computational Physics*, vol. 99, pp. 341-347, 1992.

[134] Zachary, A. L., Malagoli, A. and Colella, P., "A Higher-Order Godunov Method for Multidimensional Ideal Magnetohydrodynamics," *preprint*, 1993.

[135] Zank, G. P. and Matthaeus, W. H., "The Equations of Reduced Magnetohydrodynamics," *J. Plasma Physics*, vol. 48, part 1, pp. 85-100, 1992.

ABSTRACT

THEORETICAL AND COMPUTATIONAL INVESTIGATIONS OF NONLINEAR WAVES IN MAGNETOHYDRODYNAMICS

by

Rho Shin Myong

Chairperson: Philip L. Roe

For the purpose of developing a basic theory of the nonlinear evolution and stability of MHD waves and an approximate Riemann solver for MHD, the Riemann problem is investigated theoretically and computationally. The investigation starts with an analysis of a model system that preserves exactly the MHD singularity. Shock admissibility conditions are extensively examined and it is shown that the simple geometric conditions are inappropriate for determining physically relevant shocks of non-strictly hyperbolic conservation laws. A viscosity admissibility condition is proposed that ensures the uniqueness of the Riemann problem, and a global analysis of the dynamical system of the model is presented. By observing that the MHD system is symmetrically hyperbolic, a new MHD Rankine-Hugoniot relation is derived and then connected with recent mathematical theories of the Riemann problem of a quadratic model system near a hyperbolic singularity. As a result, a proof of the well-posedness of the planar MHD Riemann problem is obtained. By studying the

nonlinear evolution of the finite-amplitude waves, it is shown that the solution to the non-planar Riemann problem is not necessarily unique, in particular, that the solutions depend not only on left and right states, but also on the associated magnetic field moments. Finally, some numerical issues in developing Godunov-type numerical methods for MHD are discussed and a new approximate MHD Riemann solver is proposed, which is remarkably simple and follows exactly the way to generate the large-time solution to the non-planar Riemann problem from the well-posed planar problem.